POLITECNICO DI TORINO

Collegio di Ingegneria Chimica e dei Materiali

Master of Science Course
in Materials Engineering

Master of Science Thesis

Selective laser melting aluminum alloys for automotive component

Tutors

Prof. Claudio Badini
Dottoressa Elisa Padovano
Dott.Fabio D'aiuto

Candidate
Giulia Di Matteo

March 2018

Summary

Riassunto 5

I. Introduzione 5

II. Processo SLM 7

III. Materiali e metodi 9

IV. Risultati ottenuti e conclusioni 12

1. Introduction 15

1.1 Additive Manufacturing 16

1.2 Additive manufacturing techniques 19

1.2.1Power Bed Fusion (PBF) 21

1.2.2Selective laser sintering (SLS) 23

1.2.3 Laser melt deposition 25

1.2.4 Selective laser melting (SLM) 26

1.2.5 SLM Process technology 26

1.2.7Effect of the process parameters on SLM 29

1.2.8 Physical issues affecting the process 33

1.2.8.2 Wettability , thermo- capillarity convention , viscosity 34

1.3Powder production methods 35

1.3.1Materials for Metal Additive Manufacturing 39

1.3.2AlSi10 Mg alloy 41

1.3.3 Problems and advantages related to the use of aluminum alloys like AlSi10Mg for SLM process 43

1.3.4Aluminum alloys in automotive 45

2.0 Materials and Methods 46

2.3.1. **Flowability** 52

2.3.4 Density and porosity 56

2.3.5.2 Determination of residual stress 60

2.3.6 Scanning Electron Microscopy (SEM) 67

2.3.7. Optical microscope 68

2.4. Mechanical characterization 69

2.4.1Tensile test 69

2.4.2 Hardness test 72

2.4.3 Charpy test 75
3 Result and Discussion 76
3.1 AlSi10 Mg powders characterization 77
3.2 Characterization of Laser Molten Samples 82
3.2.1 Density analysis and microstructure 83
3.*2.3 Mechanical characteristics* 86
3.2.3.2 Micro-Hardness analysis 99
3.2.4 Residual stress analysis 104
4 Conclusions 108

Riassunto della Tesi di Laurea Magistrale (Sessione Marzo-Aprile 2018)

"**Microfusione laser selettiva di componenti automotive in lega di alluminio"**

Candidato: Giulia Di Matteo

Relatore: prof. Claudio Badini

Riassunto

I. Introduzione

Il presente lavoro di tesi svolto , in collaborazione tra FCA e Politecnico di Torino, presso il Centro Ricerche Fiat, nel dipartimento Metals Materials Lab, in sede Mirafiori, nasce dal desiderio e dalla necessità di migliorare, le tecnologie definite di "Additive Manufacturing" per la produzione di componenti automotive . Il termine "additive manufacturing " si riferisce ad una serie di processi produttivi che permetto la realizzazione di oggetti 3D a partire da un modello CAD (computer-aided-design) del prodotto finito . Il principio alla base di queste tecnologie è l'applicazione del materiale strato per strato Queste tecnologie nell'ultimo decennio stanno diventando parte integrante dei processi di produzione di famose aziende leader in numerosi settori industriali, in particolare nei settori automobilistico e aeronautico in quanto offrono numerosi vantaggi rispetto alle tecniche di produzione convenzionali. Uno dei principali vantaggi è la riduzione dei pesi dovuta sia alla minore densità dei componenti sia all'integrazione di più parti che eliminano la necessità di assemblaggio. Inoltre, vi è anche una riduzione dei costi dovuta all'eliminazione dei costi legati a numerose fasi di progettazione dei modelli, dei sistemi, nonché della manodopera ed è anche possibile evitare lo stoccaggio di pezzi di ricambio di automobili, spesso fuori produzione, grazie alla possibilità di stampare l'oggetto di interesse solo quando richiesto. contro , le tecnologie AM presentano anche svariati limiti quali :

-elevato costo delle materie prime e delle macchine

-elevati tempi di processo

-anisotropia : dovuta al fatto che, avvenendo la realizzazione dei componenti strato per strato , le proprietà microstrutturali e meccaniche dipenderanno dall'orientazione di crescita

-difetti: elevato rugosità superficiale

- creazione di supporti e successiva rimozione : i supporti sono necessari ai fine di sostenere la crescita dei componenti soprattutto di forma e complessa e al tempo stesso permetto la dissipazione del calore e la riduzione degli stress residui

- dimensione dei componenti : limiti dovuti alla dimensione della macchina

Le tecnologie AM per la realizzazione di componenti metallici hanno assistito ad un notevole sviluppo solo nell'ultimo decennio , motivo per il quale si presentano come un campo ancora da esplorare. Sono state messi a punto varie tipologie di processi produttivi per la realizzazione di componenti metallici che posso essere essenzialmente classificati in base a :

- Tipologia di materiale usato
- Fonte di energia : laser o fascione di elettroni

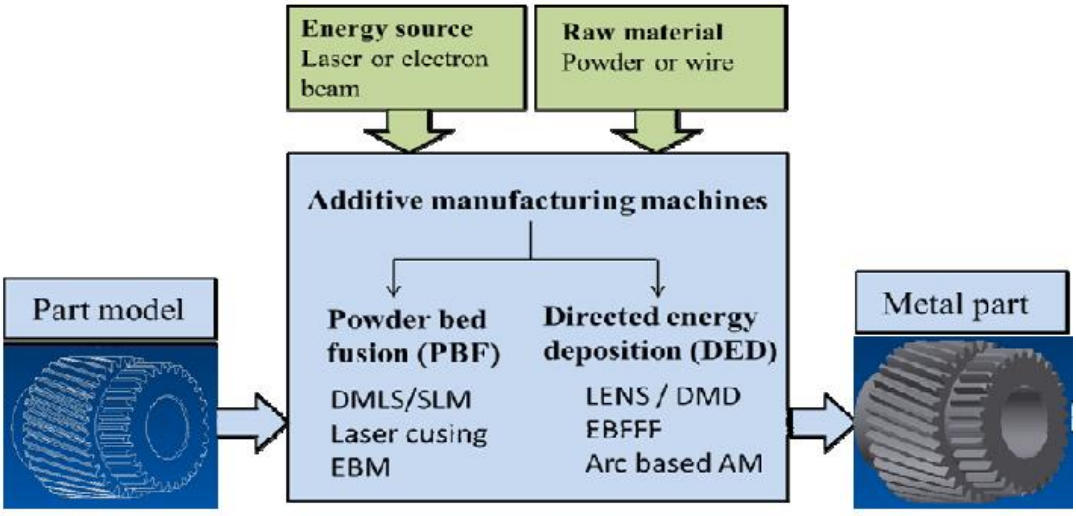

Figure 1: processi AM per realizzazione di componenti metallici

Un ulteriore classificazione è tuttavia possibile :

-Direct energy deposition (DED) :la polvere viene distribuita già fusa lungo la piattaforma di crescita in quanto viene parzialmente o totalmente fusa da una fonte di energia termica mentre avviene la deposizione

-Powder bed fusion (PBF) : la polvere dopo essere stata distribuita lungo la piattaforma di crescita(layer) viene totalmente o parzialmente fusa da una fonte di energia termica, viene aggiunto un secondo strato di polvere che viene scansionato dal laser e il processo si ripete fino alla creazione del prodotto finito. A seconda della fonte di energia :

-Fascio laser : Laser powder bed fusion (LPBF)

.-Fascio di elettroni ad elevata energia :Electron beam melting (EBM)

Tra i processi LPBF ritroviamo il processo Selective Laser Melting oggetto di studio del presente lavoro di tesi . L'uso del processo SLM per la produzione di componenti metallici di alta qualità e a basso costo è cresciuto esponenzialmente dalla metà degli anni '90 in quanto con il processo SLM è possibile realizzare componenti ad alta densità (fino al 99,9%), caratterizzati da microstrutture estremamente fine ,con geometrie complesse che non possono essere ottenuti con metodi convenzionali. La microstruttura molto fine permette di avere proprietà meccaniche migliori rispetto ai processi convenzionali. La microstruttura molto fine consente ai componenti realizzati attraverso il processo SLM di avere proprietà meccaniche migliorate rispetto ai processi di produzione convenzionali

E' stato condotto uno studio su campioni in AlSi10Mg prodotti attraverso SLM , fine a valutare le proprietà sia da un punto di vista meccanico sia morfologico. Considerando che una delle caratteristiche principali dei componenti realizzati attraverso SLM è l'anisotropia , l'influenza delle diverse orientazioni di crescita sul prodotto finito è stata oggetto di studio . Inoltre l'attenzione è stata anche focalizzata sull'analizzare e confrontare le differenti proprietà meccaniche e morfologiche tra i componenti as built e quelli sottoposti a trattamento termico e sull'influenza dello spessore del letto di polvere sulle proprietà del prodotto finite .

A tal proposito, vari campioni in AlSi10Mg sono stati realizzati attraverso il processo SLM. I campioni sono stati realizzati attraverso quattro differenti job uno dei quali differisce per il diverso spessore del letto di polvere .

Anche la polvere con la quale sono stati realizzati i provini è stata oggetto di studio in quanto sia i parametri processo sia le proprietà della polvere giocano un ruolo fondamentale sul processo SLM e di conseguenza sulle proprietà del prodotto finito

II. Processo SLM

Nel processo SLM la realizzazione del componente finito avviene a partire da un letto di polvere .

Uno strato sottile di polvere è distribuito, attraverso un sistema di distribuzione della polvere , lungo la piattaforma di crescita che può essere preriscaldata .Una volta depositato lo strato di polvere , un fascio laser viene focalizzato su una zona localizzata del letto di polvere portandola a parziale o totale fusione generando i

cosiddetti melt pool .Successivamente la piattaforma si abbassa, un nuovo strato di polvere viene depositato e re- inizia il processo .

Il processo viene ripetuto fino alla al raggiungimento della forma del prodotto finito . Il processo SLM dipende da alcune variabili riassunte in tabella 1.

Powder Properties	Process Parameters	
Particle shape	Laser power	Layer thickness
Particle size and distribution	Scanning speed	Scanning strategy
Chemical composition	Hatching distance	Building orientation
Thermal conductivity	Protective atmosphere	Gas flow
Melting temperature	Laser beam radius	Bed temperature
Absorptivity/reflectivity	Laser type	-

Tabella 1 : SLM variabili del processo

- **Proprietà della polvere**

Le proprietà della polvere quali densità bulk, proprietà termiche influenzano le caratteristiche del prodotto finito. Inoltre un ruolo importante è giocato dalla forma, dimensione e distribuzione granulometrica che dipendono essenzialmente dalle materie prime e dai metodi di produzione della polvere . La forma e la distribuzione granulometrica delle particelle influenza la flowability della polvere. Generalmente particelle di forma sferica , ottenibili attraverso l'atomizzazione in fase gas, assicurano una buona flowability . Anche l'omogeneità del letto di polvere influenza il processo in quanto letti di polvere troppo spessi potrebbero causare una non totale consolidazione delle parti e conseguenti fenomeni di instabilità . Bisogna anche prestare attenzione alla purezza della polvere in quanto eventuali contaminanti potrebbero inibire la densificazione delle parti e inficiare le proprietà meccaniche del prodotto finito .

- **Parametri di processo**

La densità di energia del fascio laser è uno dei parametri chiave del processo SLM. E' definita come la potenza del laser P(w) divisa per il prodotto tra la velocità di scan e il dimetro del fascio laser

$$E_\rho = \frac{P}{u\delta}\ (J/mm^2)$$

(Equazione 1)

Vari studi condotti da Liu et al hanno dimostrato che un elevata densità di energia del fascio laser causa la formazione di melt pool molto profondi e conseguente balling. Ciò può essere spiegato attraverso la sferoidizzazione della polvere fusa nel melt pool durante l'interazione del fascio laser con il letto di polvere .

La densità del fascio laser può essere diminuita aumentando la velocità di scan .

Altri parametri chiave del processo sono la direzione di crescita dei componenti e la strategia di scansione . Un corretta strategia di scan può minimizzare la presenza di difetti, porosità ed anisotropia .

Per quanto riguarda la direzione di crescita , essa modifica l'evoluzione microstrutturale dei componenti e può causa la nascita di difetti ed anisotropia.

III. Materiali e metodi

- **Polvere $AlSi_{10}Mg$**

La polvere $AlSi_{10}Mg$, con composizione chimica mostrata in figura 2, fornita dalla Eos è stata usata per la realizzazione dei campioni in questo lavoro di tesi

Element	Min	Max
Al	Balance	
Si	9.0	11.0
Fe	---	0.55
Cu	---	0.05
Mn	---	0.45
Mg	0.25	0.45
Ni	---	0.05
Zn	---	0.10
Pb	---	0.05
Sn	---	0.05
Ti	---	0.15

Figura 2 : $AlSi_{10}Mg$ composizione chimica

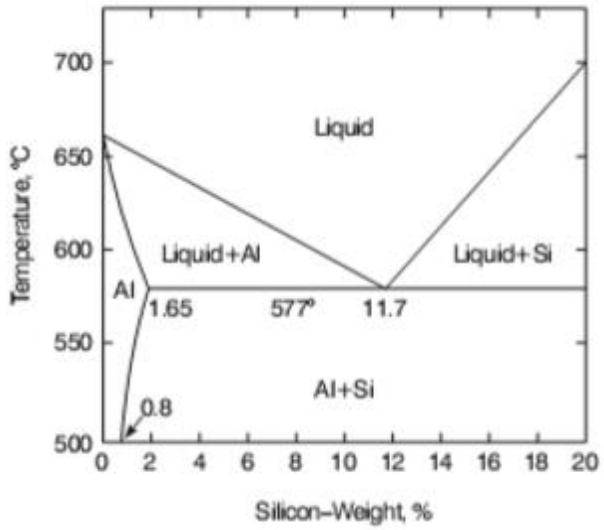

Figura 3 : diagramma di stato Al-Si

Il sistema Al-Si è un sistema eutettico binario. Il punto 'eutettico si ha ad una temperatura pari a 577 °C ed è caratterizzato dal 11 %-12% wt di Si. La lega AlSiMg è una lega ipoeutettica in quanto contiene 11% wt di Si.

- EOS M290

I campioni analizzati sono stati realizzati attraverso la macchina EOS M290 usando i parametri mostrati in tabella

	DIRECT PART		POSTCONTOURS		
	COLD	200 °C	COLD	200 °C	
DISTANCE	0,19	0,19			mm
SPEED	1300	1300	900	900	mm/s
POWER	370	370	80	80	W
BEAM OFFSET	0,02	0,02	0,02	0,02	mm
HATCHING	X	X			ROTATED
STRIPE WIDTH	7	7			mm
STRIPES OVERLAP	0,02	0,02			mm
LAYER	0,03	0,03	0,03	,03 or 0,06	mm
TEMP. ON PLATFORM	50	200	50	200	°C

Figura 4 : EOS M290 parametri di processo

La macchina EOS 290 è costituita da :

-Camera di processo : riscaldata termicamente e contenete gas inerte e sensori per monitorare il contenuto di ossigeno.
- Piattaforma di crescita : muovendosi lungo l'asse Z permette la realizzazione del componente finito
- Sistema elevatore : costituito da sistema di dosaggio della polvere e pistoni
- Recoater : distribuisce uniformemente la polvere dopo la scansione del laser
- Scanner : guida il fascio laser per mezzo di de specchi attraverso il letto di polvere E' necessario affinché si abbiano elevate precisione del prodotto finito
- Laser : ha lunghezza d'onda compresa tra 960-980 nm e permette la totale o parziale fusione del letto di polvere a seconda dell' energia del fascio.

Possono essere adottate differenti strategie di scansione per la realizzazione dei component attraverso SLM . In questo lavoro di tesi, per la realizzazione di tutti I campioni , è stata adottata una strategia di scan basata sulla rotazione di 67° della direzione di scansione .

- **Medoti di caratterizzazione**

Differenti tipi di provini sono stati realizzati in FCA presso il prototypes experimental construction department (CS). Quattro differenti job sono stati realizzati in modo da analizzare le proprietà strutturali e meccaniche dei vari campioni . Il quarto job è costituito da provini destinati al test Charpy .

Alcuni campioni sono stati sottoposti ad un trattamento di " stress relieving " a 300°C per due ore con successivo raffreddamento in forno come raccomandato dalla EOS. Le analisi ed I test effettuati sono riportati in tabella 2.

Analisi / test effettati	Caratteristiche /Proprietà analizzate
Flowability	Capacità di fluire della polvere
Tap density	Aumento della densità bulk apparente della polvere
Analisi granulometrica	Distribuzione e dimensione delle particelle di polvere

Bilancia di Archimede	Porosità e densità
Diffrazione Raggi X	-identificazione delle fasi cristalline - determinazione stress residui
Microscopio ottico	Analisi morfologica dei provini in piani paralleli e perpendicolari rispetto la direzione di crescita
Scanning electron microscopy (SEM)	-Analisi superficie di frattura dei campioni sottoposti a trazione
Test di trazione	-Determinazione e confronto proprietà meccaniche dei provini cresciuti lungo differenti direzione as built e trattati
Test di micro-durezza	-Determinazione durezza in facce parallele e perpendicolare alla direzione di crescita e confronto tra i campioni as built e trattati
Test charpy	Determinazione e confronto del lavoro di frattura dei provini cresciuti lungo differenti direzione as built e trattati

Tabella 2: analisi /test effettuati

IV. Risultati ottenuti e conclusioni

Nel presente lavoro di tesi sono stati caratterizzati dal punto di vista meccanico, microstrutturale , provini realizzati mediante il processo SLM.

Due differenti tipi di polvere sono stati analizzati.
Polvere A : realizzazione provini job A,B C
Polvere B : realizzazione provini job D
Dalle analisi FESEM si è osservato che entrambe le polveri sono costituite da particelle di forma sferica con valori identici di d10,d50 e d90 .In figura 5 è possibile notare che la forma delle due curve di distribuzione è differente : la polvere A ha una distribuzione Gaussiana mentre la polvere B più irregolare con massimo centrato a valori più elevati rispetto la polvere A . La presenza di particelle di dimensione maggiore fa si che la polvere B presenti una migliore flowability rispetto la polvere B. Esaminando i valori di densità e porosità ottenuti è possibile affermare che i provini mostrano minori valori di densità e di

conseguenza maggiore porosità percentuale rispetto i dati forniti dalla EOS . Ciò è probabilmente dovuto ad una non completa consolidazione delle parti particolarmente evidente lungo le zone di confine tra i vari melt pool . La presenza di porosità è stata evidenziata dalle micrografie effettuate su piani paralleli e perpendicolari alla direzione di crescita che hanno anche permesso di evidenziare la microstruttura dei campioni .
Prove di trazione eseguite sui campioni hanno dimostrato che le caratteristiche meccaniche dipendono dalla direzione di crescita del campione, dal trattamento termico e dallo spessore del letto di polvere. I campioni cresciuti lungo l'asse Z mostrano una maggiore resistenza alla trazione rispetto a quelli coltivati sul piano XY, ma a volte hanno una minore resistenza allo snervamento e un minore allungamento a rottura. Studiando la microstruttura dei campioni è stato possibile capire come la direzione della crescita influenza le proprietà meccaniche. Il diverso comportamento meccanico può essere spiegato dal diverso orientamento dei vari strati che può essere parallelo o perpendicolare rispetto alla direzione di applicazione del carico. Nei campioni Z, la frattura avviene perpendicolarmente alla direzione di crescita , cioè attraverso interfacce deboli tra gli strati, mentre nei campioni XY la frattura avviene parallelamente alla direzione di crescita. La microscopia elettronica eseguita sulle superfici di frattura di campioni as built e trattati termicamente (cresciuti secondo entrambe le direzioni sopra menzionate) mostrava sempre una microstruttura costituita da grani di alluminio molto piccoli circondati da silicio, segregati ai bordi dei grani. In ogni caso è stata osservata una frattura duttile inter-dominio a basso ingrandimento e la frattura duttile inter-granulare è stata osservata a un ingrandimento maggiore. Il trattamento termico ha causato il miglioramento della segregazione del silicio; i bordi del grano sono chiaramente decorati da particelle di silicio e Mg2Si in modo continuo. Nessuna crescita significativa del grano si è verificata durante il trattamento termico a causa della segregazione del silicio che ha impedito la crescita dei grani. Inoltre, è possibile affermare che il trattamento termico di stress relieving ha interessato principalmente la resistenza a trazione e l'allungamento. In particolare, questo può essere visto nei campioni cresciuti lungo l'asse Z. Per quanto riguarda i campioni costruiti con maggiore spessore del letto di polvere, il trattamento termico influenza molto meno le proprietà meccaniche dei campioni, in quanto essendo il letto di polvere più spesso c'è una diversa storia termica durante la fusione laser selettiva. L'anisotropia del materiale ha influenzato anche i valori di durezza e il lavoro di frattura. Dai risultati ottenuti attraverso il test di micro durezza HB è possibile affermare che i campioni mostrano valori di durezza più elevati sulle facce perpendicolari alla direzione di crescita rispetto a quelle parallele. Le facce

parallele e perpendicolari alla direzione di crescita hanno una diversa storia termica. Il campione è cresciuto lungo Z, quindi la durezza del campione nella faccia perpendicolare alla direzione di crescita si riferisce allo strato che si è solidificato per ultimo, mentre nel caso delle facce parallele gli strati sono rimasti ad alta temperatura per molte ore durante la costruzione campione strato per strato. Inoltre, il trattamento termico fine a ridurre gli stress non ha influenzato in modo significativo la durezza dei campioni. Anche il lavoro di frattura è stato influenzato dall'orientamento alla crescita dei campioni e dal trattamento termico. I campioni cresciuti nel piano XY hanno mostrato un lavoro di frattura più elevato e anche la duttilità (allungamento a rottura) rispetto a quelli cresciuti lungo l'asse Z. In entrambi i casi si è verificato un aumento del lavoro di frattura dopo il trattamento termico, in particolare per i campioni cresciuti lungo Z. L'analisi degli stress residui ha mostrato che esiste uno stato complesso di compressione e sforzo di taglio sulle facce del campione parallele e perpendicolari alla direzione di crescita. Nella faccia perpendicolare alla direzione di crescita, sono stati ottenuti valori di stress più elevati, confermando l'importanza della diversa storia termica sulle proprietà meccaniche. Tuttavia si dovrebbe tener conto del fatto che i valori delle tensioni termiche sono calcolati attraverso la misura della distanza inter planare , che è anche influenzata dalla presenza di silicio in soluzione solida in alluminio. Questa caratteristica ha quindi influito sulla valutazione dello stress.

Chapter 1

1. Introduction

The present thesis work, in collaboration between FCA and Turin Polytechnic, at the Fiat Research Center, in the Metals Materials Lab department, at Mirafiori, is born from the desire and the need to improve, the technologies of Additive Manufacturing for the production of automotive components. These technologies in the last decade are becoming an integral part of the production processes of famous leading companies in numerous industries sector , particularly in the automotive and aeronautics fields as they offer numerous advantages respect of conventional manufacturing techniques. One of the main advantages is the reduction of weights due to both the lower density of the components and the integration of several parts that eliminate the need for assembly. In addition, there is also a reduction in costs due to the elimination of costs related to numerous design phases of the models, systems, as well as manpower and it could also avoid the storage of spare parts of cars, often out of production, thanks to possibility to print the object of interest only when requested. In particular the use of SLM technology for the production of high quality, low cost metallic components has grown exponentially from the mid-1990s as the SLM technology allows the fabrication of high-density components (up to 99.9%), exhibiting extremely fine microstructures with complex geometries that cannot be fabricated by conventional methods. The very fine microstructure allows components made through SLM process to have improved mechanical properties compared to conventional production processes. A study on the properties of AlSi10Mg produced by Selective Laser Melting has been carried out both from a mechanical and a morphological point of view. Considering that one of the intrinsic characteristics of the components realized through SLM and in general by additive manufacturing

technologies is the high anisotropy, the influence of the different building direction on the characteristics of the finished product has been investigated. Furthermore, the attention has also been focused on comparing the different mechanical proprieties of the materials subjected to heat treatment with respect to those as built and on the influence of the thickness of the powder layer. In this regard, a series of samples in AlSi10Mg alloy were made through SLM process . Samples were realized through four different jobs , one of which differs for the different thickness of the powder layer. The specimens were printed in two different building orientations and the mechanical behavior of the as-built and treated specimens was studied, through tensile test , HB micro-hardness test and Charpy test. It has been possible to observe that the mechanical behavior of the specimens strongly depends on the growth direction and the heat treatment. In particular, observing the stress-strain graphs, related to the tensile tests, this dependence was confirmed as regards the values of elastic modulus, tensile strength and elongation at break and it was also possible to highlight the dependence of this values from the powder layers thickness. Interesting results were also obtained by observing the fracture surfaces of the samples subjected to traction. To understand how the mechanical behavior depends on the structure of the specimens, which differs in the different directions of growth, a micro structural characterization has been carried out. The powder through which the specimens were obtained has also been subject of study since the properties of the finished products depend on powder characteristics such as shape , particle size and distribution , composition . In the various chapters the main characteristics of additive technologies will be presented, in particular the study of SLM technologies, the advantages and limitations of this with respect to traditional technologies will be explored. The results of the mechanical tests carried out will be reported, and of the various analyzes carried out respectively on the specimens and on the powder

1.1Additive Manufacturing

Additive manufacturing (AM) is a technology that build three-dimensional objects by adding layer by layer materials (metal, polymer or ceramic ones) starting from a computer-aided design (CAD) model of the final product [1] .

For many years AM has been known as Rapid prototyping (RP), a term that was coined in the mid-1980s to describe a series of technologies that make prototypes of products in the early stages of development in a quick and automated manner . Nowadays the AM technologies represent a significant development respect to the pure prototyping.

The scientific community has chosen the general nomenclature of "additive manufacturing " to refers to any manufacturing technology using layer-by-layer or drop-by-drop processes that offers the possibility to create the final product by adding materials in contrast with conventional subtractive manufacturing methodologies which are based on removing material from a solid block[2] . Many are the advantages of using AM process respect to more traditional techniques: The object, even of complex shape, can be developed in a single process without (or with limited) needing further processing to improve mechanical properties or surface finishing. Moreover the AM process is particularly advantageous when is necessary to lighten a component, to realize elements with dense, porous or trabecular parts and for the production of a limited number of complex objects which need the creation of ad hoc supports to be removed later. However to create a very simple geometry, casting will always be the most economical technology.

AM techniques have also the potential to achieve zero wastage through the use of recycling within the processes and this also results in a reduction in emissions because of fewer raw materials need to be produced. Usually, in molding processes, such as die casting, lots of energy and resources are consumed to produce tools like dies and molds; moreover, in comparison to conventional manufacturing technologies, AM techniques do not directly use toxic chemicals, such as lubricant or coolant.

On the other hand, additive manufacturing has various limitations like:

- Speed: It takes time to realized a component which becomes available in few hours

-Defects : it can cause problems concerning surface roughness and dimensional accuracy,

-Anisotropy :it is due to the fact that, since there is a layer by layer growth, the properties of the material depend on the orientation

-Size limitation : the size of the components is limited by the dimensions of the machine

- Creation of support and its removal: depending on the direction of growth, supports are required in order to dissipate the internal heat flow, to minimize the residual stress and, above all, to support the growth of the pieces during the process especially if complex objects are realized [3]

- Cost : the effectiveness in terms of production costs is low because of the high cost of machines and raw materials.

The costs associated with a production process can be divided into fixed and recurring costs. Fixed costs are correlated to tools, molds, buildings, etc.; they are amortized on the number of produced items. On the other hand the recurring costs are the regular ones such as those for materials and labor; they are mainly associated with the produced pieces. Figure 1 illustrates the comparison between the costs associated with -conventional methods and those correlated with additive manufacturing. The total cost shows a linear increase in function of the amount of the produced pieces. The intercept on the y axis represents the value of fixed costs while the slope of the curve corresponds to the ratio between the variable costs of the AM and those of the conventional processes[4] .

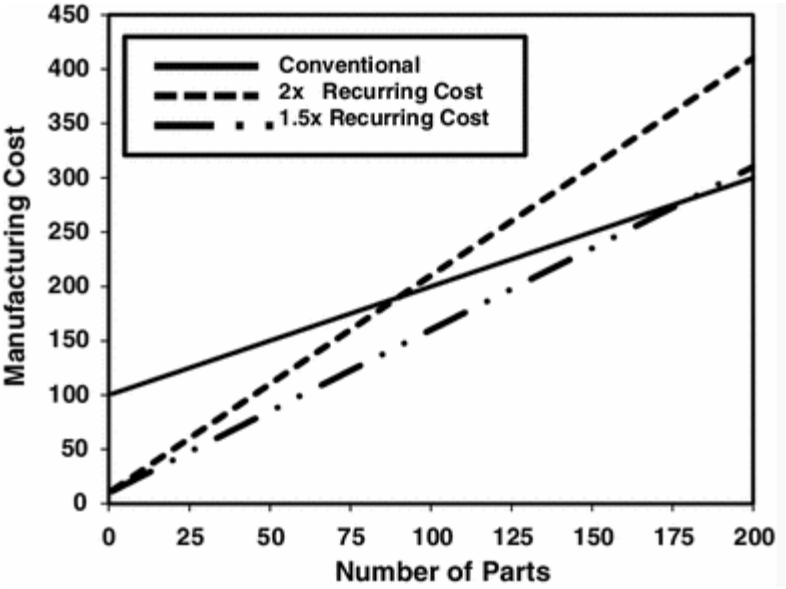

Figure 1 : Comparison between AM costs and conventional methods ones[4]

It is evident that the fixed costs of the Additive Manufacturing process are much lower because of there is no need for molds and models. On the other hand the

recurring costs are 1.5 (or even 2) times higher respect to conventional methods; this is mainly due to the high cost of the powder .

However, thanks to the numerous advantages it can offer , despite of the disadvantages, additive manufacturing has found application in the last years in three main industrial sectors:

- Aerospace industries have a growing interest in AM process because it makes possible the creation of lightweight and high performance products with complex shape such as
  cooling channels, internal honeycomb structures, etc.. Actually lots of components for military aircraft are made with polymer; however the greatest interest is for direct metal fabrication system in order to realize composites, such those based on carbon –titanium, that are useful for aircrafts design .
- Medical industries are particularly interested in additive manufacturing because with this process
  the3D medical imaging data can be converted into solid objects; moreover they can be designed and tailored in order to satisfy
  the needs of an individual patient. Nowadays one of the most used3D print application is linked to the production of dental prostheses [5].
- Automotive industries have been some of the earliest adopters of AM.

  Roll hoops created with additive manufacturing technology have been realized for a number of F1 team. New processes aimed at increasing tensile strength, electrical conductivity, hardness, and impact strength using nanomaterials are under development . It was also created an AM device capable to realize fiber carbon components .Carbon fiber allows to make lightweight auto components like car roofs and windshield frames[6].

While there is already a flourishing industry for making polymer automotive parts only in the last few years famous automotive companies have invested in the production of metal components through AM process[2]

1.2 Additive manufacturing techniques

The first additive manufacturing process, Stereholitography (SLA), was developed by Chuck Hull in 1980: he used monomers in a water suspension that, by using UVs light, polymerized in the desired shape.

Few years later, in 1986 Carl Deckard developed the first SLS machine: he mixed metallic powders together with polymers powders and used a laser beam to consolidate them .
Nowadays additive techniques for the polymeric materials have reached notable results. At the same time, metallic AM development has been considerable since in the last years different firms have subsequently developed these technologies, also thanks to the availability of powerful laser . This has brought to an increase of the materials available for AM.
As reported in literature, available AM techniques for the production of metal parts can be classified based on two parameters:

1. input raw material: metal powder or wires
2. energy source: laser/electron beam or arc

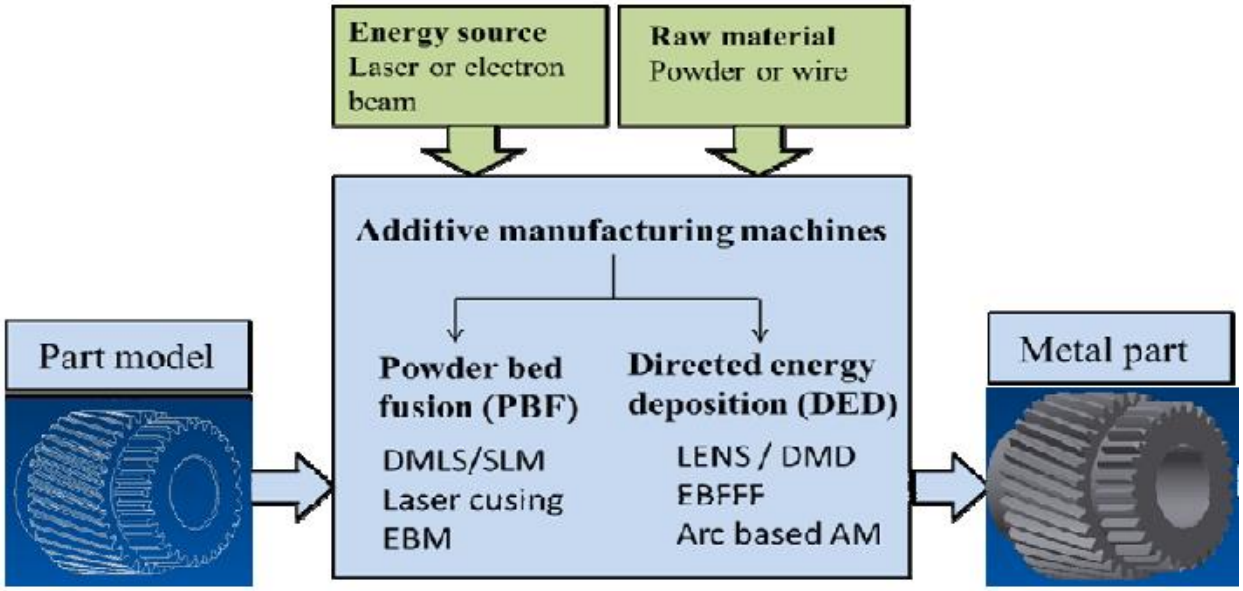

Figure 2 : Common metal additive manufacturing process[7]

Another classification for metallic AM techniques is possible :

- Powder Bed Fusion based technologies (PBF) : powder is spread on the building platform and the powder bed formed is partially or totally fused by thermal energy

-Directed Energy Deposition (DED): materials (powder or wire form) are fused while they are being deposited. Direct Metal Deposition (DMD), Laser Engineered

Net Shaping (LENS), Electron Beam Free Form Fabrication and arc based AM are the most popular DED technologies.

PBF requires more time to build part respect to DED but with PBF process it is possible to obtain better surface finishing and complex components [7]

1.2.1Power Bed Fusion (PBF)

As we said in the previous paragraph , an energy source (Laser or electron beam) is used to melt each layer of the powder bed .After the laser scans one layer , the piston of building chamber goes downward , the piston of the powder chamber goes upward and the laser scans another layer . This cycle is repeated layer by layer in order to realize the component . The building chamber operates in inert atmosphere or partial vacuum in order to avoid the powder's contamination . On the base of the used energy source we can distinguish laser powder bed fusion (LPBF) process, which uses a laser beam to locally melt the powder bed, from EBM (Electron Beam Melting) process that uses a high energy electron beam in high vacuum to melt the powder bed.

In Electron beam melting process the electron beam is generated by a heated tungsten filament that emits electrons at high speed . A magnetic field, a focus coil and a deflection coil control and direct the beam towards the powder bed .

When electrons hit the powder bed they cause its fusion because of their kinetic energy gets converted into thermal energy [9]. The process consist in two steps :

1 Preheating step: the powder layer is pre-heated by high current beam and high scanning speed
2 Melting stage: the powder layer is melted by a low current beam and low scanning speed

The process takes place under high vacuum.

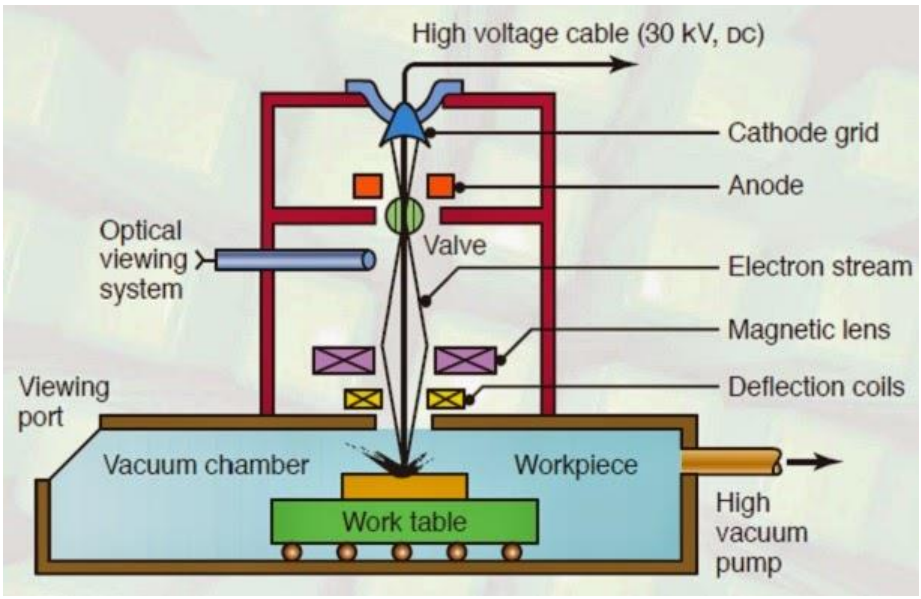

Figure 3 : EBM schematic representation

Laser power bed fusion techniques are divided into three large families:
- Selective laser melting (SLM) also known as Direct metal laser sintering (DMLS)
- Laser melt deposition (LMD)

-Selective Laser Sintering (SLS)

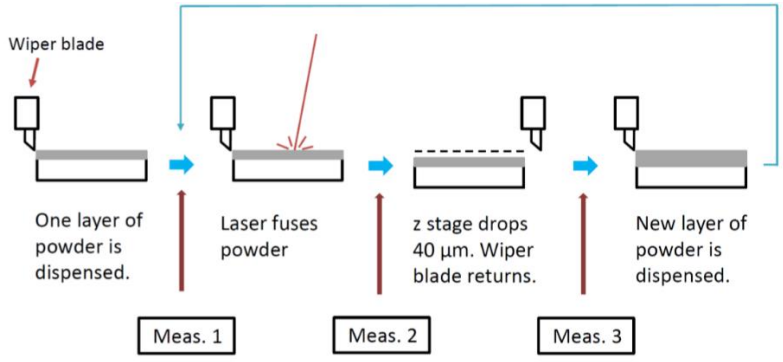

Figure 4: schematic representation of LPBF process [8]

This three families have some common features: a powder bed is wholly or partially fused from one or more sources, the mechanisms of adding the layers of powder and a method to get localized melting are similar but they differ in the way powder is distributed on the building platform , the use of support .

With this processes it is easy to manufacture a lot of metal alloys like aluminum, titanium and cobalt alloys obtaining high density materials.

The process takes place in an inert atmosphere of argon gas for reactive materials and nitrogen gas for non-reactive materials. The main processing parameters are: the power of laser source, the scan speed, the hatch distance between laser tracks and the thickness of powdered layer . In the PBF techniques illustrated previously residual stresses are developed due to rapid heating and cooling , however in EBM the preheating minimize the thermal gradient and eliminates post heat treatment . Preheating also reduces the number of support required in order to hold the powder particles together. Moreover EBM takes place under vacuum so oxidation , contamination and thermal convention phenomena are reduced, while the components realized by LPBF show higher oxygen content. Despite the above mentioned advantages, EBM is not good for large build up volumes , in addition it shows a lower accuracy and a high machine cost [8].

The remainder of this chapter will specifically describe the technique of Selective laser Melting (SLM) while the other techniques will be just mentioned. Giustificalo dicendo che la tua tesi è basata su produzione e caratterizzazione di materiale processato con questa tecnica.

1.2.2Selective laser sintering (SLS)

The SLS (Selective Laser Sintering) technology, invented by Carl Deckard at the University of Texas (Austin) in 1984 , uses a laser for sintering (melt or soften) thermoplastic or metallic powders. The machine rolls out layer after layer of pwder on a board, moving down progressively. Among plastics the most used are polycarbonate, nylon, ABS ,polystyrene PS, polyetheretherketone (PEEK);

moreover metal and ceramic powders can be coated with thermoplastic resins, mixing together and acting as a binder . After the material was being treated in a furnace to remove the polymer , that has a lower melting point than ceramics and metals, the resultant product presents a porosity between 30 and 40%, and others treatments are needed in order to reduce the porosity. Actually the use of SLS is limited to the production of polymers.

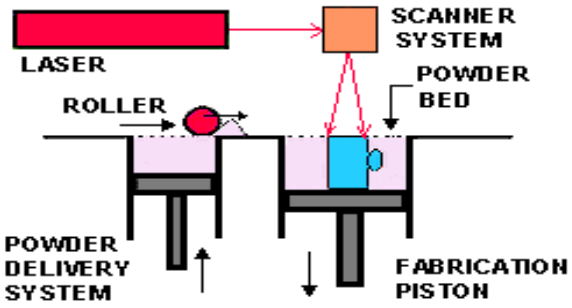

Figure 5: schematic representation of SLM process

SLS techniques use a roller system to form the bed of powder and a CO_2 laser to melt the powder. In order to avoid the degradation of polymers, an inert gas fluxes in the working chamber . The plate can be heated to minimize the laser power required for the merger. The main advantages of this technology are:
-possibility of using different materials
-support structures are not required in the production of parts with undercuts, because of the powder deposited in layers and not sintered act as support. SLS can be utilized to realized aesthetic prototypes with high surface finish and functional object . The prototypes realized with SLS are more resistant and accurate than those obtained using Stereo lithography (SLA), but their finish is much smaller depending on the powder grain size.

1.2.3 Laser melt deposition

Laser Metal Deposition (LMD) is an additive manufacturing technique that can be used to produce functionally graded materials because it can handle different materials at the same time. Laser metal deposition is particularly attractive for the production of aerospace parts because it can greatly increase fly-to-buy ratio [8]

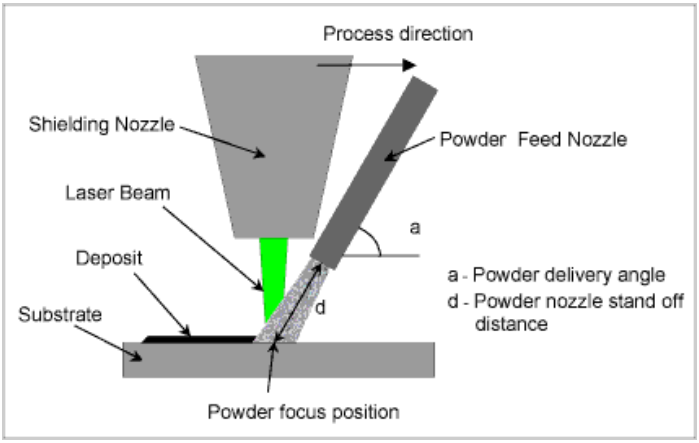

Figure 6: scheme of LMD process

This technology is used both to produce metal components and MMC composites .

Unlike DMLS and SLS methods, powder arrives already fused on the building platform because it is distributed on the substrate through a nozzle ,thanks to a gas flow. The powder is invested and melted by a laser beam before arriving on the building platform. The interaction between the substrate and laser beam creates melt pools . The support is mobile to allow the construction of the piece layer after layer while the laser is maintained in fixed position.

1.2.4 Selective laser melting (SLM)

The SLM process belongs to the class of powder bed fusion technologies ; it allows the creation of components layer-after-layer, through a localized melting of the metallic powder by using a laser and subsequent solidification reached with a quick cooling; the process lets to obtain materials with very fine microstructure and compact grain size. Moreover the mechanical properties result even better than those obtained through more traditional processes since it is possible to use single-phase metallic powders without the addition of organic binders or elements with low melting point. High cooling rates are achieved (103-108 K/s) in the melting pools. In this way, the crystalline grains do not have time to grow and a very fine microstructure is obtained. There is anisotropy of mechanical properties because of the crystals grow along the direction of heat flow. Moreover the reached densities are often close to the theoretical values (99.5-99.8%)[2] .This technique is used to realize metal artifacts, inserts for molds and other objects with complex geometry in a unique fully automated process. In fact the selective laser melting process is generally used for the production of complex geometries and structures with thin walls and hidden voids or channels; their production is generally limited to a low amount of pieces. Advantage can be gained when producing hybrid components. The SLM is able to process different metals and alloys, including stainless steel, nickel-based super alloys or cobalt-based super alloys and light alloys. Among the light alloys the most used are titanium alloys such as Ti6Al4V, and aluminum alloys like AlSi10Mg. EOS, one of the most important producer of AM machines, focuses the attention on aluminum alloys . These aluminum alloy components find many applications in automotive and aeronautic fields[3]

While traditional manufacturing techniques have a relatively high set-up cost, SLM shows a high cost per part (mostly because it is time-intensive), so it is advisable if only very few parts are to be produced. This is the case e.g. of spare parts of old cars (like vintage ones) or individual products like implants.

1.2.5 SLM Process technology

This section provides a brief description of the main steps of the process

Schematically illustrated in Figure 7:

A workpiece is built up from a powder bed. A thin powder layer is distributed over the building area which can be preheated through a powder spreading system called blade for coating .Once the powder layer has been deposited, a direct laser source (controlled by a scanner system) selectively melts the material. The portion of material subjected to the melting caused by the laser beam is greater than the thickness of the layer, generating the melt pools.

When the material solidifies, a melt metallurgic connection between adjacent and subjacent lines is formed. This type of consolidation is very effective in creating well-linked and high-density structures [4]

The building platform is lowered, a new powder layer is delivered and the process starts from the beginning.

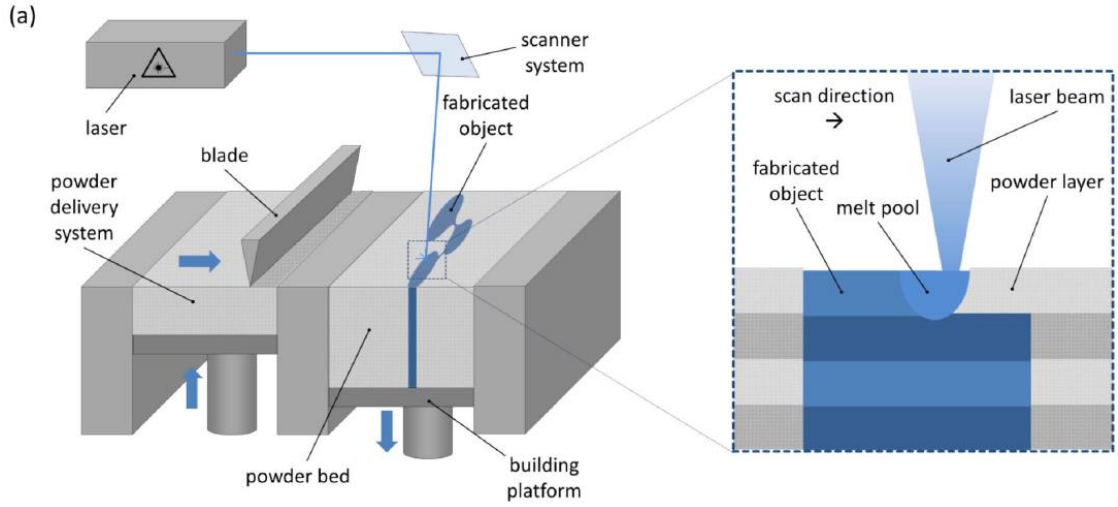

Figure 7: Schematic representation of the SLM process

The microstructural and mechanical properties of the products, are linked to various factors summarized in the table 1. They can be divided into two categories: process parameters and powder properties[9] .

Table 1. Selective Laser Melting (SLM) variables.

Powder Properties	Process Parameters	
Particle shape	Laser power	Layer thickness
Particle size and distribution	Scanning speed	Scanning strategy
Chemical composition	Hatching distance	Building orientation
Thermal conductivity	Protective atmosphere	Gas flow
Melting temperature	Laser beam radius	Bed temperature
Absorptivity/reflectivity	Laser type	-

1.2.6 Effect of the powder proprieties on SLM process

Powder bed properties, including bulk density and thermal properties, affect the final part properties. Powder particle size distribution plays an important role in both the sintering kinetics and the powder bed formation; it directly depends on the powder-processing route: powder production methods, type of feeding stock, process parameters, sieving and classification steps. All these factors influence the powder quality[9]

The particles shape greatly affects the flowability of the powder: the spherical shape is the most suitable one because it allows for good flowability and high density. Particles of spherical shape are easily obtainable through the gas phase atomization process , which allows having particles with a regular shape, necessary to have good fluidity of the powder.
The homogeneity of the powder bed is another issue to be taken into account: thicker regions of the powder bed may lead to insufficient re-melting of the underlying layers causing instability. As observed by Liu et al. [10], a possible direct correlation exists between the powder bed density and the part density: the density of a powder layer with a specific granulation has to be as high as possible. Only in this case the effective layer thickness remains at acceptable values, e.g. about 50µm for a powder layer density of 60% and a machine layer thickness of 30µm.

However, if the powder consists of too many particles, which have to be classified as “coarse” in relation to the effective layer thickness and if fine particles are absent, the density of the resulting single powder layer can be lower than the corresponding density of the powder itself[11] . Layer thickness is also fundamental because of the size of powder influences the physical interaction between powder and the laser beam. Fine powder particles have in fact a high

surface energy which leads to superior densification kinetics while large particles require higher incident laser density to be melted correctly. The thinner the powder layer, the greater degree of interlayer bonding and so the higher the final density can be obtained. However, if a too small value in chosen the speed of manufacturing become too slow. Another fundamental aspect is the chemical composition of the powders. They often have a high degree of contamination, which can be caused by moisture, organics, adsorbed gases and oxide films that are present on the particle surface, due to their high surface area per unit volume: these contaminants not only inhibit the successful densification of the material, but also degrade the mechanical properties of the consolidated products[12]

1.2.7Effect of the process parameters on SLM

Optimal fabrication of parts using SLM requires a comprehensive understanding of the main processing parameters. In SLM, energy input, powder bed properties and build conditions are three leading factors that can affect the parts quality usually evaluated in various ways, including final part density, surface finishing and mechanical properties.

Laser energy density, Eρ, is a key factor that affects the final parts quality in the SLM process and quantify the energy input [13]It is defined by the laser power P (W), the laser scanning speed u (mm/s), and the laser beam diameter δ (mm) according to the equation below

$$E_\rho = \frac{P}{u\delta}\ (J/mm^2)$$

(Equation 1)

Louvis et al [10] attributed the use of high laser power and low scanning speed during the SLM processing of aluminum and its alloy powders to the formation of uncontrollable large melt pool; which causes balling and consequent increase of both the build time and the manufacturing costs of components. This phenomenon can be described as the sphereodization of the liquid melt pool during laser

interaction with the powder bed. In order to mitigate the balling process, they explored the changes that can be made to the SLM of aluminum by reducing the laser power required and increasing the laser scanning rates, while still producing components with a high relative density. They concluded that since it is unlikely that the formation of oxide films can be avoided completely in the SLM process, further research on the SLS/SLM of aluminum should be primarily orientated towards new methods of controlling the oxidation process and disrupting oxide films formed within the components[10]

Scanning strategy, which is the geometrical pattern that the laser beam follows during the hatching to melt and consolidate a section onto a layer, is also a fundamental parameter because influences the porosity and the microstructure of the materials in the SLM process and adopting the correct scanning strategy helps to create final parts that are free from distortions, warping, porosities, and anisotropy .

It is important to say that the machine has different parameters for the core of a part, for its lower and upper surfaces parallel to the building plane and for the lateral outer surfaces called the contour.

Core and skin correspond to 2-dimensional surfaces scanner by the laser source, while the contour corresponds to a 1-dimensional closed-type line. First of all , the contour of the layer structure is exposed to the layer action. Then all of the inner area delimited by the contour is scanned through hatching : the laser beam moves line after line several times and the distance between the line is called hatching distance . Finally, a second exposure of the exterior part contour is carried out to make sure that the part edges correspond exactly to the CAD data.

Regarding the scanning strategy associated to the core and to the skin there are a lot of procedures, but a certain degree of rotation between the layers leads to a better overlapping of these. This should make the properties of the obtained parts more isotropic in comparison with more conventional scanning strategy. The hatch angle (h) defines the raster changing angle between two neighbor layers, as shown in figure (8).

Obviously, it is hard to eliminate the anisotropy of mechanical properties if improper hatch angle is adopted, which would affect the whole performance of the fabricated parts. However, it is ambiguous that hatch angle, whether has defined, can affect the tensile properties. Furthermore, in most SLM researches, the hatch angle of 90°is thought as the best-fit value to get excellent mechanical properties.

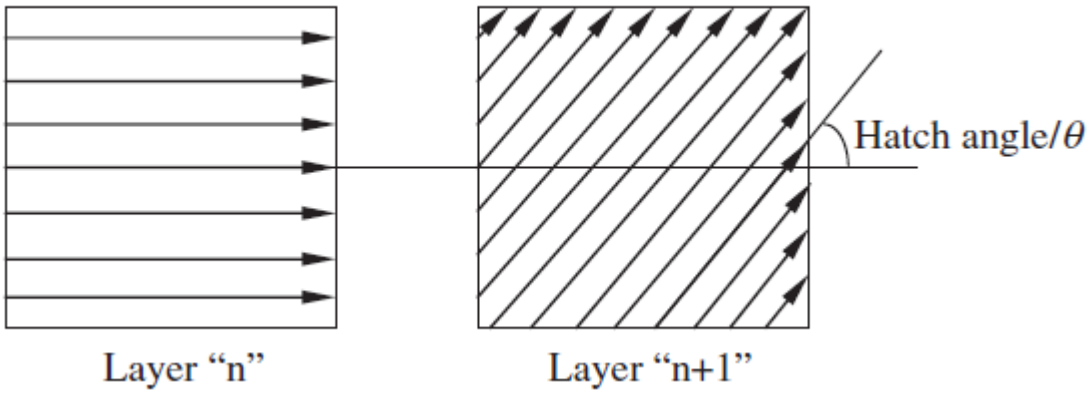

Figure 8 The schematic of hatch angle in raster filling patterns

In this case, the cross section of the sample represents a column structure resulting in the superposition of a large number of vectors in the vertical direction. The contact zones between separate columns are not smooth and have discontinuities and pores. A further increase of the hatch distance results in a strong increase in porosity, the loss of the contact between columns and the lack of the continuous structure[14]

An alternative strategy has been employed to achieve the maximum density of the samples, so-called ‘‘two-zone technique’’: each layer of powder is processed by the laser beam twice. For instance, first a layer of powder is processed with a hatch distance of 120 mm, and then the laser beam passes in between the melted vectors of the same layer thus re-melting no powder but two neighboring melted vectors. The most monolithic structure, compared to the above reviewed ones, is formed with less than 1% porosity.

Another important parameter is the building orientation: ‘‘Z’’ cylinders have their long axis parallel to the build direction; while the long axis is within the XY plane (parallel to the powder spreading plane) for ‘‘XY’’ samples.

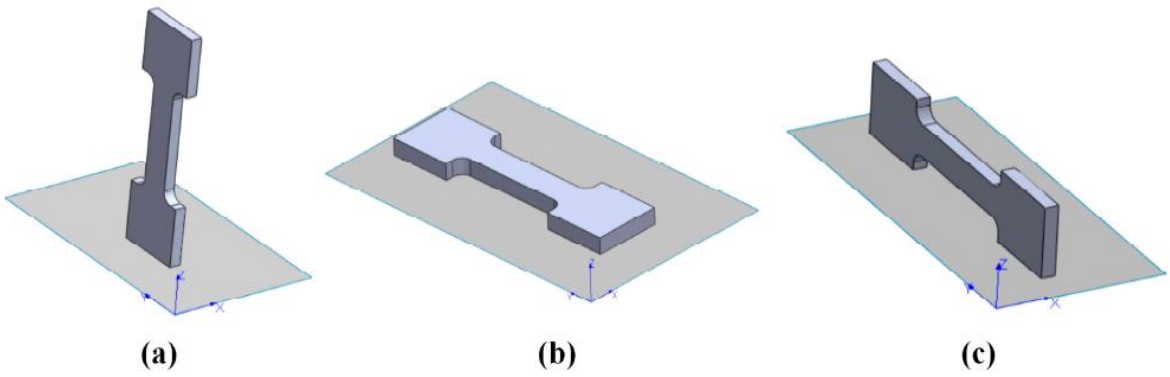

Figure 9: different building orientation a) z plane b) c) xy plane

The orientation can modify the microstructural evolution of the material and can introduce anisotropy and defects. Many studies[15] [have demonstrated that the vertical specimens had a lower elastic modulus than the horizontal ones. The reason for this anisotropy was correlated to the higher number of defects, which were caused by a higher concentration of residual stress and the local heat transfer condition. Based on the heat transfer one has a preferential growth of the grains which, as previously mentioned, brings to a heterogeneous microstructure. The presence of columnar grains, characteristic of some materials obtained by SLM, generates anisotropy in the mechanical response and therefore changes mechanical behavior of the material during the application of stress. For examples, Frazier found[14] that titanium alloys produced by AM show anisotropy in both the microstructure and the mechanical properties; the Z direction shows the lower properties in particular a lower ductility. At least in some cases, directionality narrative was held by melting problems perpendicular to the construction direction. As far as samples of AlSi10Mg are concerned, it has been shown that they also display different mechanical behavior when the orientation changes. The earliest failure for Z-oriented samples is probably related to the micro-residual stress, resulting from the difference in thermal expansion of the aluminum matrix and of the cellular silicon. From other studies[15] conducted on samples of AlSi10Mg, it was found that, after observing the fracture surface, there are large pores near the edge of the sample from which the fracture will begin. These "borderline pores" are formed at the start / end of a scan vector. These borderline pores are more numerous in the specimens grown along the Z direction, compared to the parts produced in the XY direction. When a stress is applied, they causes irregular

deformations. Because of their location near the edge of the sample they easily caused the complete fracture of the samples[16]

The process atmosphere during SLM is another factor able to influence the amount and the type of defects inside the material and therefore the mechanical behavior. Fine metal powders are very sensitive to oxygen, due to their elevated surface areas, and the formation of an oxide layer alters the stability of the melt track during laser scanning, favoring balling phenomenon . Moreover, when reactive powders such as Al and Ti alloys are considered, the O_2 content should always be kept below 0.1% to avoid dangerous reactions[10]

Some studies have been conducted at the University of Western in Australia [17]on AlSi12 samples produced by additive manufacturing under three different process atmospheres: argon, nitrogen and helium. These studies have shown that for all atmospheres, the density of the samples increases as the laser energy density increases until it reaches the theoretical density values. There is no improvement in density by further increasing energy. Excess energy can be detrimental to the surface finish when, as mentioned earlier, it can cause balling.
In all the three atmospheres, the material shows the same behavior and there is no difference in density; however the sample processed in He contains significantly more porosity on the fracture surface than those produced in Ar or N_2. The properties, in particular the ductility of cast Al-Si alloys have a strong correlation with the amount of porosity present on the facture surface.

Although the overall bulk density is similar in all three atmospheres, there is clustering of pores in the samples produced in He. These clusters, therefore, contribute to the reduced ductility of the samples produced in He.

There is no significant difference in the mechanical properties or nitrogen content of the samples processed in Ar or N_2. During conventional sintering, enhanced densification occurred due to the formation of AlN, which takes some time to form. However, during SLM, the material is only molten for very short time and therefore it is unsurprising that AlN does not form [18]

1.2.8 Physical issues affecting the process

In order to optimize the production process it must be taken into account not only the process and the powders parameters but also the physical parameters of the process that can affect the quality of the final product.

1.2.8.1Absorbance

The absorbance is an important aspect of the SLM process as when the laser beam interacts with the bed of powder only part of the radiation is absorbed by the layers of powder while the rest is reflected. The absorption depends on several factors such as the depth of penetration of the radiation, the wavelength of the laser, the powder morphology and packing factor .When powder melting takes place, thermal energy is needed ,and if powder has low absorbance laser power must be optimized . In addition, we must also consider the fact that the absorbance of the powder layers and that of consolidated material is different; in general, the absorbance is higher in powder [16]. Therefore, to resolve this issue you should increase the laser power but this will affect the cost of the process and consequently the cost of the finished product. For these reasons, it is important to use lasers that guarantee a good absorption by the layers of powder.

1.2.8.2 Wettability , thermo- capillarity convention , viscosity

In order to obtain materials with high density by SLM it is necessary to guarantee a good wettability between the molten metal layer and the underlying layer. The wettability depends on the surface tensions of solid-liquid , solid-vapor, liquid-vapor interfaces that determine the contact angle, as can see in the formula below.

$$cos\theta = \frac{\gamma sv - \gamma s}{\gamma lv} \qquad \text{(Equation2)}$$

Considering a solid/liquid system, if the contact angle is $\theta > 90°$ the system is wettable, while if $\theta < 90°$ the system is not wettable.

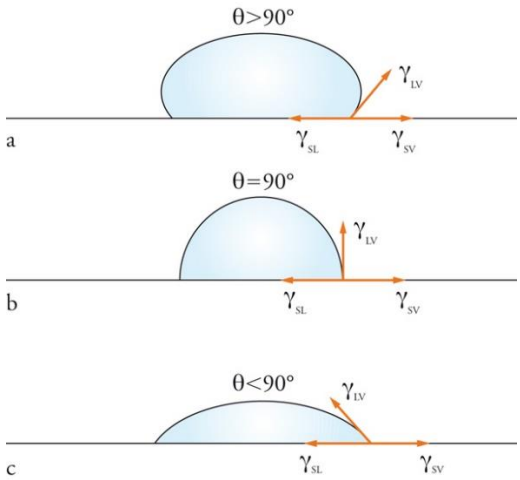

Figure10: solid-liquid system wettability

The presence of metal oxide layers decreases the wettability of the solid-liquid system, forming spherical deposits that prevent the uniform deposition of the subsequent layers of powder, thus causing an increase in porosity. Precisely to avoid this, the working chamber is protected by inert gases. Moreover, in order to have dense materials it is important to control the viscosity of the melted powder which can lead to the formation of metallic aggregates. Viscosity can be reduced by increasing temperature. Another effect to consider is the Marangoni one, also known as thermo-capillary convection flow, which is due to the viscosity and the presence of stress gradients in the melt pools . Generally the temperature of the melt pool reaches a maximum in its center and a minimum in the borders and for these reason there is a stress gradient. This effect can be evidenced by observing a section of the alloy under an optical microscope: it can be noted that the melting wells have an elongated shape due to the fact that the metal melt is pushed to the sides due to a thermal gradient from the warmer central areas to the zones colder sides.

The kind of Marangoni flow has indeed a great influence on the consolidation process and on the shape of the melt pool: an outward flow generally produces wide melt pools and enhances the consolidation while an inward flow produces deep and thin melt pools [19]

1.3Powder production methods

The spherical particle shape is one of the main requirement of metal powders used in additive manufacturing in order to obtain reliable and repeatable results .

Particles of spherical shape partially minimize the physical problems of the process mentioned above. The technologies of production of metal powders are divided into chemical-physical methods and mechanical methods. In physical methods, changes in the chemical composition and in the structure of the final product are obtained. The mechanical methods use high pressure or various types of milling process [20]

Atomization is the most widespread technology for the mass production of metal powders for additive manufacturing. The main principle of all atomization technologies is a disintegration (dispersion) of a thin stream of molten metal by subjecting it to impact of gas, high pressure of water, plasma, rotating forces etc. During this impact, molten metal is divided on small droplets, which rapidly crystallize in flight before they reach atomizer walls

There are different atomization methods:

Water atomization: it uses high pressure of water, steam as atomizing medium. The water atomization is used mostly for the production of powders of unreactive materials such as steels. Due to higher cooling

rate particles have irregular shapes. The main advantage of water atomization

consists in the fact that it is less expensive than the other types of atomization; the main disadvantage is the limitations of purity, especially for metals and alloys inclined to oxidation.

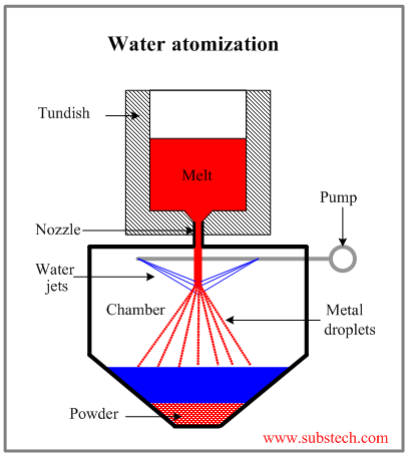

Figure11: schematic representation of water atomization process

- **Plasma atomization**: plasma atomization (PA) has been developed to produce fine and spherical powders. Unlike conventional high-pressure

atomizers, PA utilizes multiple arc plasmas to accelerate the gas atomization. In this process, metal wires are fed into the apex of the multiple plasmas, where they melt and are atomized in a single step.

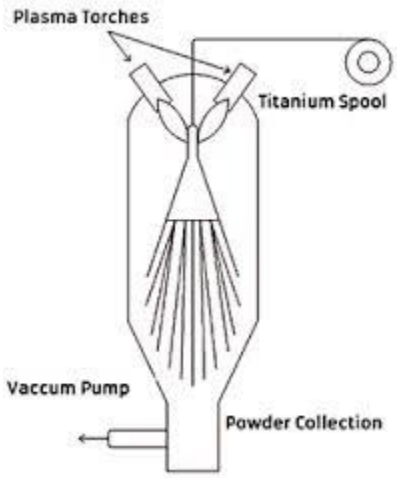

Figure 12 : schematic representation of plasma atomization process

This process offers the unique ability to produce spherical powders of reactive metals with a typical average particle size of 40 μm[21].

- **Centrifugal atomization**: In centrifugal atomization, a nozzle introduces fluid in a spinning cup. The nozzle moves radially away from the spinning cup and the centrifugal force moves the liquid on the edge of the disc out off the edge. The liquid breaks into fine droplets. Figure 13 shows the centrifugal atomization mechanism.

  The energy source of centrifugal atomization is the centrifugal force. With the same rotational speed at low flow rates, the droplets form closer to the edge of the disc compared with higher flow rates. With rotary atomization, operators can control both the scope and the speed of the disk independently of each other. In most applications, electrostatic charge is applied to spray to draw droplets to a target object.

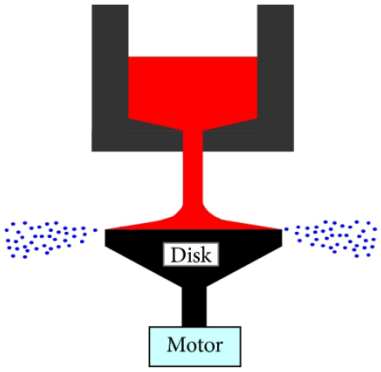

Figure 13 : schematic representation of centrifugal atomization

An example is the REP process: an electrode material in the form of a road electrode is rotated rapidly while being melted at one end by an electric arc. Molten metal spins off the bar and solidified before hitting the walls of a container filled with an inert gas. The anode rotation control as well as centrifugal forces and surface tension of metallic particles are important to have a certain particles size. Powder obtained with this technique are suitable for processes where the consolidation is done through isostatic pressing or through high temperatures [20] .

- **Gas atomization:** it is the main process for the production of metal powders for additive manufacturing. The process consists on melting, atomizing, and solidifying the respective metals and alloys. In the gas atomizers, there is a furnace for melting metals under vacuum or rarely under protective atmosphere The molten metal is atomized thanks to an inert high pressure gas; the droplets solidify during the flight in the atomizing chamber.

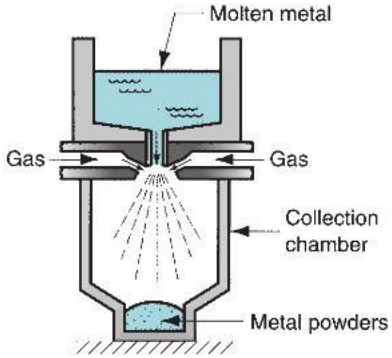

Figure 14: schematic representation of gas atomization process

Powders obtained by gas atomization process usually have a spherical or near to spherical shape and a proper particle size to be used in additive technologies. It should be noted that particle size distribution has a strong dependence on the type

of atomized alloy and used system. Powders produced by gas atomization have a spherical shape, high cleanliness, fine and homogeneous microstructure thanks to rapid solidification.

1.3.1Materials for Metal Additive Manufacturing

The growing interest in additive manufacturing techniques for metallic materials, as previously mentioned, resulted in recent years in an increase of processable materials. Following are reported some of the materials most used by EOS GmbH Electro Optical Systems for the production of components in different industrial sectors [22]

- **Ti6Al4V**: this well-known light alloy is characterized by having excellent mechanical properties and corrosion resistance combined with low specific weight and high specific strength. It also has very good bio adhesion (cell growth tested with good results).

Main applications:

- Functional prototypes
- Series-production parts
- Aerospace
- Motorsports
- Biomedical Implants
-

- **Stainless-steel 316L**: it is characterized by a high ductility and corrosion resistance. Meets the requirements of the ASTM F138 norm ("Standard Specification for Wrought 18Cr-14Ni-2.5Mo Stainless Steel Bar and Wire for Surgical Implants, UNS S31673") .The manufactured parts can be further processed or polished.

Applications

- Automotive
- Aerospace for the manufacture of mounting parts
- Food and chemical plants
- Medical filed for surgical aids, endoscopic surgery and orthopedics

-Nickel Alloy IN625: Nickel chromium super-alloys like Inconel 718 and Inconel 625 are used to produce strong corrosion-resistant metal parts. These alloys are often used in high-stress, high-temperature aeronautical, petrochemical and auto racing environments. This material is also suitable for building complex parts for high-temperature and high-strength applications. The process achieves material properties that are comparable to wrought alloys and by far exceeds those of casting. Inconel 718 performs at temperatures as low as minus 218 °C and as high as 705 °C .

The high mechanical properties are due to the use of significant amounts of nickel, chromium and molybdenum in the alloy. It resists pitting and cracking when exposed to chlorides. As a result, Inconel 625 is frequently used in metal parts adopted in marine applications. Due in part to its high resistance to both alkalis and acids, Inconel 625 is also used in components used in oil and gas production. It also resists oxidation at extremely high temperature.

Applications

- Functional prototypes
- Series-production parts
- Aerospace
- Motorsport
- Industry (e.g. high-temperature turbine components)

-Cobalt Chrome: This class of super alloys is characterized by having excellent mechanical properties (strength, hardness etc.), corrosion resistance and temperature resistance; its mechanical properties improve with the increasing of temperature up to 500-600°C. They play an important role in the performance of aero- and land-based gas turbines. While nickel alloys predominate in the hot sections of modern aero turbine engines, cobalt alloys are used in particularly demanding applications such as fuel nozzles and vanes for industrial gas turbines.

Applications

- Functional prototypes
- Series-production parts
- Mechanical high-temperature engineering applications such as in aero engines.

- Biomedical Applications such as dental and medical implants

- **AlSi10Mg**: is a typical casting alloy with good casting properties; it is typically used for cast parts with thin walls and complex geometry. It offers good strength, hardness and dynamic properties and is therefore used for parts subject to high loads.

Applications

- Functional prototypes
- Series-production parts
- Motorsports
- Automotive/Series Production Vehicle

1.3.2AlSi10 Mg alloy

The Al–Si system is a binary eutectic system, showing an eutectic at 577°C containing about 12% Si . Al-Si alloys are defined as eutectic when the content of Si is in the range from 11 to 13 wt %, as hypoeutectic when the Si is less than 11 wt % and as hypereutectic when the Si exceeds13 wt %[23]

AlSi10Mg alloy is a hypoeutectic alloy as the content of Si is in the range 9-11% (see figure 15).

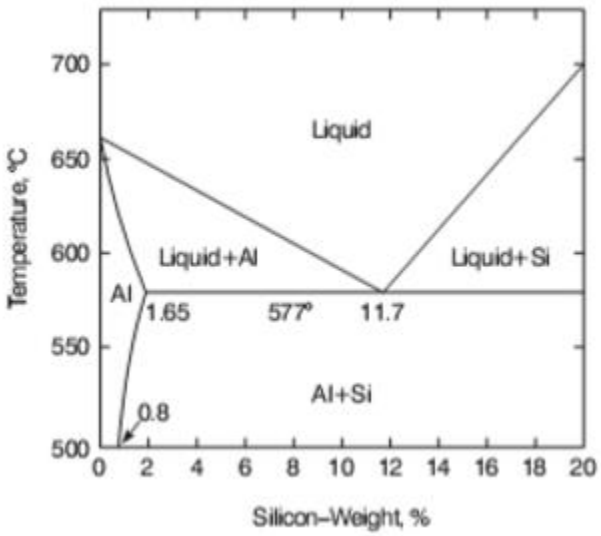

Figure15: state diagram Al-Si

This alloy has a chemical composition characterized by the presence of mainly Al and Si; other minor elements are reported in table 2

Element	Min	Max
Al	Balance	
Si	9.0	11.0
Fe	---	0.55
Cu	---	0.05
Mn	---	0.45
Mg	0.25	0.45
Ni	---	0.05
Zn	---	0.10
Pb	---	0.05
Sn	---	0.05
Ti	---	0.15

Table 2: chemical composition of EOS AlSi10Mg [22]

The presence of magnesium in the Al-Si alloy enables the precipitation of Mg_2Si which enhances the ductility and strengthen the matrix to a significant extent without compromising the other mechanical properties[24]

Sound cast ability, good weldability and excellent corrosion resistance characterize aluminum-silicon alloys. Moreover, thanks to their attractive combination of mechanical properties, high thermal conductivity and low weight, Al-Si alloys are used in a large number of applications such as automotive, aerospace and molding industries [23]

1.3.3 Problems and advantages related to the use of aluminum alloys like AlSi10Mg for SLM process

The use of aluminum powder for SLM presents various problems if compared to other SLM candidate materials (Table 3) ; the high thermal conductivity of aluminum-based powders and a reflectivity greater than 91% in UV and IR regions make necessary the use of a high laser power for melting and to overcome the rapid heat dissipation [k]. In addition, one of the biggest problem associated with the production of aluminum alloys is the porosity; in fact, because of aluminum tendency to oxidize, the formed oxide layer can compromise the powder wettability and increase the porosity.
Moreover the aluminum powder shows low flowability which does not allow falling below certain thickness layer of powder [25].

SLM candidate material	Thermal conductivity (W/mk)	Flow ability (s/50gm)	Reflectivity (%)
Stainless Steel 316L	21,4	14,6	60
Ti6Al4V	6,7	47	53-59
AlSi10Mg	146	No flow	91

Table 3: proprieties of different alloys for SLM

However during the last years various studies have demonstrated that it's possible to decrease the porosity down to the value of 1%.

According to the American classification (ASTM)AlSi10Mg alloy can be approximated to an A360 alloy as is shown in the Table 4[18]

LEGA	Si%	Fe%	Cu%	Mn%	Mg%	Ni%	Zn%	Pb%	Ti%	Sn%
A360 [9]	9,0-11	≤ 0,55	≤ 0,05	≤0,45	0,2-0,45	≤ 0,05	≤0,010	≤0,05	≤0,15	≤0,05
AlSi10Mg [12]	10,0-13,0	0,6	0,20	0,3-0,7	0,2-0,6	0,1	0,1	0,1	0,2	0,05

Table 4 : AlSi10 Mg and A360 chemical composition

The production of AlSi10Mg samples by DMLS allows to obtain breaking load values (UTS) higher than those measured for a standard A360-T6 alloy; morover other mechanical properties of AlSi10Mg are similar to that of a T6 sample . Therefore DMLS process allows to obtain good mechanical proprieties with a single step, saving time and money. The high performance is due to the high heating / cooling speeds, which allow to obtain a very fine microcrystalline structure .Thanks to its extremely high flexibility, SLM process is used in many fields of application : orthopedics , dental industries, rapid prototyping and tooling. DMLS technology also finds unexpected applications in aerospace and automotive industry [26] .

1.3.4Aluminum alloys in automotive

Aluminum (Al) is a non-ferrous metal that stands out for its lightness, ductility, good electrical and thermal conductivity and relatively low melting temperature. The mechanical properties of pure aluminum are quite poor, but the addition of a small amount of alloying elements (such as copper, silicon or magnesium) can strongly enhance its mechanical behavior preserving the advantage of its lightness. Aluminum also shows good corrosion resistance due to the fact that, when it is exposed to air, it is covered with an alumina layer protecting the bulk material from any further oxidation and corrosion too. Its face-centered cubic crystal structure, similar to that of iron, ensures an excellent ductility even at low temperatures. Thanks to these characteristics, aluminum alloys are used for aeronautical constructions and in the automotive field. For good road holding, it is important to reduce the weight of the wheels and all the elements connected to them. Even if the use of aluminum in the automotive field has been limited by cost reasons, it was already used since the birth of automobile history , when the production was still at the craft level. The first application of Al alloys was in 1897 for the crankcase of the Clark engine, a three-wheeled car. Aluminum is lighter than steel generally used for the production of the rims, and allow to better absorb bumps in the road.

Nowadays aluminum is mainly used in many car components:

- operating groups: engine head, intake manifolds, gearbox, alternator casing and starter motor cups, oil pan
- in the chassis: wheels rims, steering box, side protection bars;
- in the cooling system: radiator, water pump and fittings for sleeves;
- In the components of the air conditioner: condenser, evaporator, compressor casing.

2.0 Materials and Methods

2.1 AlSi10Mg powder

An $AlSi_{10}Mg$ powder provided by EOS was used in this thesis; its nominal chemical composition is shown in table 4 .

Si	Mg	Fe	Cu	Mn	Fe	Zn	Ti	Sn	Pb	Al
9,0-11,0	0,2-0,45	≤0,55	≤0,05	≤0,45	≤0,55	≤0,10	≤0,15	≤0,05	≤0,05	Balance

Table 4: Nominal chemical composition (wt %) of $AlSi_{10}Mg$ powder

$AlSi_{10}Mg$ powder was produced by gas atomization. Among the different manufacturing processes which are available for the production of AM powders, gas atomization is generally used for Al ones. Since Al shows the tendency to oxidize , the use of an inert gas as atomizing media allows to reduce the risk of oxidation and contamination of the metal. The formation of oxidized layers on the surface of the drops resulting from the melting process is believed to reduce their tendency to spheroidize and because of a local modification of the surface tension[15]

2.2 EOS M290

All the AlSi10Mg samples were produced by using EOS M290 system that realizes metallic components directly from CAD data . A Yb laser beam with a nominal power of 400W allowed for the realization of dense component by melting layer-by-layer the metallic powder .

Technical data EOS M 290	
Building volume	250 mm x 250 mm x 325 mm (9.85 x 9.85 x 12.8 in)
Laser type	Yb fibre laser; 400 W
Precision optics	F-theta lens; high-speed scanner
Scanning speed	up to 7.0 m/s (23 ft./sec)
Focus diameter	100 µm (0.004 in)
Power supply	32 A / 400 V
Power consumption	max. 8,5 kW / average 2,4 kW / with platform heating up to 3,2 kW
Inert gas supply	7,000 hPa; 20 m³/h (102 psi; 706 ft³/h)
Dimensions (W x D x H)	
System	2,500 mm x 1,300 mm x 2,190 mm (98.4 x 51.2 x 86.2 in)
Recommended installation space	min. 4,800 mm x 3,600 mm x 2,900 mm (189 x 142 x 114
Weight	in)approx. 1,250 kg (2,756 lb)

Figure 16 : EOS M290 [27] system and its technical data

EOS M290 system is constituted by :

- Process room : it is thermally insulated, contains a protective inert gas and uses sensors in order to control the amount of oxygen. Blowing nozzles create a continuous flow of inert gas which allows the elimination of the secondary components which could disturb the process. Subsequently, the inert gas is sucked by a nozzle and then filtered.
- Building platform : it moves along the z axis and the component is built on it.
- Elevator system: which is constituted by a constructive system (after exposure to the laser beam, it lowers the platform of one layer thickness) and a dosing system (it transports the powders necessary for the building process)
- Overflow system : it allows to collect metallic powder in excess
- Recoater : it uniformly spreads the powder before the laser beam scan
- Scanner : it guides the laser beam towards the metal powders using two mirrors. Scanner is necessary in order to have high construction precision of the pieces.
- Laser : it has a wavelength of 960-980 nm that leads to a good absorption of laser energy from the metals. The optical fibers coming from the laser end with a collimator that is fixed to the expansion optics in order to give shape to the laser beam[27]

The creation of a component takes place through a cyclical process repeating layer by layer the various procedural steps. The building platform is constituted by a heating system that minimizes the laser power necessary for melting the powder. This heating system also reduces the thermal gradient between the already solidified area and the molted zone, thus reducing the residual stresses that could lead to crack formation. In the first step the powder is spread over the building platform. A laser beam totally melts a precise area of the powder according to the CAD model of the component. Below the first layer a mechanical connection is created between the powders and the platform. The piece is fixed to the platform directly or through supports. Subsequently the platform is lowered by a height equal to the thickness of the powder layer, a second layer of powder is then deposited and melted .

Different scanning strategy can be used in DMLS systems as reported in Figure 17 . For this thesis a scanning strategy involving the rotation of the scanning direction of 67° was adopted for all the samples.

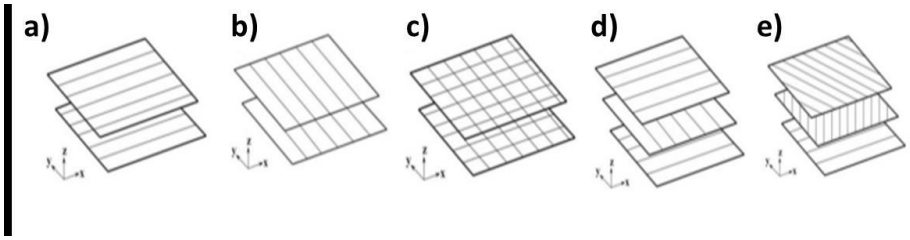

Figure 17: Different scanning strategies.

This process is repeated until the component is created. Once the process is finished, the process room is opened , the powder in excess is removed and then sieved in order to be collected and reused. Once the powder is removed from the platform, a stress relieving treatment is carried out, treating the piece in an oven at a certain temperature and for a certain time. The used thermal cycle depends on the type of alloy or composite produced. Finally the piece is removed and can be polished.

Eos M290 process parameters used for the production of samples in this thesis work are shown in figure 18

	DIRECT PART		POSTCONTOURS		
	COLD	200 °C	COLD	200 °C	
DISTANCE	0,19	0,19			mm
SPEED	1300	1300	900	900	mm/s
POWER	370	370	80	80	W
BEAM OFFSET	0,02	0,02	0,02	0,02	mm
HATCHING	X	X			ROTATED
STRIPE WIDTH	7	7			mm
STRIPES OVERLAP	0,02	0,02			mm
LAYER	0,03	0,03	0,03	0,03 or 0,06	mm
TEMP. ON PLATFORM	50	200	50	200	°C

Figure18 : Eos M290 process parameters

2.3 Characterization methods

In the SLM process a fundamental role is played by the properties of the starting powder because they affect the mechanical properties of the final products in addition to their compositional and microstructural characteristics. In this thesis the starting AlSi10Mg powder was investigated in term of flowability and tapped density; the particle size distribution and particles shape distribution were also investigated .

Different kinds of samples were produced at the prototypes experimental construction department (CS) of FCA. Four different jobs were realized in order to analyze the structural and mechanical properties of the samples. The following figures (fig. 20, 21 and 22) show the main geometries of the samples produced in the jobs from 1 to 4 . The fourth job involved the preparation of the specimens that were submitted to the Charpy tests.

- Cubic and parallelepiped samples were built along Z axes; they were subjected to hardness tests, x-ray analysis , optical microscope examination and density measurements.
  Cubic : 1x1 cm
  Parallelepiped : 2,65x1,4 cm

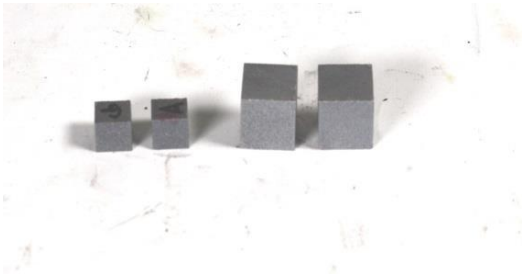

Figure 20: cubic and parallelepiped samples

- Cilyndrical samples growth according to different building orientations (in the XY plane or Z axes) were used for tensile test and their fracture surfaces were analyzed by SEM

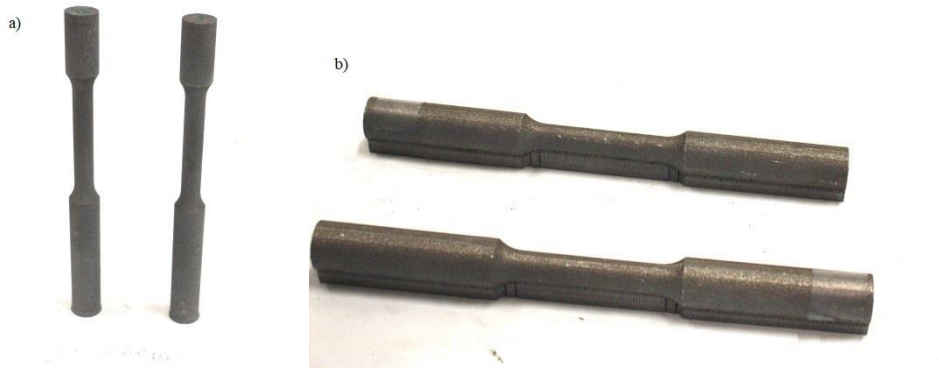

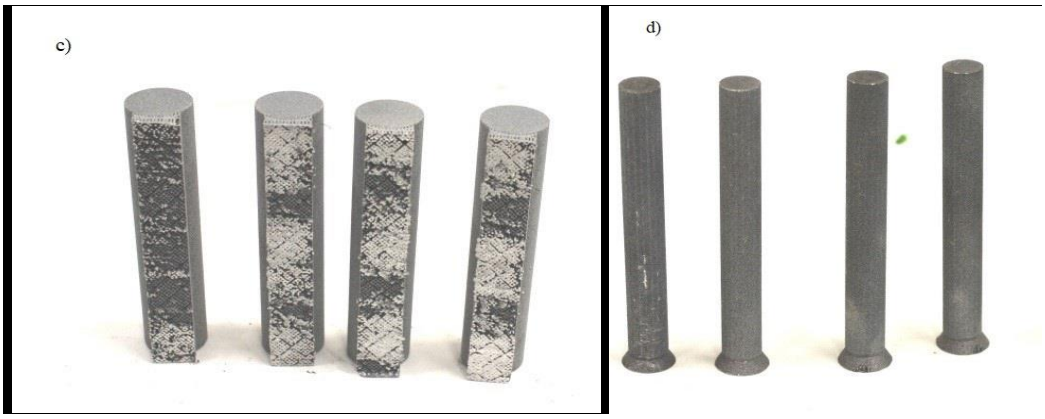

Figure 21: main samples geometries a), d) samples with building orientation along z-axes , b), c) samples with building orientation in x-y plane

-Charpy test samples(55mm x 10mm) realized along different building orientations (Z and XY)

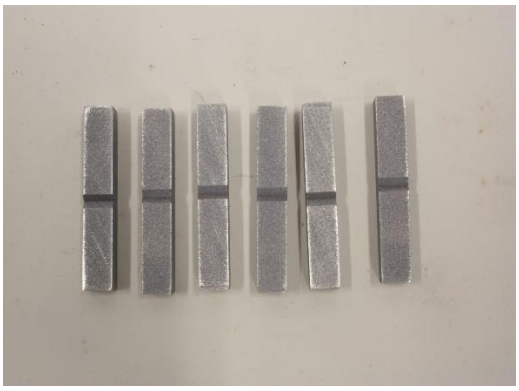

Figure 22: charpy test samples

Some specimens were subjected to a stress relieving treatment for 2h at 300 ° C and then slowly cooled in air inside the furnace. The used thermal cycle is recommended by EOS in order to eliminate residual stresses[27]. AlSi10Mg casting alloy components are generally heat treated to improve the mechanical

properties (for example according to T6 heat treatment). The laser sintering process is characterized by quick melting and solidification; this produces as-cast samples showing mechanical properties similar to T6 heat-treated cast components. For this reason a hardening treatment is not recommended for AM processed materials, but preferentially a stress relieving cycle.

2.3.*1.* ***Flowability***

Flowability is the ability of granular powder to flow and it depends on various factors : the properties of the powders such as their shape, morphology and particle size distribution, the environmental conditions, the equipment used for handling and the storage conditions.

Very fine powder (less than 10 μm) generally has poor flowability or does not flow at all. The general principle of flowability assessment is to measure the time that 50g of powder takes to flow inside a 2.5mm diameter orifice under the action of their own weight.

If the powder has a high density, it will flow faster. The spherical powder flows better than the irregularly shaped one, because of particles do not cling each other.The humidity of the powder has a negative effect as it causes particles agglomeration and therefore decreases their smoothness [28]

2.3.2 ***Tapped Density***

The tapped density is an increased bulk density attained after mechanically tapping a container containing the powder sample.

The tapped density is obtained by mechanically tapping a graduated measuring cylinder or vessel containing the powder sample. After observing the initial powder volume or mass, the measuring cylinder or vessel is mechanically tapped, and volume or mass readings are taken until little further volume or mass change is observed. The mechanical tapping is achieved by raising the cylinder or vessel and allowing it to drop, under its own mass, a specified distance of dropping should be

adopted for the three methods as described below. Devices that rotate the cylinder or vessel during tapping may be preferred to minimize any possible separation of the mass during tapping down.

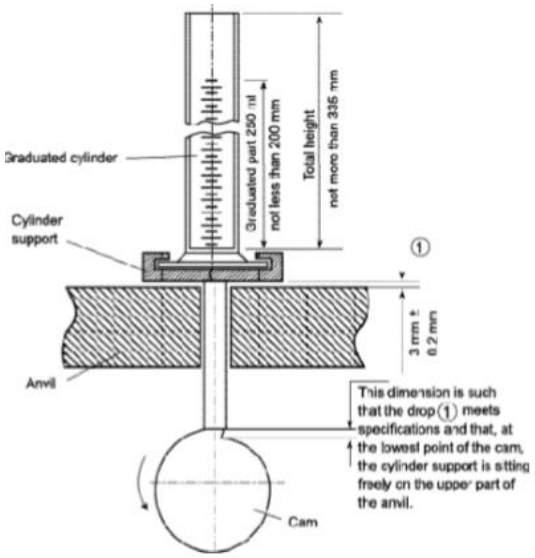

Figure 23 : tapping system

The tap density was measured in Polytechnic of Turin laboratory by using a cylindrical steel vessel; the tapping system is illustrated in the figure 23. The cylinder is filled with powder until is completely full. Then the excess of the powder is carefully removed from the top of the vessel by moving the blade of a spatula perpendicular to the top vessel surface [25] .

Subsequently the amount of powder present is measured, after calibrating the balance with the weight of the cylinder, and the vessel is put on the tapping system.

The mechanical tapping is achieved by raising and dropping the cylinder, thus allowing the powder to drop under its own weight lowering its level on the cylinder .The cylindrical container is filled with additional powder, a second weighing is carried out and the process is repeated until the powder is completely compacted.

Tapped density (g/mL) is calculated using the following equation:

$$\text{Tap density} = \frac{MF}{100} \quad \text{(Equation 4)}$$

where MF is the mass of powder in the measuring vessel.

It's also possible to calculate the Compressibility index (CI) and the Hausner ration (HR) that gives a sort of evaluation of powder to be compressed .

$$CI = \frac{bulk\ density - tap\ density}{bulck\ density})*100 \quad \text{(Equation 5)}$$

$$HR = (\frac{tap\ density}{bulck\ density}) \quad \text{(Equation 6)}$$

Where bulk density is defined as the mass of material's particles divided by the total volume they occupy. The total volume includes particle volume, inter-particle void volume, and internal pore volume. Tapped density is the value obtained applying the Equation 4

The compressibility index and Hausner ratio are measures of the powder ability to settle, and permit an assessment of the relative importance of inter -particular interactions. In a free-flowing powder these interactions are less significant and the bulk and tapped densities will be closer in value. For poorly flowing materials, there are greater inter-particle interactions and a greater difference between the bulk and tapped densities will be observed. The differences are reflected in the compressibility index and Hausner ratio.

Flow Character	Hausner Ratio	CI (%)
Excellent/very free flow	1.00-1.11	≤10
Good/free flow	1.12-1.18	11-15
Fair	1.19-1.25	16-20
Passable	1.26-1.34	21-25
Poor/cohesive	1.35-1.45	26-31
Very Poor/very cohesive	1.46-1.59	32-37
Very, very poor/ approx. non-flow	>1.60	>38

Figure 24 : determination flow character through Hausner ratio e compress index

Metti una tabella vera, non uno screenshot

2.3.3 *Particle size distribution*

Samples mechanical and microstructural characteristics are influenced by the properties of the metallic powder used . Depending on the size of the particles, various interactions with the laser can occur, which will consequently influence the efficiency of the powders fusion . Particle size distribution of AlSi10Mg powder has been analyzed at the Polytechnic of Turin using LASER PARTICLE SIZER ANALYSETTE 22 NANOTEC. The measurement was carried out after wet dispersion . An optimally dispersed sample is a basic prerequisite for reliable determination of the particle size distribution . After selecting the method of analysis and introducing the amount of powder required by the instrument the analysis will start automatically when the correct quantity of powder has been reached.

i

FGURE 25: ANALYSETTE 22 Nanotec

ANALYSETTE 22 Nanotec has a measuring range of 0.01 - 2000 μm and offers extraordinary sensitivity even for nanoparticles.

The particle size measurement is based on the diffraction of a laser beam focused on the sample. The deviation of the trajectory of the light waves creates a

characteristic diffraction pattern consisting on a series of concentric rings, detected by an analyzer , whose intensity depends on the interference between the different waves diffused by each particle .The particle size is calculated based on the distance between the rings of diffraction: large particles generate very close rings; small particles produce more spaced rings. When the light illuminates a particle the weakening of the incident ray is essentially due to absorption. During absorption, each particle collects a portion of the electromagnetic energy converting it into heat . Mie theory is the complete solution of the Maxwell equations for the scattering of electromagnetic waves by spherical particles and it can be used to analyze the intensity of particles distributions even for very small particles. It is necessary to know the index of refraction and the absorption coefficient of the powder . Through the FRITSCH software, that includes a complete database containing the refractive index values of many materials ,it is possible to determine the distribution of the particles. [29]

2.3.4 Density and porosity

Some of mechanical properties such as fatigue resistance and tensile strength are influenced by porosity so it is important to minimize it by optimizing the process. Cubic samples resulting from additive manufacturing were firstly mechanically polished in order to remove the surface roughness. Density measurements were performed on cubic and parallelepiped samples using the Archimedes' balance based on Archimede 's principle; their porosity was also evaluated. ,

The balance consists of two plates : one is immersed in the liquid and on it the weight of the immersed sample (Wwet) is obtained; the second one is not immersed and on it the weight of the sample in air(Wair) is measured .

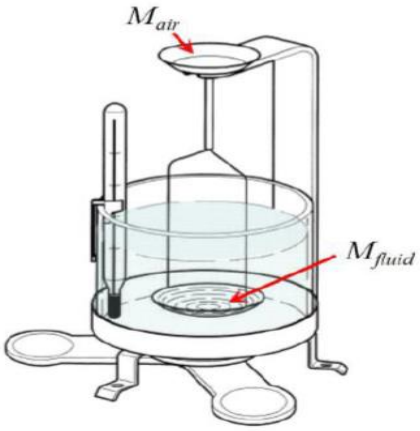

Figure 26 : Archimede's balance

When the sample is immersed the open porosity is filled with liquid and the volume of liquid displaced (V_d) by the immersion is equal to the sum of the filled volume (V_{filled}) and the volume of the closed pores (V_{ch}) as is shown by the formula

$V_d = V_{filled} + V_{ch}$ (Equation 6)

Subsequently, the sample is dried in order to eliminate the surface water and allowing only the water inside the open pores to remain. Calculating the dried sample weight it is possible to determine the geometric density by the formula were ρfl is the fluid density (distilled water was used)

$$\rho = \frac{\rho fl * Wair}{Wdried - Wwet} \quad \text{(Equation 7)}$$

Porosity (P) is given by the formula :

$$P = \left(\frac{Vpore}{Vfilled + Vpore}\right) \quad \text{(Equation 8)}$$

V_{pore}: is the volume occupied by the pores

V_{filled}: is the volume occupied by the material

The porosity was then evaluated by comparison with the theoretical density (TD) of the

material.

Porosity can be divided in three types :

- Open porosity : pores accessible from the outside with a volume V (op)
- Close porosity : pores inside the material not accessible from the outside with a volume V_{ch}
-

Total porosity (Pt) is the sum of the two and it is given by the formula

$$Pt = \frac{Vch+Vop}{Vfilled+Vop+Vch} \qquad \text{(Equation 9)}$$

Porosity and density are related by the formula :

$$Po = \frac{dapp-dgeo}{dapp} \text{ Equation 10}$$

$$Pc = dgeo\left(\frac{1}{dapp} - \frac{1}{dth}\right) \qquad \text{(Equation 11)}$$

Suppongo che P_A sia la porosità aperta (meglio chiamarla P_o) e P_c la porosità chiusa.

Comunque bisogna dire cosa sono P_O e P_c.

$$Pt = (\frac{dth-dgeo}{dth}) \qquad \text{(Equation 13)}$$

The geometric density and apparent density can be determined by Archimedes principles After obtaining the density, in this way, the value of porosity can be derived indirectly from the bulk density .

It is necessary to follow certain precautions because this technique is subject to different sources of error; for example it can remain humidity inside the sample that influences the weighing in air as it involves an increase in weight . Regarding the weigh in water is necessary to leave the samples soaked for a period of time

sufficient to allow the porosity to be filled totally. If there are air bubbles on the surface, the measurement must be repeated.
On the contrary the drying of the sample, must be fast, so that the water present in the pores is not absorbed. Various measurements have been performed on the samples in order to be able to average the values obtained and minimize errors.

2.3.5. X- ray diffraction

2.3.5.1 Identification of crystalline phases

The X-ray diffraction (XRD) is a non-destructive analytical technique used for the identification and quantification of the crystalline phases present in a polycrystalline material; moreover it provides information about the crystallographic structure of them.

X-rays are generated by a cathode ray tube,filtered to produce a monochromatic radiation, collimated and then directed toward the sample

When an X photon hits with θ angle on several atom planes separated by the distance d, a diffraction will take place. Interference is constructive if the path difference between two diffracted waves is a discrete multiple of wavelength; these are the conditions which satisfy the Bragg's law:

$n\lambda=2d \sin\theta$ (Equation 13)

where θ is the incident angle, d is the distance between two adjacent planes, λ (lambda) is the wavelength of incident x-ray beam and n is a positive number.

The diffracted X-rays are then detected, processed and counted. By scanning the sample through a range of 2θangles, all possible diffraction directions of the lattice are attained. XRD analyses were carried out by using a Panalytical X'PERT PRO PW3040/60 diffractometer in a Bragg-Brentano configuration (Cu K_α radiation with λ=1.540 nm, generator voltage of 40 kV and generator current of 40 mA)

The obtained diffraction pattern shows the intensity in y-axes and the 2θ diffraction angle in x-axis. The recognition of the phases takes place through comparison of the position of the signals and their intensity with the data present in the literature.

X-ray diffraction was used to determine the composition of the starting $AlSi_{10}Mg$ powder. Specifically the compositional differences between two different batches of powder supplied by EOS, a well as between the virgin powder and the one collected after the job were investigated at the Polytechnic of Turin.

XRD analysis was also carried out on the surface of cubic samples obtained by additive manufacturing.

2.3.5.2 Determination of residual stress

X-rays diffraction analysis gives also information about the residual stress present within the materials . The diffractometer used for this kind of measurement is basically a powder diffractometer, however it differs from Bragg-Brentano configuration in the following ways:

- It can accommodate large and heavy champions,
- The maximum 2θ angle is 165 ° while a standard diffractometer can reach 2θ angle of 145 °.
- Samples can be tilted because a residual stress diffractometer has more rotations than a standard powder diffractometer.

At CRF Metals Material's lab residual stress measurements on cubic and parallelepiped, as built and heat treated samples were performed by using the GNR Stress X diffractometer shown in figure 26 .

Figure 27 : CRF Metals Lab diffractometer

The determination of residual stress was carried out both on parallel and perpendicular sample faces respect to the growth direction. Two measurements in two different points have been done in order to verify the repeatibilty of the obtained values. The specimens surface must be flat in order to allow the correct execution of the test.

The measurement of residual stresses relies on the interactions between the wave front of the X-ray beam and the crystal lattice. The basis of all XRD measurements is described by the Bragg's law that has been previously discussed .There is a clear relationship between the diffraction pattern and the distance between atomic planes in the crystal lattices . If a material is free of strain it will produce a specific diffraction pattern; when a material is strained the inter-planar spacing changes. In fact elongations and contractions are produced within the crystal lattice and these cause variations in d value and consequently in the diffraction pattern. By a precise measurement of this shift, both d variation and the strain within the material can be evaluated by using the following equation:

.

$$\varepsilon_z = \frac{d_n - d_0}{d_0} \qquad \text{(Equation 14)}$$

Where do is the unstrained inter-planar spacing and dn is strained inter-planar spacing.

So the strain ε_z can be measured by comparing the inter-planar spacing when the material is free of stress with the strained ones.

In order to calculate to stresses connected to the strains we can use the Hooke's law which directly relates stress and strain according to the following equation:

$\sigma = E\varepsilon$ (Equation 15)

where σ is the stress , E is the material elastic modulus and ε is the strain

It is known that a tensile force, for examples in the X-direction, will produce not only a linear strain in that direction, but also a strain in the transverse direction (Y)

Assuming that a state of stress exists and that the stresses are biaxial :

$\varepsilon_y = \varepsilon_x = -\upsilon\varepsilon_z = \frac{-\varepsilon\sigma}{E}$ (Equation 16)

where υ is ratio between the transverse and the longitudinal strains that is the Poisson's ratio.

If we assume that $\sigma_z = 0$ because of the measurement is made within the surface then

$$\varepsilon_z = -\nu(\varepsilon_x + \varepsilon_y) = \frac{-\nu}{E}(\sigma_x + \sigma_y)$$

(Equation 17)

Combing the equations (14 and 17):

$$\frac{d_n - d_0}{d_0} = -\frac{\nu}{E}(\sigma_x + \sigma_y)$$

(Equation 18)

Having stress that act in a specific direction on the surface $\sigma_{\phi;}$ the elasticity theory shows that the strain along an inclined line is:

$$\varepsilon_{\phi\psi} = \frac{1+\nu}{E}(\sigma_1 \cos^2\phi + \sigma_2 \sin^2\phi)\sin^2\psi - \frac{\nu}{E}(\sigma_1 + \sigma_2)$$

(Equation 19)

Where $\varepsilon_{\varphi\psi}$ is strain measured in the direction of measurement defined by the angle phi, psi.φ (phi) is the angle between a fixed direction in the plane of the sample and the projection in that plane of the normal of the diffracting plane. Finally ψ (psi) is the angle between the normal of the sample and the normal of the diffracting plane (bisecting the incident and diffracted beams)

Considering the strains in terms of inter-planar spacing and by using these strains to calculate the relative stresses, it is possible to evaluate the stress in any chosen direction through two measurements: one is carried out in a plane normal to the surface and a second one contains the direction of the stress to be measured.

$$\sigma_\phi = \frac{E}{(1+\nu)\sin^2\psi}\left(\frac{d_\psi - d_n}{d_n}\right)$$

(Equation 20)

The $\sin^2\psi$ method is the method used at CRF for stress determination: different XRD measurements are done at different psi angles. The inter-planar spacing is measured and then plotted as a function of $\sin^2\psi$.

The position (2θ value) of a XRD peak (e.g. 422 reflex of aluminum) and the relevant inter-planar distance can be detected by recording the XRD pattern at different angles ψ (See Fig. 28).

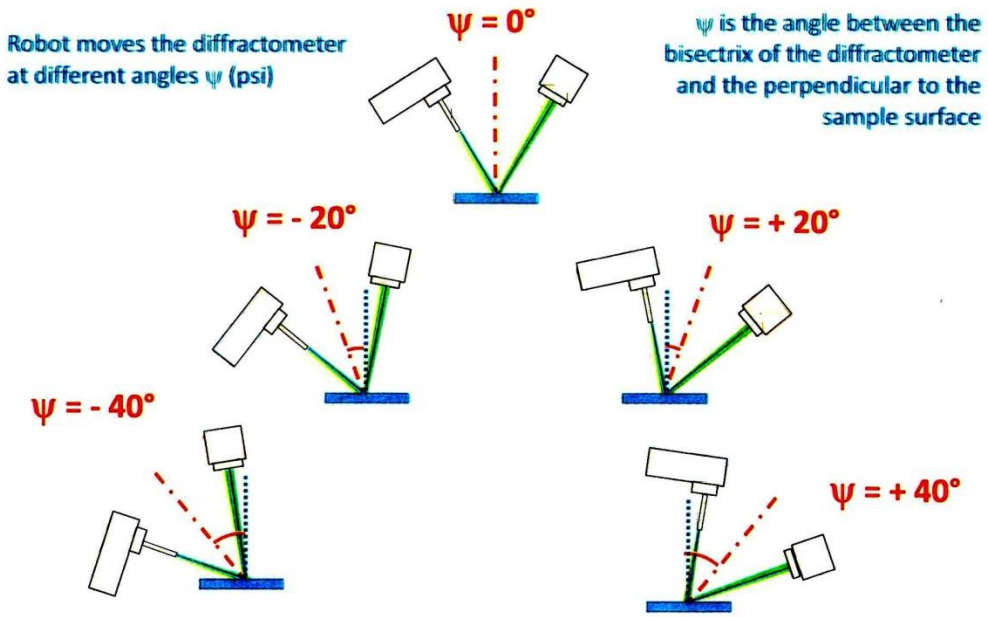

Figure 28: Positions of XR source and detector for resisual stress measurements.

In this manner crystals with (422) crystallographic plane differently oriented with respect to the sample surface will be responsible for the diffraction (see Fig 29). The different orientation will result in different changes of planar spacing and then in different shift of 2θ for the peak in the XRD pattern. Conclusively from the peak position and for each ψ value it is possible to calculate the corresponding d value and the deformation ε.

When mono axial stress state exists, the equation 20 applies and it can be written as:

$$\sigma = \frac{E}{(1+\nu)\sin 2\psi}\varepsilon$$

By plotting the planar interspace or the deformation against the corresponding $\sin^2\psi$ it is possible to obtain a straight line, whose slope "m" is related to the stress (see Fig. Z).

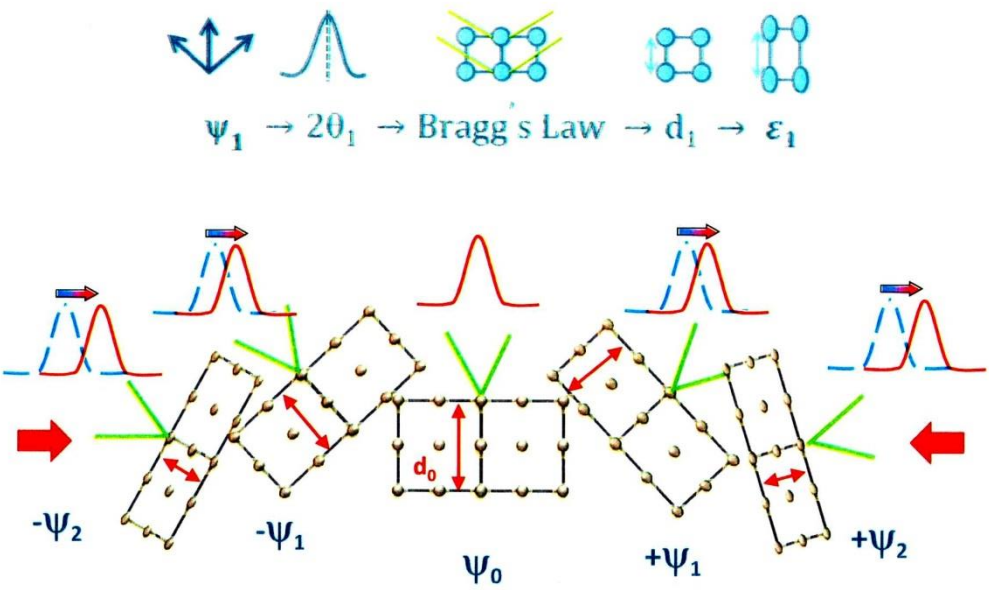

Figure 29 Effect of stress on plane spacing in crystals with different orientation.

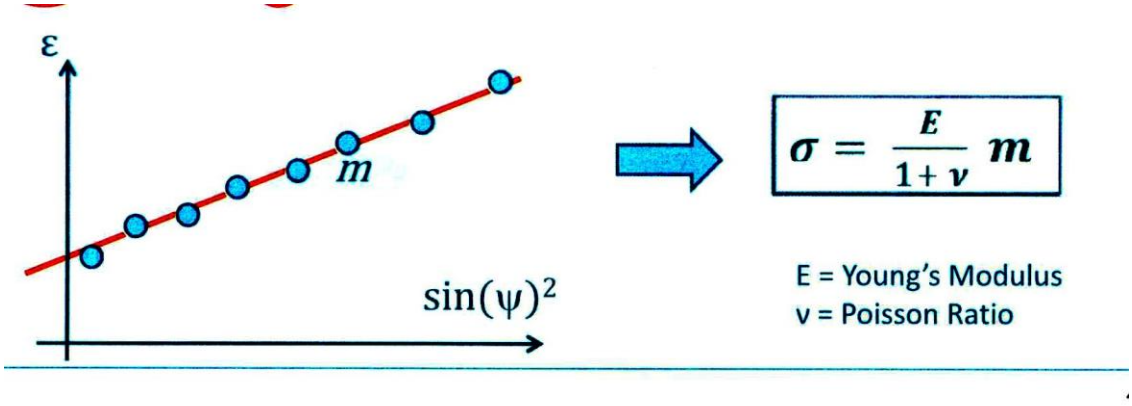

Figure 30 Calculation of residual stress from the slope of the plot

Figure 30 shows the linear dependence of d upon $\sin^2\psi$.

The true stress is given by the formula :

$$\sigma_\phi = \left(\frac{E}{1+\nu}\right) m$$

(Equation 21)

Different solutions can occur for non-ideal situations: the presence of shear stresses can for example cause psi splitting (Figure 31b) or there can be an inhomogeneous stress state within the material (Figure 31 c)[30]

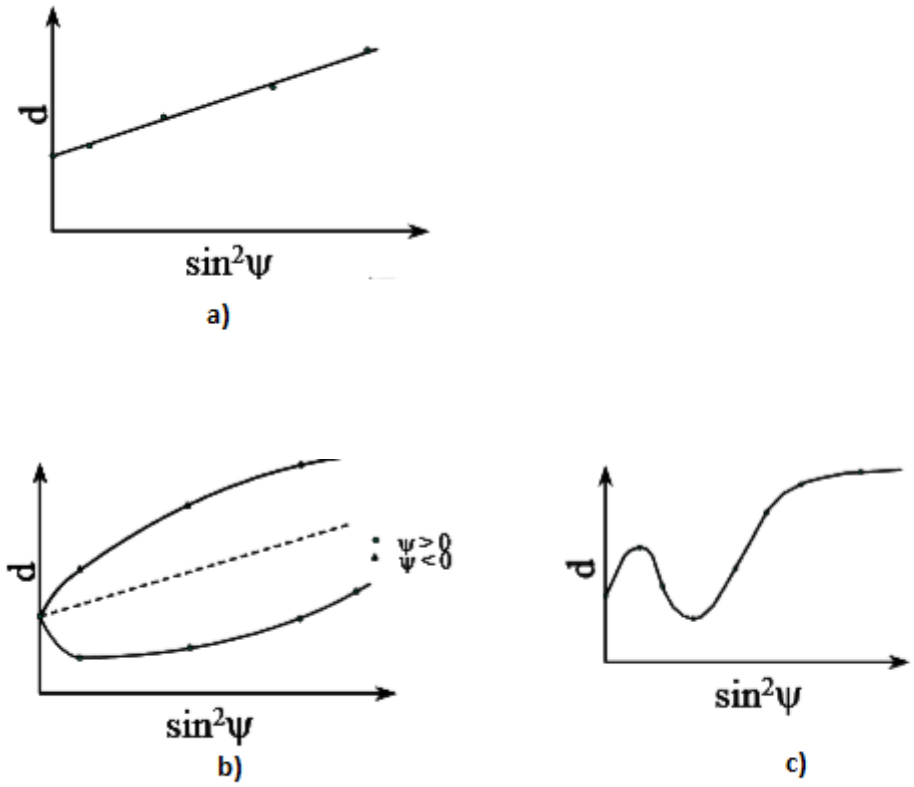

Figure 31 : inter-planar distance as a function of $\sin^2 \psi$ a) Regular behavior b) ψ splitting c) Oscillatory -indicating the presence of an inhomogeneous stress/strain state within the material [30]

2.3.6 Scanning Electron Microscopy (SEM)

The scanning electron microscope (SEM) analysis is considered to be "non-destructive" and gives information about morphology, chemical composition and crystalline structure of the material. The analyzed signals come from the electron-sample interactions. Accelerated electrons carrying significant amounts of kinetic energy, strike the solid sample where energy is dissipate producing a variety of signals : secondary electrons, backscattered electrons, diffracted backscattered electrons (that are used to determine crystal structures and orientations of minerals), photons (characteristic X-rays that are used for elemental analysis and continuum X-rays), visible light and heat. Secondary electrons are used to obtain information about the morphology of the sample while backscattered electrons are useful for revealing contrasts in multi-phase samples [31] .

The signals of greatest interest for this work thesis are mainly the secondary electrons (SE), because they are strictly linked to changes in surface topography and they give information on sample surface morphology. The secondary electron emission is confined to a very small volume near the beam impact area and it allows to obtain images with very high resolutions. Scanning Electron Microscopy (SEM) Leo 435VP was used at the CRF .

The equipment is divided in four main parts: the electron column (the most conventional gun is a tungsten wire of 0.25 mm of diameter as electron source, where the tungsten filament is heated to approximately 2500°C), the specimen chamber, the vacuum pumping system and the electronic control of the imaging system.

The electron beam is generated by a Tungsten (W) filament which , emits electrons by thermo-ionic effect. These electrons are accelerated through a potential difference reaching energies ranging between a few hundred and a few tens of thousands of eV (generally from 200 eV to 30 keV) .

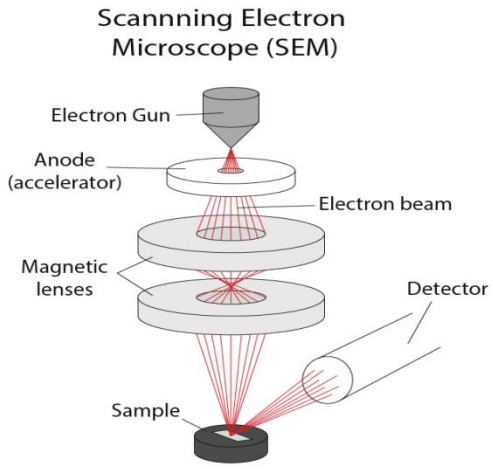

Figure32: scheme of SEM

The electron beam is subsequently collimated by a series of electromagnetic lenses inside the column. At the bottom of the column, the beam is focused in such a way that it covers a predefined area of the sample surface.

It is moreover possible to perform chemical analysis with SEM equipment by measuring the energy and intensity distribution of the x-rays generated by the electron beam. One of the most common x-rays detectors are the so called Energy-Dispersive X-ray Spectrometer (EDS). In EDS, the impact of a X photon on the sensor generates an electron-hole couple with an energy proportional to those of the photon.

After passing through a thick beryllium window (8 μm) the X-rays are detected by a Silicon diode; this is generally cooled to reduce noise. The analysis of the spectrum can ensure a qualitative and semi-quantitative chemical nalysis of the specimens.

Fracture surfaces of the tensile specimens were analyzed by SEM in order to determine their morphology and consequently the fracture mode.

2.3.7. Optical microscope

The metallographic microscope is an optical microscope that works in reflected light: for this reason it is necessary to prepare the samples by polishing the surfaces. The reflected light allows to obtain information about the microstructure

of the material such as: dimensions and shape of the crystalline grains, distribution of phases, presence of inclusions, porosity, possible precipitates and cracks. Optical Microscope (OM) Leica DMI 5000 M was used to obtain samples micrographs at different magnifications (from 50 to 500x) in order to observe the morphology of the specimens (specifically the shape and the distribution of the melt pools) and their porosity. This analysis was carried out on the cubes, the parallelepipeds and some tensile tested samples after cutting them in both parallel and perpendicular directions with respect to the growth (z-direction) one . A BUEHLER ISOMET 4000 cutting machine with Cermet blade (cutting speed of 2 mm/min and rotation blade speed of 1800 rpm) was used to cut the specimens . The so cut samples were embedded in a two component epoxy resin (Technovit 4006 resin obtained by mixingthe liquid and the powder components) .The samples were polished by using SiC abrasive papers and polishing cloths with 3 μm and 1 μm diamond pastes. The specimens were then washed with ethanol in order to eliminate any abrasive surface particles and dried at the end. In order to better highlight the microstructures, some samples were subjected to chemical attack . The etchant used for AlSi10Mg specimens was the Keller's reagent . It is constituted by a mixture of HF, HCl, HNO_3 acids and water. (1.0 mL HF + 1.5 mL HCl + 2.5 mL HNO_3 + 95 mL water) Once the micrographs have been collected, they were elaborated by using an the image analysis software (Image Pro Plus) in order to evaluate the residual porosity . This analysis was performed on 5 photos taken in different areas for each sample (all the micrographs were collected at a 50x magnification) .

2.4. Mechanical characterization

2.4.1Tensile test

Tensile test is one of the most important destructive mechanical tests as it allows to determine the tensile strength, the yield strength, the elongation and the elastic modulus of the materials submitted to it.

The tensile tests have been carried out according to the UNI EN ISO 6893.

According to this standard , the specimens can be either circular or rectangular in shape and the most important parameters to take into consideration are the gauge length of the calibrated section, the diameter of the circular section and the section area.

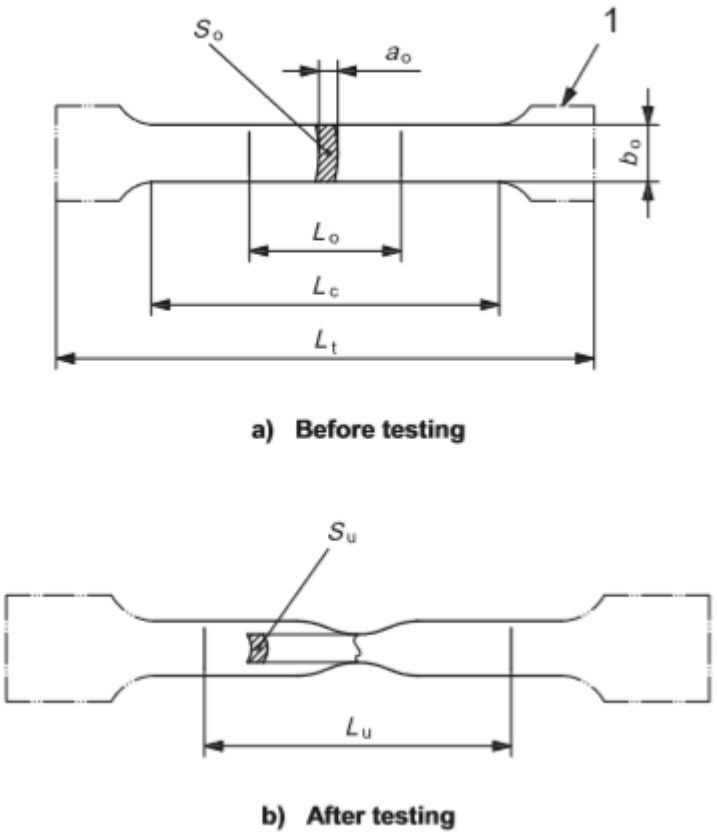

Figure 33: tensile test sample a) before testing b) after testing

There must be a direct relationship between the original gauge length (L_o) and the original cross section area (S_0) expressed by the equation:

$L_0 = k \sqrt[2]{So}$ (Equation 22)

where k is a coefficient of proportionality (the internationally adopted value for k is 5,65)

While Lc is equal to

$L_c \geq L_0 + b_0$ (Equation 23)

Where b_0 is the original width of the parallel length of a flat test piece

The test specimens shall be gripped by suitable means, such as wedges, screwed grips, parallel jaw faces, or shouldered holders.

Circular samples have been produced according to the standard parameters; some of them were manufactured and tested at the Polytechnic of Turin while others at the CRF Metals Lab . At Polytechnic the tensile tests were carried out by using MTS CITERION MODEL 43 machine with a rate of 5 mm/min; at the CRF the test were carried out using GALDABINI mod. SUN40 .

Figure 34: MTS CITERION MODEL 43 machine

The obtained results (e.g. fracture and yield loads) are function of the specimen dimensions; in order to make the test independent from them , both the load and the deformation were normalized obtaining the *nominal effort* (σ) that is the ratio between the force (F) applied along the axis and the initial section and *the nominal deformation* (ε) ratio that is given by the ration between the elongation (Δl)and the initial length (l_0).

$$\sigma=\frac{F}{So} \qquad \text{(Equation22)}$$

$$\varepsilon=\frac{\Delta l}{l0.} \qquad \text{(Equation 23)}$$

The obtained graphs report the nominal load [N / mm^2 or MPa] versus the percentage deformation.

2.4.2 Hardness test

Hardness is defined as the resistance of a material to be penetrated by a harder object. Several indentation methods have been developed such as Rockwell, Brinell, Vickers and Knoop ones. Each of them requests a specific geometry and size of the indenter, a specific equation, and presents also specific load conditions.

Hardness tests are some of the most widespread measuremets because they :

- do not deal with the realization of specimens of predefined shape
- give information on mechanical properties of the materials
- give information on the quality of some processes such as heat treatments, coatings and welds
- are fast
- are not destructive

In Vickers and Brinnel techniques the hardness is calculated by measuring the footprint left from the indenter on the surface of the sample, while in case of Rockwell technique it is calculated by measuring the penetration of the indenter. In this thesis the hardness of AlSi10Mg cubic and parallelepiped specimens was evaluated by Brinnel tests performed at the CRF metals laboratory

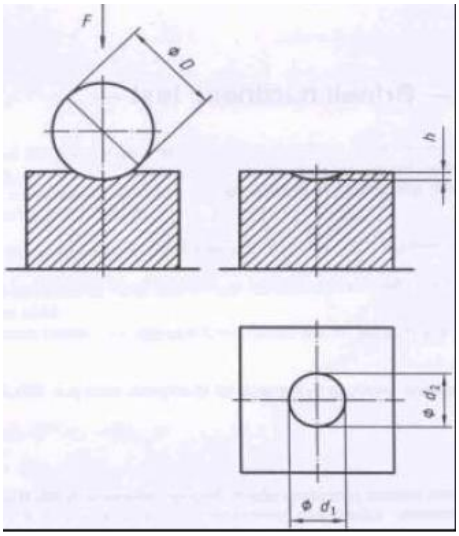

Figure 35 : principle measurement of the Brinell hardness.

The Brinell Hardness test is defined by the UNI EN 6506-1 standard. The operative procedure of the test consists in indenting the tested material with an indenter made of a hardened steel sphere or tungsten carbide ball; a load is applied for a fixed time leaving an imprint on the sample surface.The formula below is used to express the mean diameters of the indentation

$d = \frac{d1+d2}{2}$ (Equation 24)

where d_1 ,d_2 are the indention diameter measured at approximately 90°. The depth of indentation (h) is calculated as:

$$h = \frac{D}{2}\left(1 - \sqrt[2]{1 - \frac{d2}{D2}}\right) \quad \text{(Equation 25)}$$

It is possible to calculate Brinell hardness using the formula

$$HB = 0.102\frac{2F}{\pi D2\left(1-\sqrt[2]{\frac{d2}{D2}}\right)} \quad \text{(Equation 26)}$$

Where F is the force [Newton] and D is the diameter of the sphere in [mm][30] .

At the CRF laboratory a durometer with a tungsten carbide sphere (diameter of 2,5 mm) was used . The applied load was 10 N and it was maintained for 10 seconds. The hardness tests were carried out on cubic specimens and on parallelepipeds by repeating the measurements on 3-points for each samples face. Both the parallel and the perpendicular faces respect to the growth direction(Z axes) were submitted to the test in order to evaluate any differences of hardness in function of the orientation .
The test was carried out also on stress relieved specimens in order to determine the effects of the treatment on the material hardness.

Figure 36 : Brinnel EMCOTEST M5U 300/030 machine [30]

2.4.3 Charpy test

The Charpy test is one of the most used methods for quantifying impact energy. According to ASTM E 23 the test is performed on notched samples with a square section; the geometry is shown in figure 36. The test consists in applying a load that impacts through a hammer / pendulum dropped from a height H. Because of the impact, the sample breaks and the pendulum continues its way going back to a height (h'), lower than H because of it has lost energy after the impact. From the difference between the two heights H and h' it is possible to calculate the absorbed energy.

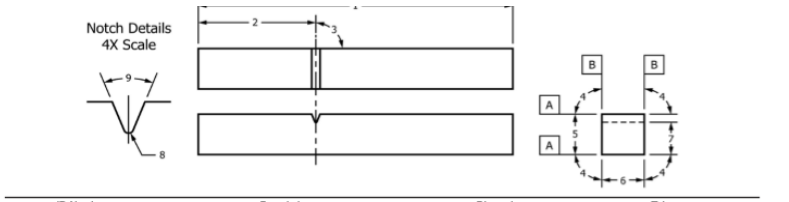

ID Number	Description	Dimension	Tolerance
1	Length of specimen	75 mm	+0/-2.5 mm
2	Notch to top	28 mm	
3	Notch length to edge	90°	±2°
4	Adjacent sides angle	90°	±0.17°
5	Width	10 mm	±0.025 mm
6	Thickness	10 mm	±0.025 mm
7	Ligament length	8 mm	±0.025 mm
8	Radius of notch	0.25 mm	±0.025 mm
9	Angle of notch	45°	±1°
A	Surface finish requirement	2 µm (Ra)	≤
B	Surface finish requirement	4 µm (Ra)	≤

Figure 37: ASTM E23 Charpy samples

For this test, notched specimens have been produced along two different building orientations (respectively Z and XY); half of them were then subjected to stress relieving treatment. The effect of both building orientation and thermal treatment on the material impact energy was evaluated and compared.

3 Result and Discussion

In this chapter the properties of the starting AlSi10Mg powder and the characterization of samples produced by DMLS process is reported and discussed. Samples produced along two different building orientation (XY and Z directions) were characterized in term of microstructure, density and mechanical properties .The influence of the powder layer thickness and the geometry of samples on the material properties were also evaluated.

In this chapter the properties of the starting AlSi10Mg powder and the characterization of samples produced by DMLS process are reported and discussed. Samples produced along two different building orientation (XY and Z directions respectively) are characterized in term of microstructure, density and mechanical

properties .The influence of the powder layer thickness and the geometry of samples on the materials properties are also evaluated.

3.1 AlSi10 Mg powders characterization

In the SLM process a fundamental role is played by the properties of the starting powder because they affect both the mechanical properties and the microstructural characteristics of the components.
The samples characterized during this work of thesis have been prepared starting from AlSi10Mg powder provided by EOS. However, the use of two batches of powders (reported as A and B respectively) was necessary in order to complete the experimental work. Both of them were characterized in order to verify their shape, particles size distribution and densities.

Figures 38 and 34b show the FESEM micrographs of the two AlSi10Mg powders: in both cases the particles show a roughly spherical shape; this configuration is typical of powders produced by gas atomization process. Powder with spherical shape and appropriate particle size distribution favorites a good flowability and a homogeneous deposition of each powder layer during the DMLS process.

Some satellites were observed for both powders A and B; generally these smaller particles are present as agglomerates .

The average particles size was observed to be around 27 μm for both the powders.

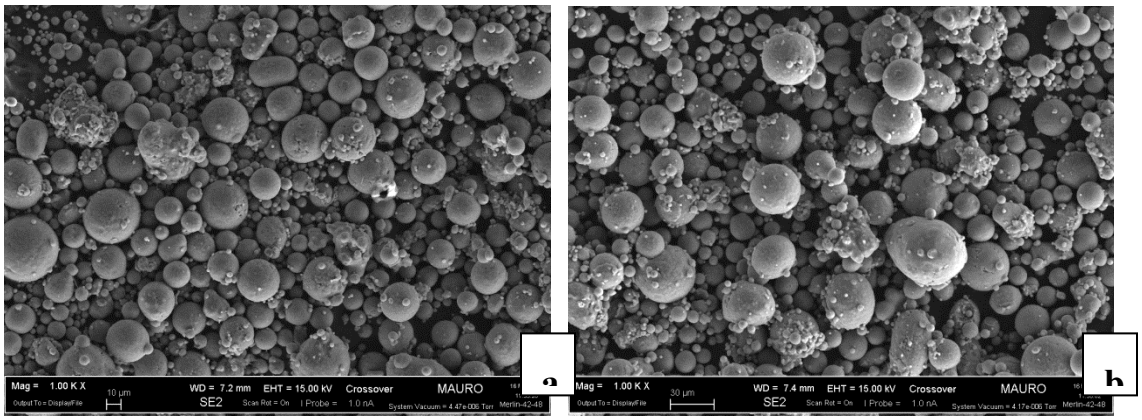

Figure 38 : SEM image of the two AlSi10Mg powders: A) first batch and B) second batch

The particles size distribution of the these two powders is reported in Figure 39. The d10 d50 and d90 of powder A are 19.3 µm , 40.7 µm and 74.8 µm respectively; the corresponding values for powder B are 19.1 µm (d10) , 40 µm (d50) and 74 µm (d90).

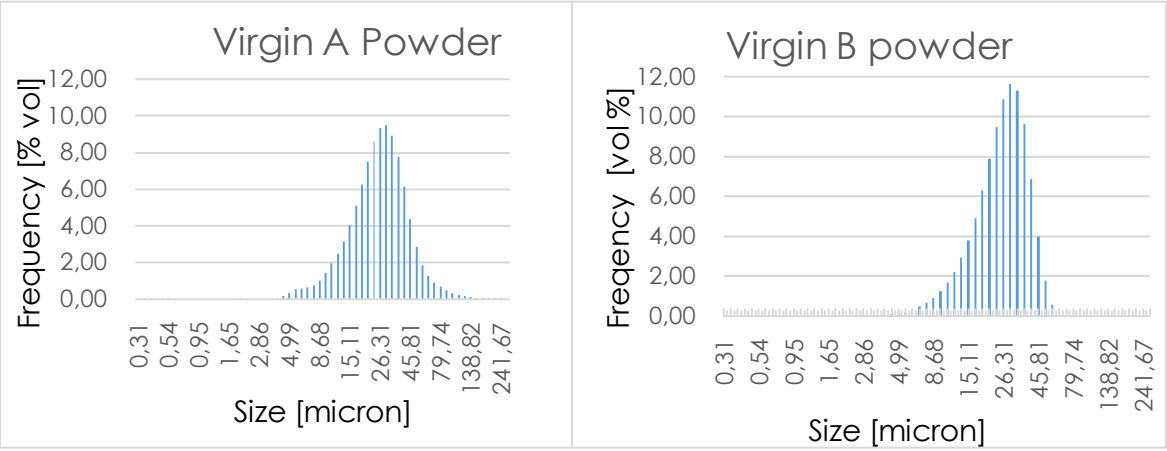

Figure 39 : particle size distribution; A virgin powder and B virgin powder

Powder	D10 (µm)	D50 (µm)	D90 (µm)
A	19,3	40,7	74,8
B	19,1	40	74
EOS data sheet	29	46	70

Table 5: diameters corresponding to 10% (d10), 50% (d50) and 90% (d90) of the cumulative size distribution

The shape of the two distribution curves is different; nevertheless the average particles size for both powders is around 27 µm .

While a Gaussian distribution is observed for powder A, the data for powder B seems not to fit a normal distribution showing an asymmetrical shape with the maximum centered at higher values than that of powder A.

The higher amount of bigger particles of powder B allows to predict a better flowability respect to powder A. In fact the presence of fine particles (with size lower than 10 µm) generally has poor flowability or does not flow at all because tend to cling each others.

EOS M290 datasheet confirms that powder morphology is quite spherical with a regular shape, ranging from 1 to 70 μm, with an average size which can be set in the range from 21 to 27 μm.

The differences in particles size distribution were also highlighted by the different flowability and tapped density values of the two powders.

Regarding the powder flowability powder A did not flow, so its flowability cannot be quantified. Poor flowability means that deposition of a uniform layer during DMLS process can present some difficulties.

On the other hand the flow rate of powder B was measured of 65sec/50 g. The better flowability of powder B respect to the A one is due to the fact that powder B has coarser particles and narrower particles size than powder A which in contrast contains some amounts of finer particles . As particles become finer the Van Der Waals attraction forces between them increase and, at the same time, the gravitational forces decrease . In conclusion it is possible to say that coarser powder flows better that finer ones .

The tapped density was measured for both the powders; moreover the compressibility index (CI) and Haussner ratio (HR) were calculated in order to compare their flow characteristics. The reference values for CI and HI are reported in Table 6

Flow Character	**Hausner Ratio**	**CI (%)**
Excellent/very flow	1.00-1.11	≤10
Good /free flow	1.12-1.18	11-15
Fair	1.19-1.25	16-20
Passable	1.26-1.34	21-25
Poor/cohesive	1.35-1.45	36-31
Very Poor /very cohesive	1.46-1.59	32-37
Very,very poor/approx non flow	>1.60	>38

Table 6 : CI and HI values for powder A (red) powder B (green)

According to the table 6 it is clear that the powder B presents an excellent flowing character if compared to the only passable one of powder A.

The CI are in fact 24.6% and 9.5% for the powder A and B respectively; the corresponding HR values are 1.27 and 1.1.

This confirm the fact that powder B flows better than powder A according to the smaller particles size distribution and different result of the flowability test .

The flowability of a metal powder is affected by its morphology and size distribution: powders A and B have the same morphology but different size distribution, with .

Probably the differences in A e B powders flowability is also due to the to the difference in moisture present inside the powder in addition to the storage conditions.

X-ray diffraction measurements were performed in order to compare the crystalline phases constituting the two starting powders. Moreover the powder A, which was the most used one, was collected in the platform after the job and as residual from the nozzle; the corresponding XRD spectra were obtained and compared to that of starting powder in order to highlight possible differences .

Figure 40shows the normalized spectra of A and B virgin powders.

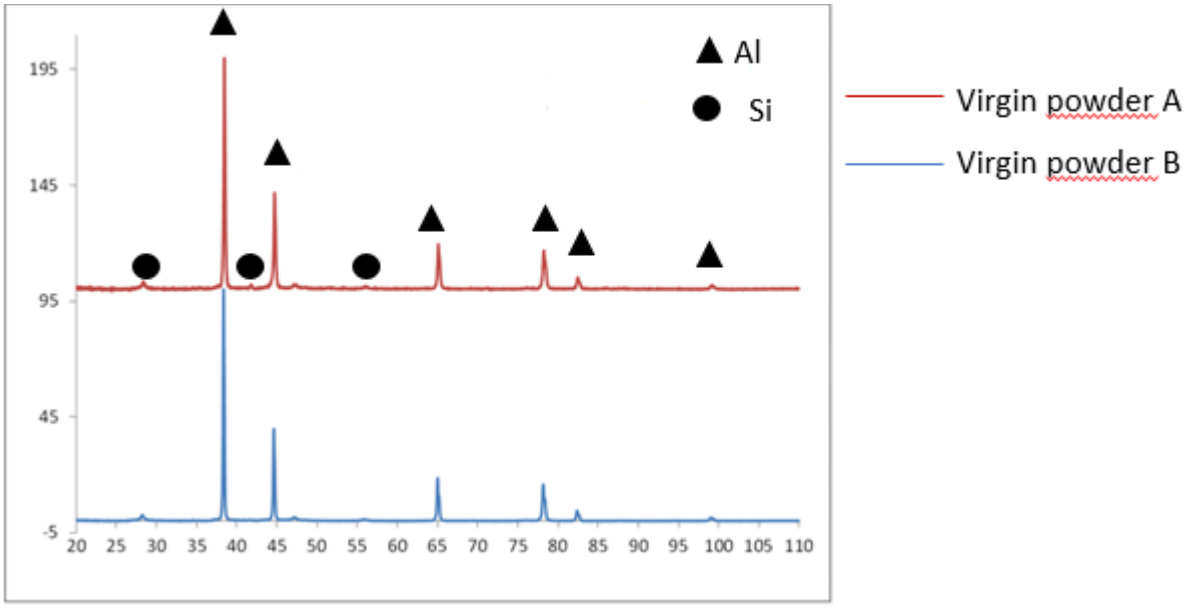

Figure 40 : A and B virgin powder spectra

The two spectra are identical revealing the presence of aluminum and silicon as the only crystalline phases.

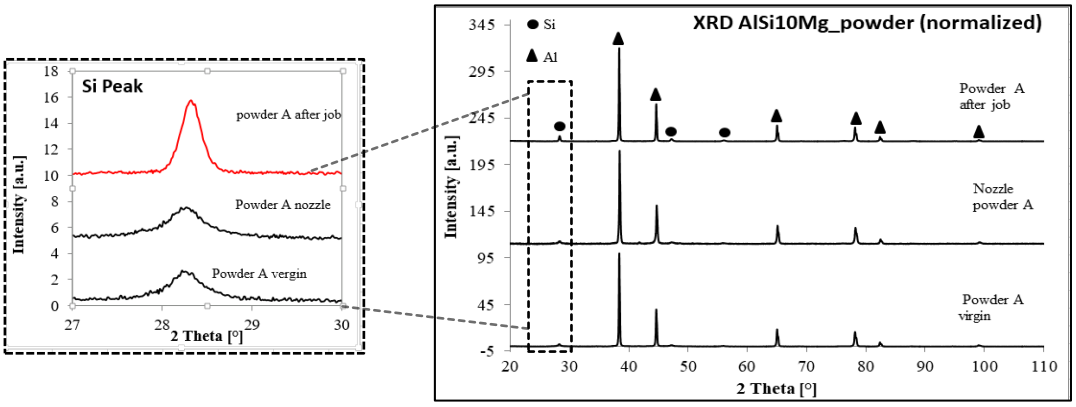

Figure 41 : XRD spectrum of powder A: a) comparison among virgin powder, powder collected after DMLS job and as residual coming from nozzle; b) zoom on Si peak.

As previously reported for starting powders, all the spectra reveal the presence of aluminum and silicon as crystalline phases. It is interesting to observe the variation of silicon peak in the three spectra. In fact silicon peak is more intense in the spectrum of powder collected after job with respect to peak of both virgin powder and material coming from the nozzle.

This is probably due to the fact that the powder is subjected to high temperature during the process which causes better crystallization of silicon.

3.2 Characterization of Laser Molten Samples

In this paragraph the characterization of the laser molten samples is presented; the effects on the samples properties of the different building orientations, the powder layer thickness, the sample shape and geometry in addition to the effect of a stress relieved treatment is also discussed.

In this thesis all the samples were produced in four different jobs:

Jobs A – B → process parameters shown in Figure 42

Job C → same process parameters of jobs A and B, but different powder layer thickness (0,06 mm instead of 0,03 mm)

Job D → same process parameters of jobs A and B, but samples are produced only with Charpy test configuration.

	DIRECT PART		POSTCONTOURS		
	COLD	200 °C	COLD	200 °C	
DISTANCE	0,19	0,19			mm
SPEED	1300	1300	900	900	mm/s
POWER	370	370	80	80	W
BEAM OFFSET	0,02	0,02	0,02	0,02	mm
HATCHING	X	X			ROTATED
STRIPE WIDTH	7	7			mm
STRIPES OVERLAP	0,02	0,02			mm
LAYER	0,03	0,03	0,03	0,03	mm
TEMP. ON PLATFORM	50	200	50	200	°C

Figure 42: jobs process parameters

3.2.1 Density analysis and microstructure

The density measurements and microstructural analysis were the initial steps for samples characterization. Changes in samples density and microstructure are compared for the different jobs; the effect of the deposition powder layer thickness and stress relieving heat treatment were also evaluated.

In the Table 7 density values of parallelepiped samples, built along Z axis, are reported. In addition, the theoretical density and porosity of AlSi10Mg alloy which are respectively 2,67g/cm^3 and 0,998% , are indicated as reference

	2 JOB		**3 JOB**		**4 JOB**	
	Bulding orientation Z axis					
	Parallelepiped					
	T building platform 200°C					
	As built	**Stress relieved**	**As built**	**Stress relieved**	**As built**	**Stress relieved**
Bulk density (g/cm^3)	2,63	2,63	2,63	2,63	2,63	2,61
Densità EOS data sheet (g/cm^3)	2,67					
Relative bulk density (%)	98,37	98,29	98,37	98,28	98,24	97,92
Porosity (%)	1,63	1,71	1,63	1,72	1,76	2,1
Porosity EOS data sheet (%)	0,998					

Table 7: Porosity and bulk density values for jobs A, B and C

Results show lower density values for all the three jobs A, B and C respect to the theoretical values supplied by EOS. There are not significant differences in term of porosity percentage comparing samples produced in the different jobs; however a very little porosity increase is observed for stress relieved samples compared to as built ones. These small differences can be mainly due to the experimental error. It is therefore possible to say that neither the heat treatment nor the powder layer thickness affect the densities values and consequently, the porosity of the manufactured products .

Figure 43 shows the micrographs of the Job A as built and heat treated sample cut in both parallel and perpendicular directions respect to the building one (Z axis); the black areas represent the porosities(highlighted using red arrows) . For all three jobs (A,B,C) similar microstructures are observed.

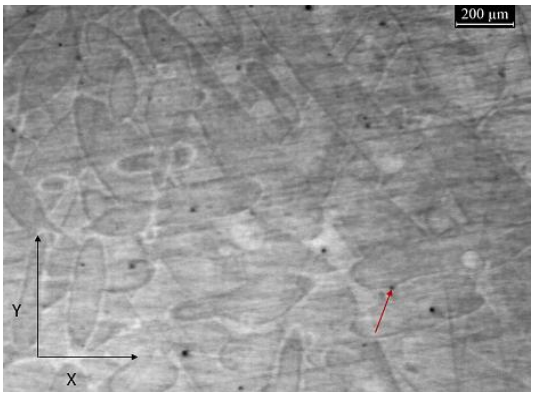

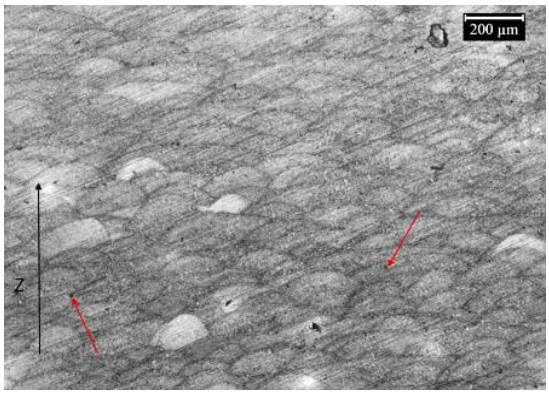

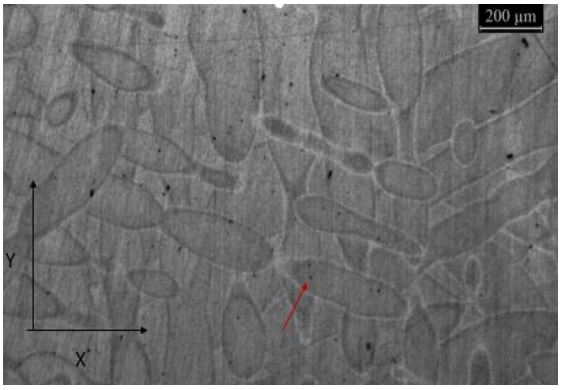

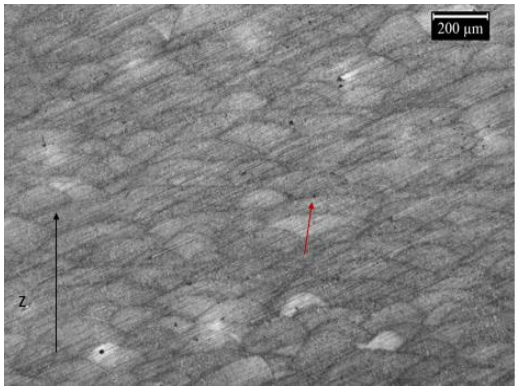

Figure 43: Job A as built and heat treated samples micrographs (magnification 50 x): on the left is presented the section parallel to the building direction, on the right the perpendicular one.

The pores size in both parallel and perpendicular sections is smaller than 10 μm. The higher residual porosity respect to the theoretical values is probably due to a not complete consolidation of the parts which result particularly evident at the edges of the melt pools; here the porosity seems to be more concentrated. Examining the micrographs of the sectioned as built samples at higher magnifications (figure 44) it is possible to analyze more in details the microstructure.

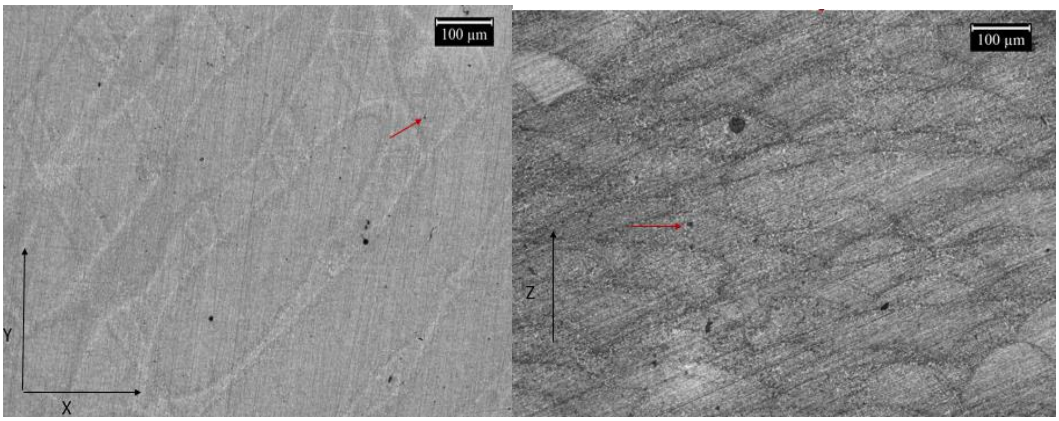

Figure 44 :Typical microstructure morphology of Laser Melted parts: on the left the section parallel to the building direction (Z axis); on the right the section perpendicular to the building direction(Z axis)

Considering the section parallel to the build direction (figure 44a) the melt pools are all oriented in the same way being the result of the superimposition of subsequent layers. Their shape is mostly half-cylindrical showing overlapping of the edges.

On the other hand in the samples sectioned perpendicular to the building direction (figure 44b) the melt pools show an elongated shape due to the heat capillarity, a phenomenon generated by different thermal gradients between the melt pools and the external zone that is at lower temperature [32].

3.*2.3 Mechanical characteristics*

3.2.3.1 Tensile test and fracture surface

In order to evaluate the mechanical properties, both the as-built and heat treated samples grown along different building orientations (Z axis and XY planes on the building platform and realized through job A, job B and job C, were submitted to the tensile test and fracture surfaces were analyzed .

Figures 45 ,46,47 and 48 show respectively job A and job B stress-strain curves for the as built and heat treated samples built along Z axis and in XY plane .

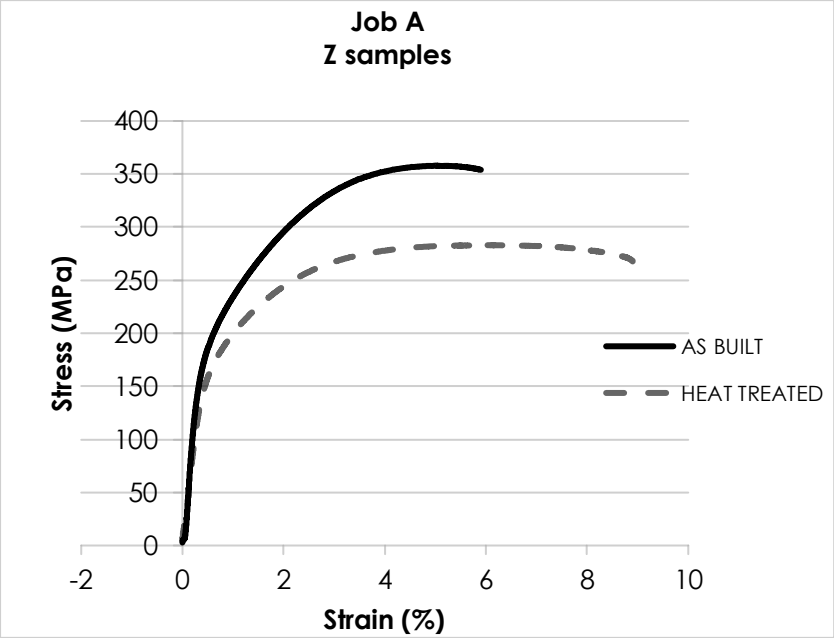

Figure 45 : Job A, Z samples as built and heat treated ,Stress-strain curves.

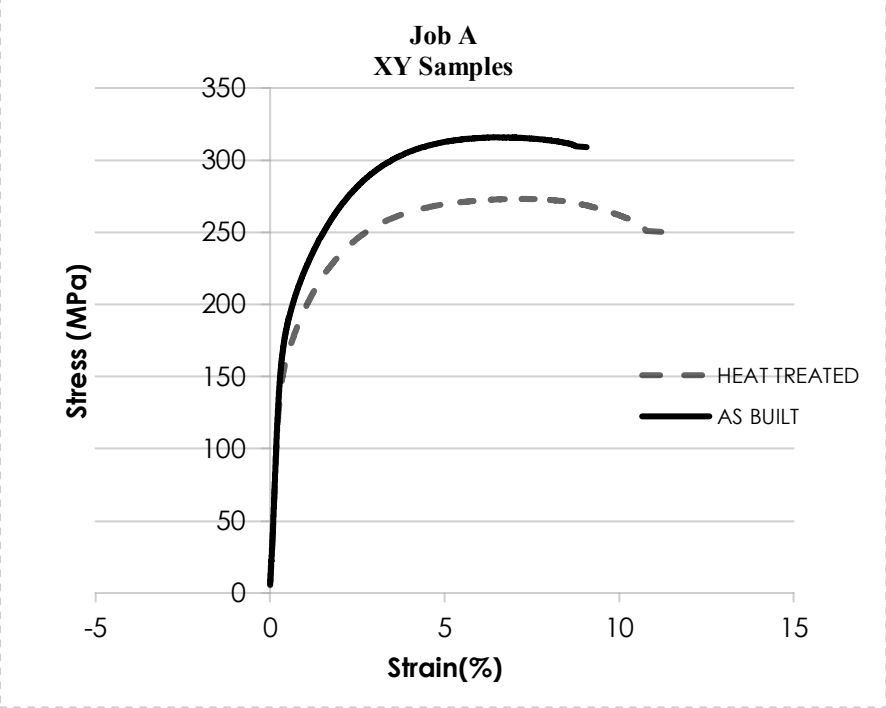

Figure 46: Job A, XY samples as built and heat treated ,Stress-strain curves.

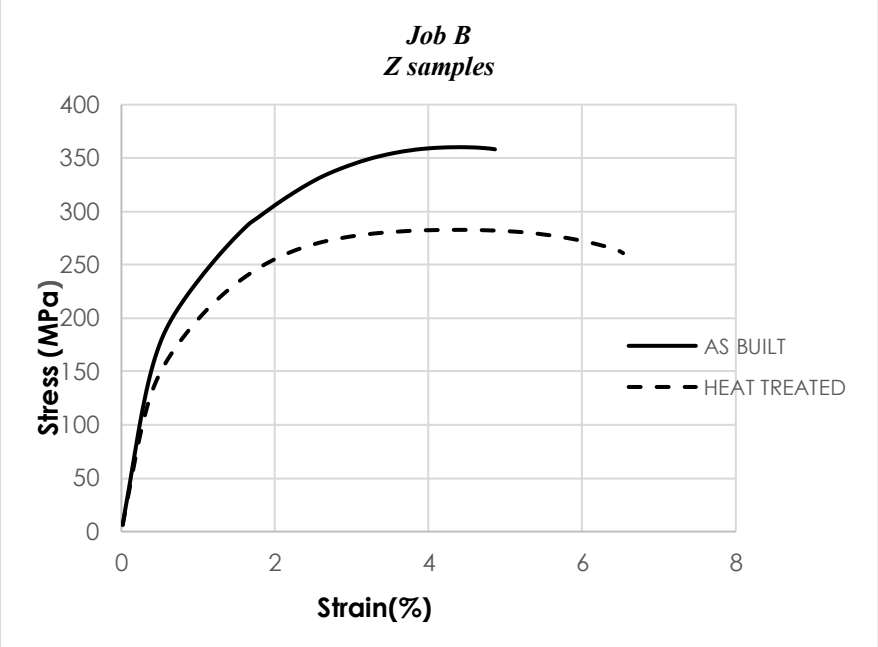

Figure 47: Job B, Z samples as built and heat treated ,Stress-strain curves.

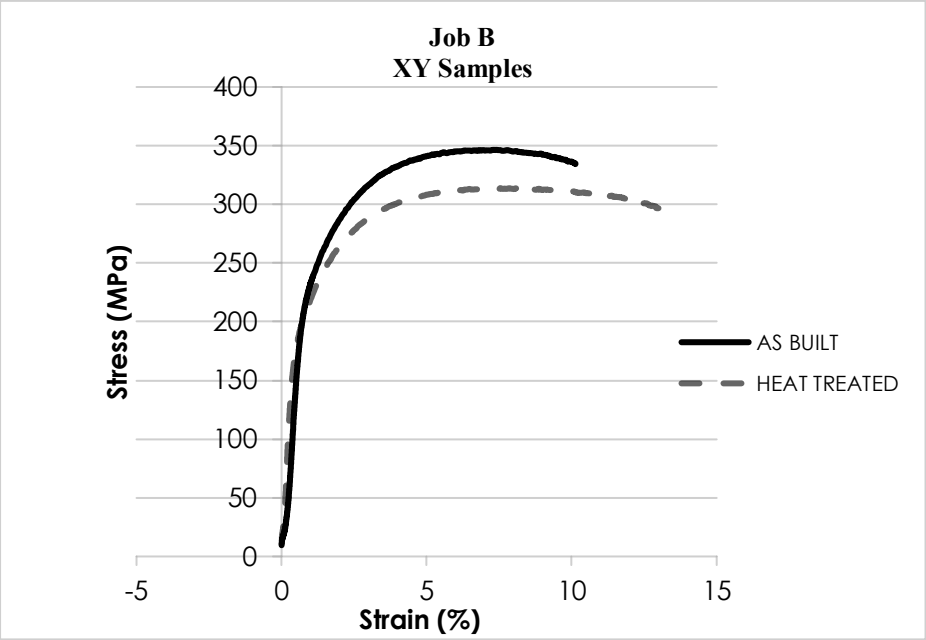

Figure 48: Job B, XY samples as built and heat treated ,Stress-strain curves.

It is possible to see that there are not significant differences in the tensile behavior of the job A and job B specimens produced according to the same building direction, as they have similar values of Rm and Rp , elastic modulus, elongation. These results are also comparable with the data provided by Eos. On the other hand there are evident differences (found in the values of Rm, Rp, elongation) between the specimens grown with different orientation due to the fact that the SLM process is characterized by providing a certain degree of anisotropy. Z samples are characterized by higher Rm value than XY samples but they show lower Rp and elongation. Therefore Z samples are more resistant but less ductile than XY samples. Other remarkable differences were found between heat treated and as built samples. Table 8 shows Rm, Rp and elongation values of the heat treated and as built Job A and Job B samples build along Z and XY axis.

JOB A	Z Samples as built	Z Samples heat treated	XY samples as built	XY samples heat treated
RM average value (MPa)	352,3	283,2	315	274,1
RMEos data sheet (MPa)	390		360	
Rp average value (MPa)	184,4	163,4	188,8	165,7
RP Eos data sheet	210		220	
Elongation average value (%)	5,55	7,10	8,45	8,50
Eos data sheet	6		8	
JOB B	Z samples ab built	Z samples heat treated	XY samples as built	XY samples heat treated
RM average value (MPa	351,33	279,55	346,2	344,1
RM Eos data sheet (MPa)	390		360	
Rp average value (MPa	186,63	153,35	225,0	186,2
RpEos data sheet (MPa)	210		220	
Elongation average value (%)	5,9	10,7	9,3	13,0
Eos data sheet (%)	6		8	

Table 8: job A and job B tensile test results

The effect of heat treatment is summarized in the following.

-Heat treatment effect on RM: specimens grown along Z and subjected to stress relieving show a decrease of Rm of about 20 % in both jobs, while Job A heat

treated samples built in XY plane show a decrease of RM of about 13%, which is higher than that of the specimens of job B, in which a negligible decrease is observed.

-Heat treatment effect on RP : an equal decrease in RP is observed in the heat treated specimens grown along the two different directions for both jobs. In particular, there is decrease of about 12% and 18% for job A and B respectively .

- Heat treatment effect on elongation : elongation in Job A heat treated samples shows an increase of about 20% in both building orientation, while job B (z orientation) heat treated samples show an higher increase in elongation (70%) than heat treated XY samples.

-Heat treatment effect on elastic modulus : no variations was observed between heat treated and as built samples .

Conclusively, it is possible to affirm that the stress relieving treatment is more impacting on the tensile strength and on the elongation. In particular, this can be seen in specimens grown along Z.

The treatment of job C , shown below, was done separately with respect to the other two jobs as this job was performed with different powder layer thickness and therefore different results could be expected.

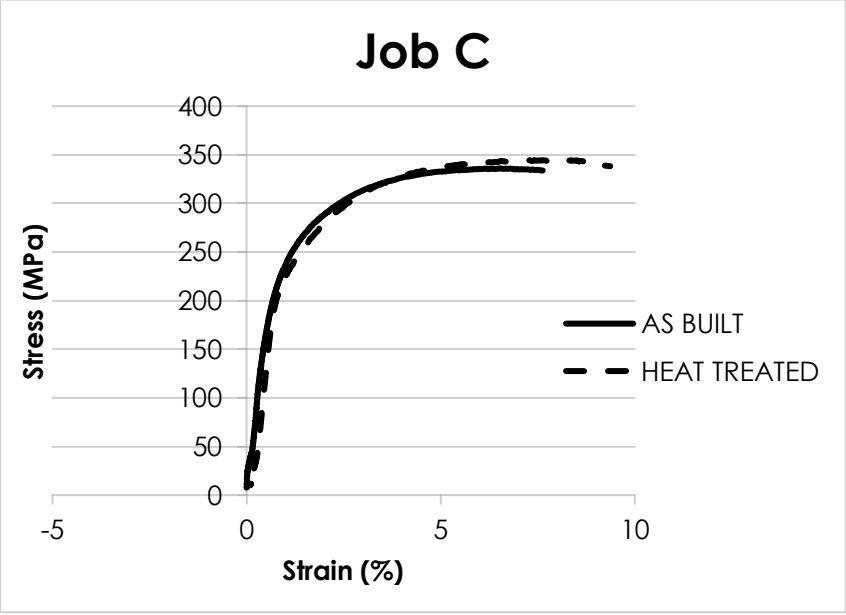

Figure 49: Job C, XY samples as built and heat treated ,Stress-strain curves

Table 9 shows Rm, Rp and elongation values of the heat treated and as built samples build only in XY plane .

JOB C	XY samples 60µm As built	XY samples 60µm Heat treated
RM average value (MPa)	355,8	339,9
RM Eos data sheet (MPa)	360	
RP average value (MPa)	204,8	216,7
RP Eos data sheet (MPa)	220	
Elongation average value (%)	6,85	7,60
Elongation Eod data sheet (%)	8	

Table 9: job C tensile test results

It is clear that heat treatment inflates much less the mechanical properties of the samples than in the case of the other two jobs previously discussed.
There is a slightly more significant variation in the elongation ,about 10%, compared to the values of m R and Rp.
This is probably due to the fact that being the powder bed thicker there is less heating of the sample and consequently lower thermal stresses. Therefore the final heat treatment causes smaller variation of mechanical behavior. .
It seems most convenient to use thicker powder layers to realized manufactured products, but the data at our disposal are not sufficient to confirm it in a definitive manner. In table 10 it is possible to see the different mechanical properties of the $AlSi_{10}Mg$ parts realized through SLM and traditional casting processes . SLM as built parts show higher values of elongation and ultimate tensile strength than

those processed by traditional casting and without finally thermal treatments . Only after ageing (T6) heat treatments, the formation of Mg2Si precipitates ensure that elongation and UTS values of cast products become comparable with those of SLM parts .

x ± s	E	UTS	ε_{break}
	GPa	MPa	%
XY direction	68 ± 3	391 ± 6	5,55 ± 0,4
Z direction		396 ± 8	3,47 ± 0,6
conventional cast and aged	71	300-317	2,5-3,5
high pressure die casting	71	300-350	3-5
high pressure die casting T6	71	330-365	3-5

Table 10 : Mechanical properties of AlSi10Mg parts after traditional casting and SLM process

Deeper investigation of the fracture surfaces microstructure of the as-built and heat treated samples , by using SEM, shows that it is made up of α-Al small polygonal grains, with Si segregated at the boundaries and that ductile fracture was dominant in all specimens, but the fracture mechanism slightly different between samples grown with different orientations

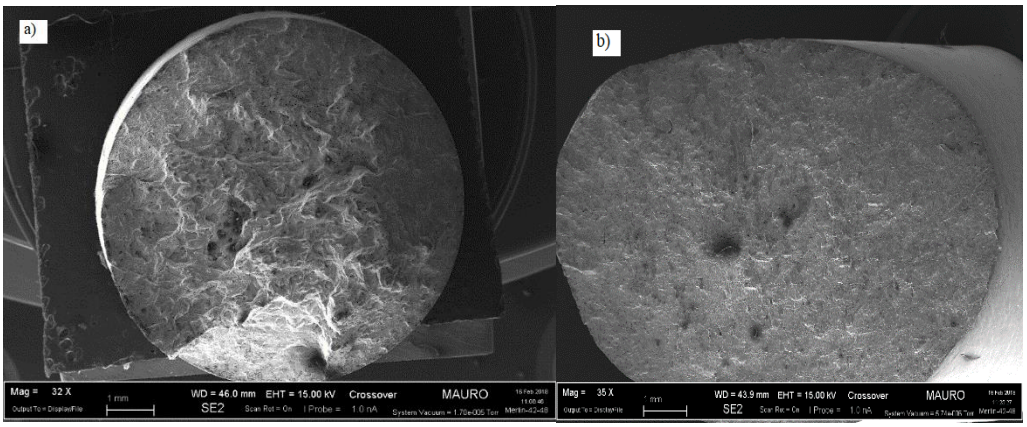

Figure 50: a) Z samples fracture surface b) XY samples fracture surface

Since the tensile direction remained constant (Z axis), in the Z and XY samples occurs different relationship between the building orientation and the tensile direction (figure 51) [32] .

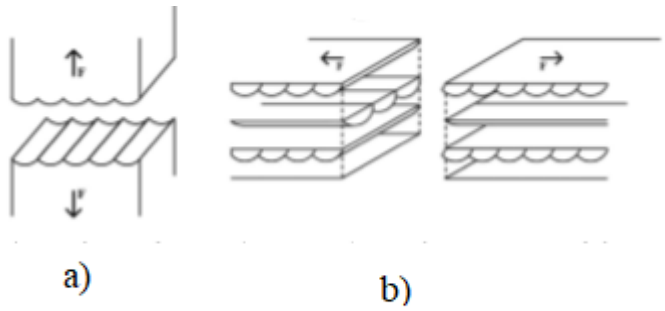

Figure 51 : Schematic representation of interactions between building orientation and the stress direction : a) Z samples b) XY samples

In Z samples failure propagates perpendicular to the building direction, through weak interfaces between adjacent layers while in XY samples failure propagated parallel to the building direction, so that the crack moves perpendicularly to the layers. Analyzing the SEM images at low magnifications , the Z sample fracture surface topography seems not regular with large flat zones (Figure 52 a). The size of these zones is well greater than the grain size and therefore they corresponds to plane of separation between domains belonging to adjacent layers. The XY samples fracture surface topography seems more flat, probably because the crack cuts the layers, in addition secondary cracks forms perpendicularly to the fracture surface. Very likely these secondary cracks moves at the interfaces between adjacent layers (Figure 52 b and 56).

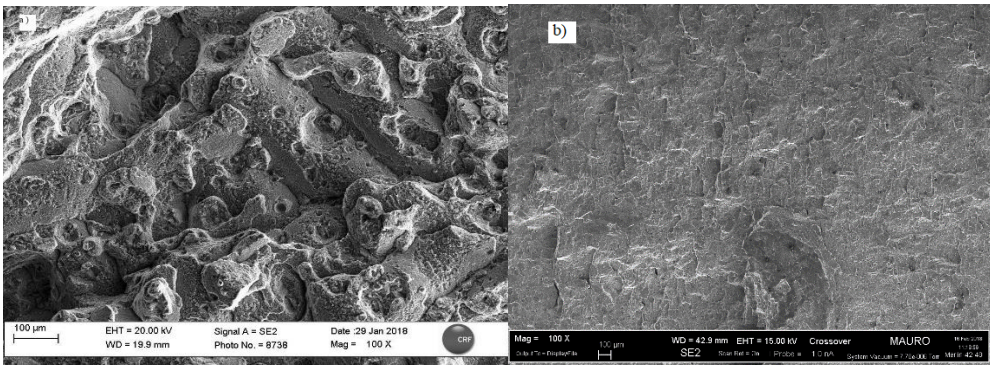

Figure 52 : a) as built Z samples fracture surface (100x) b) as built XY samples fracture surface higher magnitude (100X)

In the case of the Z samples (figure 52 a), analyzing the fracture surface, at higher magnification very flat and rather large separation surface can be seen (Fig. 55) It is clear that there is a inter -domain fracture. Inter –domain fracture occurs in the zones of separation between the various melt pools. This is probably due to the fact that the separation zones are weak areas. Many studies [32] have shown that pool melts are characterized from having a finer microstructure at the center and a coarser microstructure in the external areas. By using higher magnification these flat zones reveal that a intergranular ductile fracture occurs (Fig. 53)

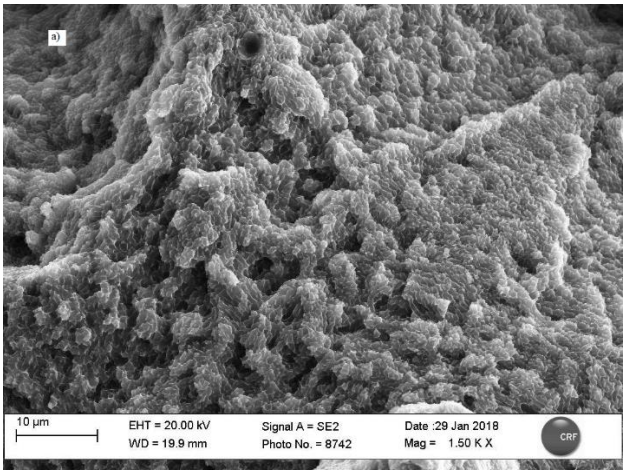

Figure 53 : as built Z sample fracture surface magnitude 1,50K,x

In the molten state, silicon is perfectly miscible in aluminum and therefore, when the laser beam is focused on a specific area of the powder bed, here a homogeneous molten solution of silicon and aluminum forms. In the state diagram it is possible to see that the solubility of the Silicon in aluminum at room temperature is equal to zero .

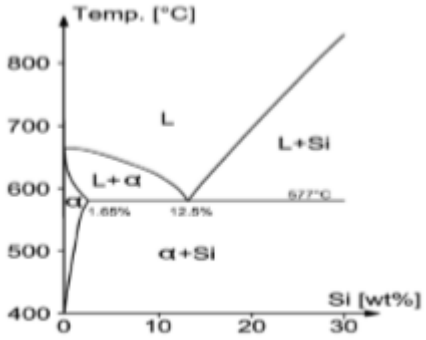

Figure 54 : Al-Si phase diagram

Considering a foundry $AlSi_{10}Mg$ alloy its micro-structure is characterized by grains of large size, since cooling takes place slowly. In these conditions the state diagram will be followed, silicon grains of silicon and aluminum have time to nucleate and grow . On the contrary In our case, the high cooling rates cause segregation of the silicon at the grain boundaries . The microstructure consisting of small sized grains surrounded by silicon. This feature is very clear when the fracture surface is observed by SEM at magnification of 2000X or more (Fig 55). The intergranular ductile mechanism of fracture is well evident.

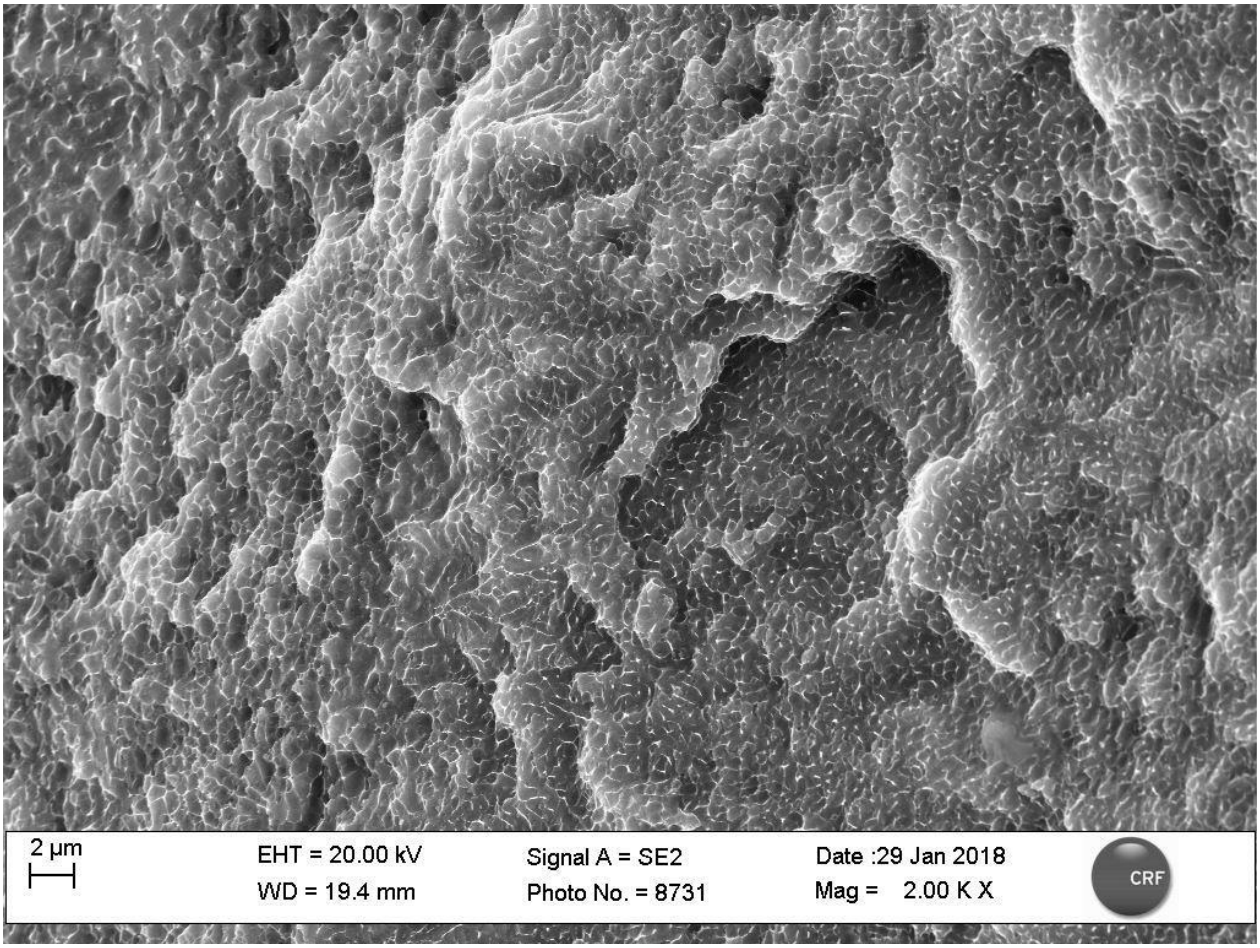

Figure 55 : Fracture surface os Z samples at high magnification: aluminum grains smaller than 2 µm with silicon segregation at the grain boundaries.

Heat treatment slightly influences the fracture mechanism of the XY and Z samples .

In every case the heat treatment causes further silicon segregation at the grain boundaries and therefore also segregation at the inter

domains. This phenomenon makes more evident the crack propagation at the interfaces between adjacent layers in the case of Z samples (Fig. 56).

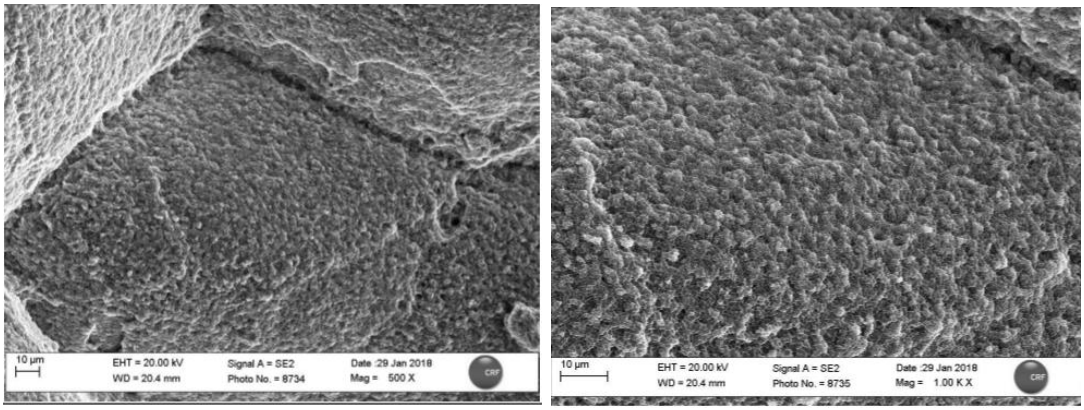

Figure 56 :heat treated Z samples inter-domain fracture surfaces different magnitude

It is possible to see from the figure 57 that the size of the aluminum grains has not increased significantly during the heat treatment (remaining lower than 2 µm) because more silicon segregate during the treatment and likely also Mg_2Si forms during this treatment. All the grains are surrounded by precipitates of silicon and Mg_2Si that prevent the grains growth. . Still interganular ductile fracture mechanism occurs.

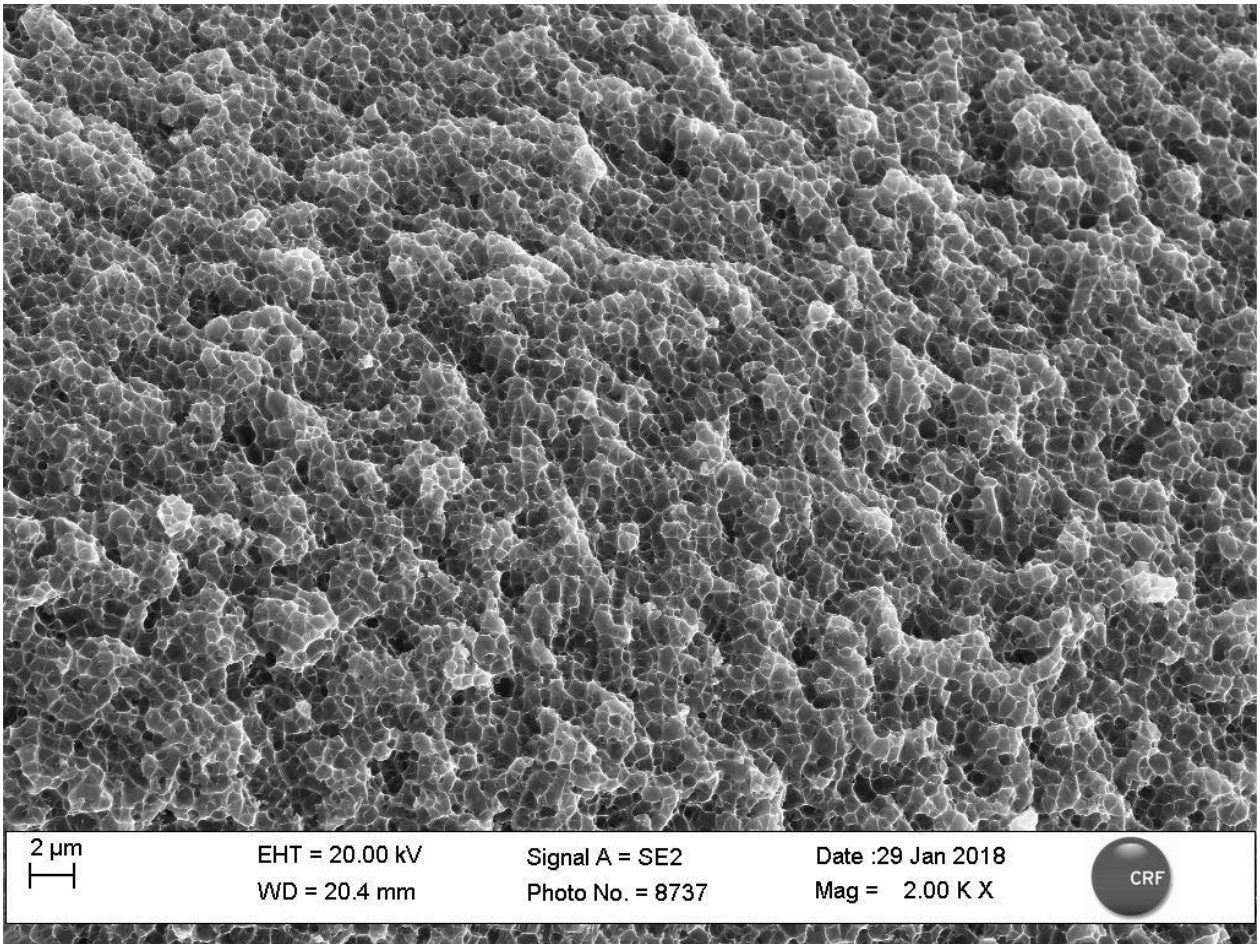

Figure 57: Enhanced segregation at grain boundaries of silicon that hinders the aluminium grain growth during the heat treatment.

Heat treatment ferformed on XY samples does not result in evident microstructural changes (aluminium grain size) and fracture surface morphology in comparison with as-built samples. Silicon segregation hinders the grain growth. The improvement in ductility achieved by the heat treatment at 300°C for 2 hours might be essentially due to the relief of internal stresses [33] .Fracture is essentially caused by micro-void coalescence (MVC) resulting in fine dimples and ductile fracture mechanism.

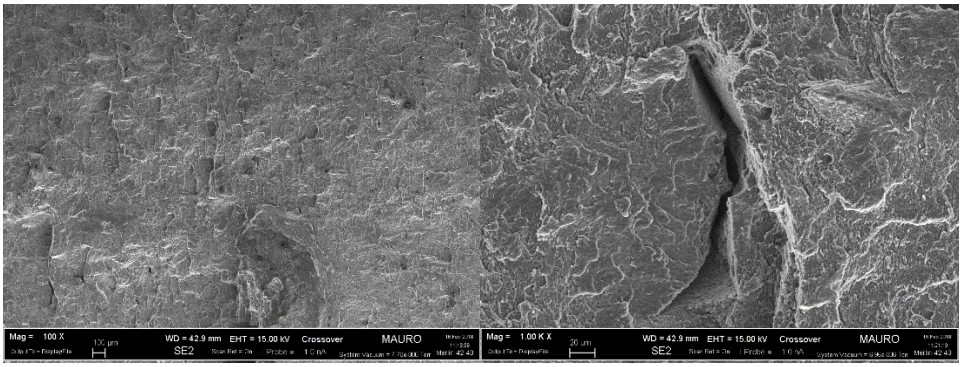

Figure 58 :heat treated XY samples fracture surfaces, different magnifications

3.2.3.2 Micro-Hardness analysis

Samples hardness , being a mechanical property ,depends on the microstructure, process parameter and heat treatment . Furthermore, this characteristic could be strongly dependent on solidification conditions and the heat treatment can cause precipitation of Mg_2Si that can enhance hardness .

Table shows the comparison between the HB hardness values, obtained on both the parallel and the perpendicular faces respect to the growth direction , of the as built and heat treated parallelepiped specimens produced in the frame of job A, job B, and job C .

HB	JOB A As built	JOB A Heat treated	JOB B As built	JOB B Heat treated	JOB C As built	JOB C Heat treated
Face parallel to the growth direction (Z)	100,5 103,92 105,066	110 108,9 109	102 107,3 107,3	111 108,43 108,88	108,5 110,33 110	109,4 110,3 109
Average value	**103,2**	**109,3**	**105,53**	**109,43**	**109,61**	**109,43**
Face(1) perpendicular to the growth direction (Z)	80,45 75,8 88,73	82,4 83 82,4	87,92 89,8 88,7	88,6 91 90	92,3 95,76 88,3	93,2 95 90
Average value	**81,66**	**82,6**	**88,806**	**89,86**	**91**	**92,73**
Face(2) perpendicular to the growth direction (Z)	80,5 73,1 84,95	85,2 80 86,7	86,3 92,2 90,1	90 92,2 92	85,9 93,66 93,46	91 95,7 95,6
Average value	**79,51**	**84,06**	**89,53**	**91,4**	**91**	**94,1**

Table 11: Hardness values relative to samples face perpendicular and parallel to the building direction

The results achieved confirm that SLM process makes possible to reach high level of hardness due to the fine distribution of the Si phase in AlSi10Mg SLM parts and to high thermal gradients at which the material is submitted during the process that lead to a very fine microstructure . The hardness of the face perpendicular to the growth direction is significantly higher than that of face placed parallel to the growth direction. Actually the face perpendicular to Z direction results from the melting and rapid solidification of the last powder layer. On the contrary the face parallel to Z direction is constituted by the layers previously melted and solified, that after solidification are kept for long time (many hours) at temperature of 200°C or more (due to the laser effect). During this period of time stress relaxation can occur to some extent, while this can not happen for the last layer (face perpendicular to Z direction).

Comparing the hardness values obtained with those of the cast $AlSi_{10}Mg$ alloy (Tab. 12) , it is evident that with the casting techniques it is possible to obtain comparable or better hardness values only by high pressure casting followed by heat treatment of precipitation hardening. As was mentioned for the UTS and

elongation also the high hardness in cast parts is reached after the formation of Mg_2Si precipitates during the heat treatment while in the SLM as built parts hardness is essentially due to residual stresses and the fine microstructure.

$AlSi_{10}$ Mg casting sample	**HV**
Conventional cast and aged	86
High pressure die casting	95-105
High pressure die casting and aged	130-133

Table 12 : Hardness of AlSi10Mg casting sample

Conclusively in SLM parts fine microstructure depends on solidification conditions and the state of residual stresses on the heat treatment [18] .

As mentioned above samples tend to have higher hardness values in the face perpendicular to the growth direction with respect to the parallel faces. Due to the very high cooling rate fine grains are obtained in every case and residual stresses arise from thermal gradients. Stress relaxation dio not occur during the building process for the layer which has solidified last while in the parallel faces the laser treated layers remain at high temperature while the others solidify and suffer a sort of softening .

The heat treatment at 300 ° C for two hours causes precipitation of Mg_2Si that can rise hardness and for this reason heat treated samples have higher hardness values than as built samples .

Eos technical data sheet only gives hardness value of approximately to119 ±5 HB for the perpendicular face of the as built samples, which is consistent with the values obtained in the present work.

3.2.3.3 Charpy test

Through the Charpy impact test it is possible to determine material toughness by hitting samples ,with a hammer, mounted at the end of a pendulum. Samples grown along different growth directions (Z and XY) as built and heat treated with a V-shaped notch (used to control the fracture process by concentrating stress in the area of minimum cross-section) were tested . Table 13 shows the absorbed energy (fracture work calculated by the height of rise subtracted from the height of fall) obtained by testing three samples as built and heat treated respectively for every building direction .

	Z samples as built	**Z samples heat treated**	**XY samples as built**	**XY samples heat treated**
absorbed energy(J/m^2)	1,7 ±0,3	4,16 ±0,2	10,33 ±0,3	19,4 ±1

Table 13 : absorbed energy during Charpy test

A clear anisotropy is observed : samples built along Z axis absorbed less energy than XY samples . This reasonably is due to the different layers orientation with respect to the length of the samples and then with respect to the direction of crack propagation. In Z samples the hammer impacts parallel to layers and when **a** crack is generated , before emerging on the surface, it will cross the border areas between the adjacent layers , which are weak areas. In the XY samples instead the hammer impacts perpendicular to layers and the crack , before emerging on the surface, will have to cross the various layers that will slow down its propagation .

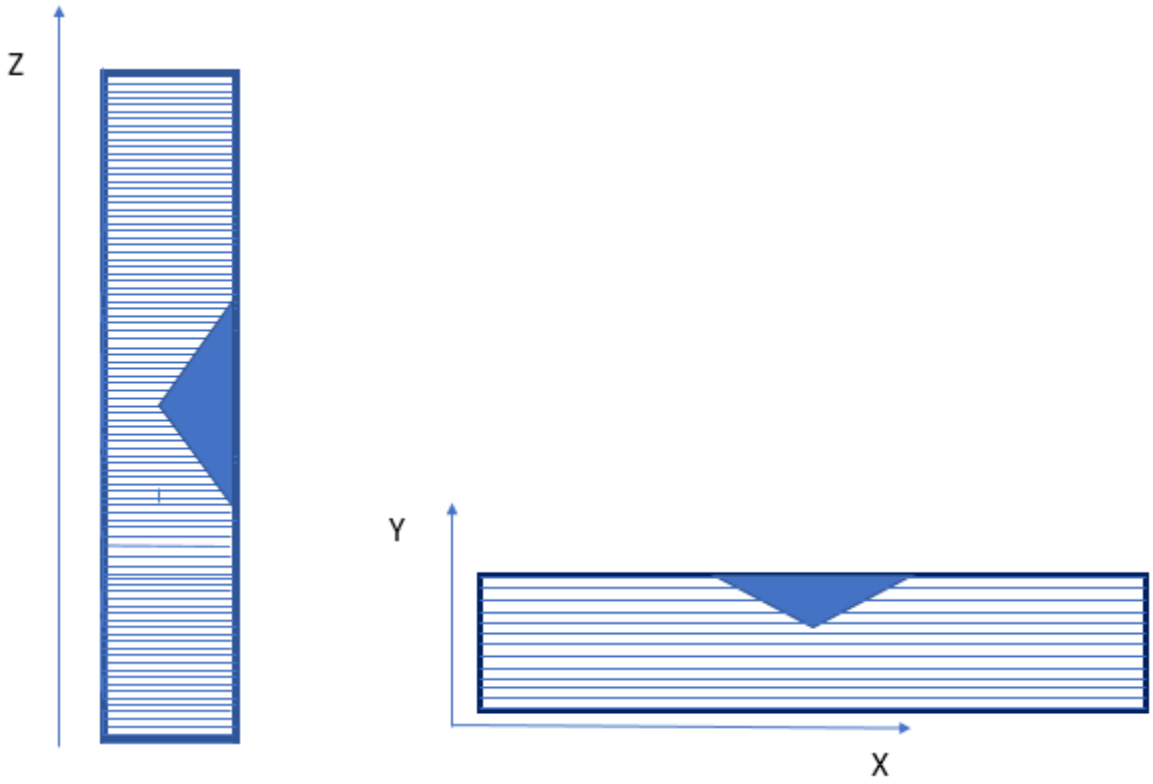

Figure 59 : cross section of Charpy samples ,different layers orientation with respect to V notch for samples built along Z axis and on XY plane

The different adsorbed energy values are due to the different fracture mechanism mentioned previously. The heat treatment cannot significantly reduce the anisotropy and then different Charpy results are observed for the two kind of specimens also after thermal treatment.. However after the thermal treatment the specimens grown along Z show an absorbed energy 5 times greater than as built samples. The fracture work also greatly increases after thermal treatment for samples placed in the XY plane. Actually thermal treatment can cause both microstructure changes (silicon segregation) and stress relaxation.

So we have the confirmation that the heat treatment has greater influence on the behavior of samples grown along Z; in fact it affects the elongation at breakage (that is synonymous of ductility) as well as the fracture toughness.

3.2.4 Residual stress analysis

The residual stress analysis was performed for each job (A,B,C) on parallelepiped samples , as built and heat treated, grown along Z axis. The analysis was carried out on a parallel and perpendicular face with respect to the building direction. The results obtained for the job A , job B and job C do not show significant differences and therefore only the most significant results will be reported.

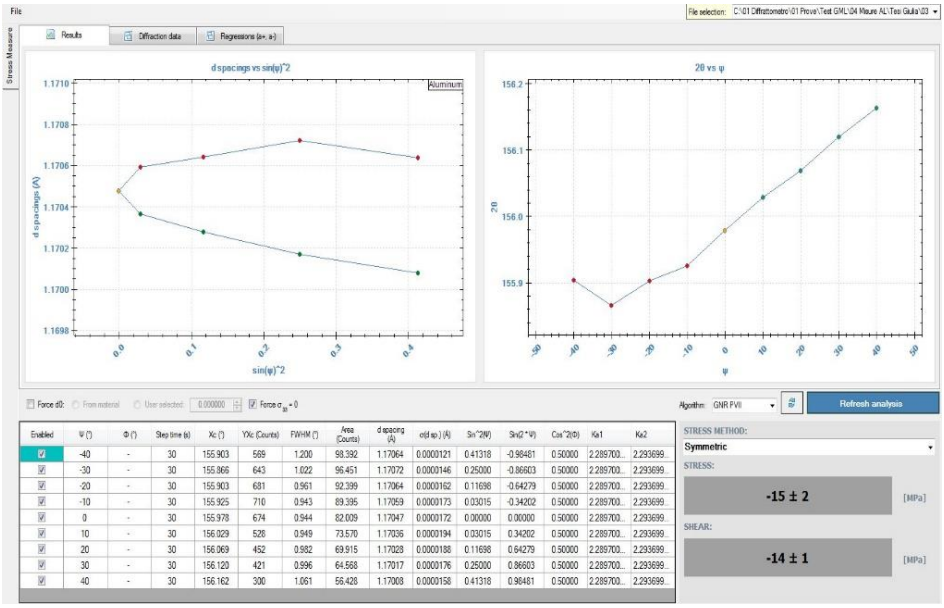

Figure 60: residual stress analysis on the perpendicular face of the as built sample

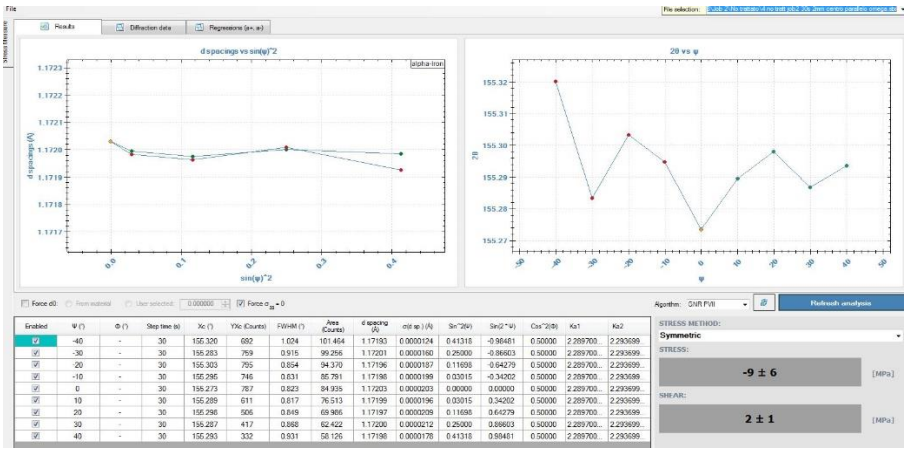

Figure 61: residual stress analysis on the parallel face of the as built sample

In both faces there is a complex state of residual stresses (compression and shear stress). A more pronounced compression state is located in the face perpendicular to the growth direction probably due to the fact that it solidify last and therefore it has less time to relax the residual stresses with respect to the parallel faces during the SLM process. . This is in accordance with the hardness data previously reported . The theoretical inter planar distance (d) is different from the one found during the analysis using φ=0. Very likely there is a distortion of the aluminium crystal lattice due to the presence of silicon in supersaturated solid solution. The presence of silicon affect the inter planar distance value. Then the d value measured results from two effects: lattice distortion due to silicon and residual stresses. Unfortunately there is no way to separate these two effects, and therefore the residual stress values are only indicative. In addition the trend of "d" variation with the φ angle was found not regular in some cases, very likely to the effect of silicon that disturbs the measurement.

The residual stresses created during the samples realization process are the sum of the effects of: rapid solidification, temperature gradients and volumetric changes caused by phase transformations and rapid cooling. The differences in temperature between the irradiated region and the surrounding zone produce transient thermal deformations on the surface and below it; when the source of heat is removed, the irradiated zones contracts and residual stresses are created. [34]

Compression and shear stresses are more evident for the face perpendiculat to Z direction, that corresponds to the powder layer that sididifies last.

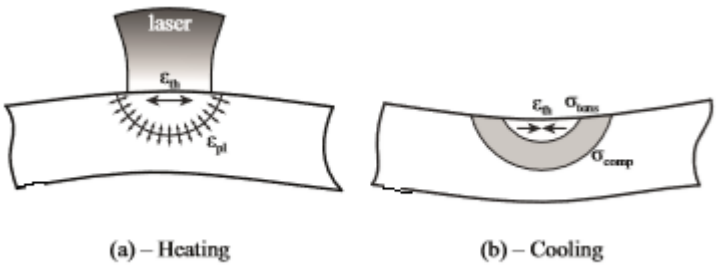

Figure 62: Temperature gradient influences on the formation of residual stress

The heat treatment seems to have only little effect on the residual stress. Residual stresses can be relieved during heat treatment because of recrystallization or plastic deformation occurring when the residual stress exceeds the yield strength of the material at the heat treatment temperature. . The possibility of having recrystallization is denied by what emerged from the SEM analyzes of the fracture surfaces: there is no evident growth of the grains during the heat treatment . It would be necessary to know the yield strength at 300°C of the alloy in order to establish if plastic deformation occurs or not. On the other hand the heat treatment pushes towards a state of equilibrium an then it modifies the silicon content in the aluminum lattice. Assuming to have a sostitutional solid solution of silicon in aluminum, as a result of heat treatment and consequent segregation of silicon there would be an increase of d and therefore a slight relaxation of compressive stresses.

The uncertainty on measured axial stresses (see standard deviation) do not allow neither to confirm nor to exclude this hypothesis.

Differently the shear stress clearly decreases after the thermal treatment.

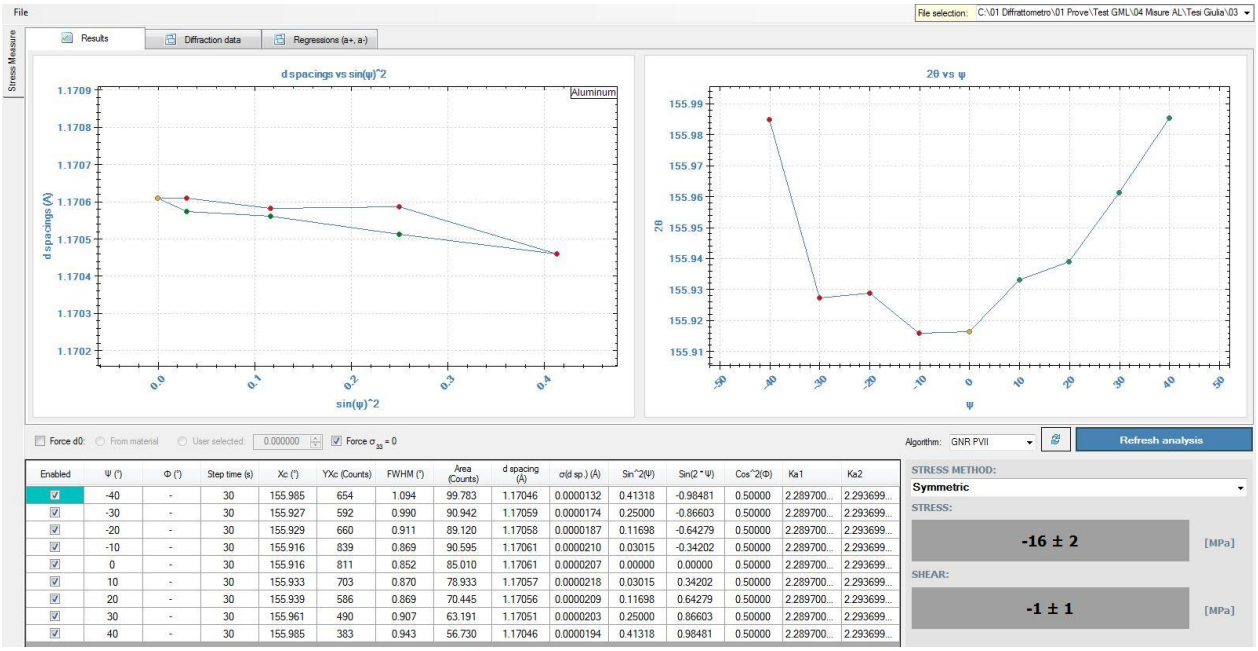

Enabled	Ψ (°)	Φ (°)	Step time (s)	Xc (°)	YXc (Counts)	FWHM (°)	Area (Counts)	d spacing (Å)	σ(d sp.) (Å)	Sin^2(Ψ)	Sin(2 * Ψ)	Cos^2(Φ)	Ka1	Ka2
☑	-40	-	30	155.985	654	1.094	99.783	1.17046	0.0000132	0.41318	-0.98481	0.50000	2.289700...	2.293699...
☑	-30	-	30	155.927	592	0.990	90.942	1.17059	0.0000174	0.25000	-0.86603	0.50000	2.289700...	2.293699...
☑	-20	-	30	155.929	660	0.911	89.120	1.17058	0.0000187	0.11698	-0.64279	0.50000	2.289700...	2.293699...
☑	-10	-	30	155.916	839	0.869	90.595	1.17061	0.0000210	0.03015	-0.34202	0.50000	2.289700...	2.293699...
☑	0	-	30	155.916	811	0.852	85.010	1.17061	0.0000207	0.00000	0.00000	0.50000	2.289700...	2.293699...
☑	10	-	30	155.933	703	0.870	78.933	1.17057	0.0000218	0.03015	0.34202	0.50000	2.289700...	2.293699...
☑	20	-	30	155.939	586	0.869	70.445	1.17056	0.0000209	0.11698	0.64279	0.50000	2.289700...	2.293699...
☑	30	-	30	155.961	490	0.907	63.191	1.17051	0.0000203	0.25000	0.86603	0.50000	2.289700...	2.293699...
☑	40	-	30	155.985	383	0.943	56.730	1.17046	0.0000194	0.41318	0.98481	0.50000	2.289700...	2.293699...

Figure 63: residual stress analysis on the perpendicular face of the heat treated sample

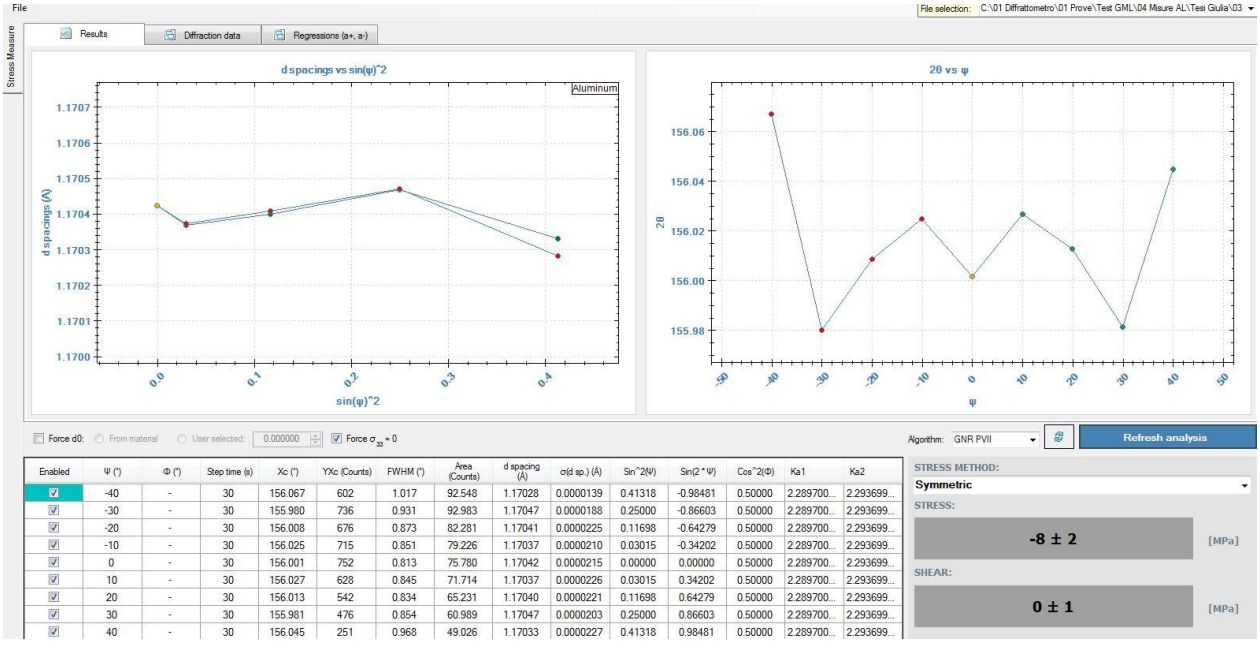

Enabled	Ψ (°)	Φ (°)	Step time (s)	Xc (°)	YXc (Counts)	FWHM (°)	Area (Counts)	d spacing (Å)	σ(d sp.) (Å)	Sin^2(Ψ)	Sin(2 * Ψ)	Cos^2(Φ)	Ka1	Ka2
☑	-40	-	30	156.067	602	1.017	92.548	1.17028	0.0000139	0.41318	-0.98481	0.50000	2.289700...	2.293699...
☑	-30	-	30	155.980	736	0.931	92.983	1.17047	0.0000188	0.25000	-0.86603	0.50000	2.289700...	2.293699...
☑	-20	-	30	156.008	676	0.873	82.281	1.17041	0.0000225	0.11698	-0.64279	0.50000	2.289700...	2.293699...
☑	-10	-	30	156.025	715	0.851	79.226	1.17037	0.0000210	0.03015	-0.34202	0.50000	2.289700...	2.293699...
☑	0	-	30	156.001	752	0.813	75.780	1.17042	0.0000215	0.00000	0.00000	0.50000	2.289700...	2.293699...
☑	10	-	30	156.027	628	0.845	71.714	1.17037	0.0000226	0.03015	0.34202	0.50000	2.289700...	2.293699...
☑	20	-	30	156.013	542	0.834	65.231	1.17040	0.0000221	0.11698	0.64279	0.50000	2.289700...	2.293699...
☑	30	-	30	155.981	476	0.854	60.989	1.17047	0.0000203	0.25000	0.86603	0.50000	2.289700...	2.293699...
☑	40	-	30	156.045	251	0.968	49.026	1.17033	0.0000227	0.41318	0.98481	0.50000	2.289700...	2.293699...

Figure 64: residual stress analysis on the parallel face of the heat treated sample

4 Conclusions

In this thesis specimens of AlSi10Mg alloy were produced via Laser Beam Melting technology and characterized. On the basis of experimental results, several conclusions can be made as listed in the following.

- Outcomes of density and porosity analyses of the as built and heat treated samples allow to state that all samples show lower density values and higher porosity with respect to the values expected according to the producer (EOS) datasheet. This was probably due to a not complete consolidation of the parts, which results particularly evident at the edges of the melt pools. It is also possible to affirm that neither the heat treatment nor the powder layer thickness affected the final density, and consequently the porosity of the manufactured products.

- Tensile tests carried out on the specimens showed that the mechanical characteristics depend on the growth direction of the specimen, on the heat treatment and on the thickness of the powder bed. The specimens grown along Z axis show greater tensile strength than those grown in the XY plane but sometimes lower yield strength and lower elongation at break. By investigating the micro-structure of the specimens it was possible to understand how the direction of growth influences the mechanical properties. The different mechanical behavior can be explained by the different orientation of the various layers that can be parallel or perpendicular with respect to the direction of load application. In Z samples failure propagates perpendicular to the building direction, that is through weak interfaces between the layers, while in XY samples failure propagated parallel to the building direction, that is perpendicularly to the building layers . Electron microscopy performed on the fracture surfaces of as built and heat treated specimens (grown according to both the above mentioned directions) always showed a microstructure consisting of very small aluminum grains surrounded by silicon, segregated at the grain boundaries. In every case inter –domain ductile fracture was observed at low magnification, and intergranular ductile fracture was

observed at higher magnification. The heat treatment caused the enhancement of silicon segregation; the grain boundary were clearly decorated by silicon particles and Mg_2Si in a continuous manner. No significant grain growth occurred during thermal treatment due to the segregation of silicon that prevented the grains growth. Moreover, it is possible to affirm that the stress relieving thermal treatment mainly affected the ultimate tensile strength and the elongation. In particular, this can be seen in specimens grown along Z axis. As regard samples built with higher powder bed thickness the heat treatment inflates much less the mechanical properties of the samples, which it is probably due to the fact that being the powder bed thicker there is a different thermal history during selective laser melting.

- The material anisotropy also affected both hardness values and fracture work. From HB micro- hardness test it is possible to state that the specimens show higher hardness values on the faces with transverse orientation with respect to the growth direction than on the parallel ones. Faces parallel and perpendicular to the growth direction have different thermal history. The specimen grew along Z, therefore the hardness of sample face perpendicular to the growth direction refers to the layer which has solidified last, while in case of the parallel faces the layers remained at high temperature for many hours during the sample building layer by layer. In addition the heat treatment for stress relieving did not significantly influence the hardness of the specimens. Fracture work was also influenced by the growth orientation of the specimens as well as by heat treatment. The specimens grown in the XY plane showed higher fracture work, and ductility too (elongation at break), than those grown along Z axis. In both cases there was an increase in fracture work after heat treatment, especially for specimens grown along Z.

- Residual stress analysis showed that there is a complex state of compression and shear stress on sample faces parallel and perpendicular to the growth direction. In the face perpendicular to the growth direction, higher stress values were obtained, confirming the importance of the different thermal history on the mechanical properties. However it should be taken into account that the values of thermal stresses are calculated through the measure of the inter-plane spacing, that is also affected by the presence of silicon in solid solution in aluminum. This feature therefore affected the stress evaluation.

Nonetheless a significant reduction of shear stress was observed after the stress relieving treatment.

Bibliography

[1] M. Javidani, J. Arreguin-Zavala, J. Danovitch, Y. Tian, and M. Brochu, "Additive Manufacturing of AlSi10Mg Alloy Using Direct Energy Deposition: Microstructure and Hardness Characterization," *J. Therm. Spray Technol.*, vol. 26, no. 4, pp. 587–597, 2017.

[2] I. Campbell, D. Bourell, and I. Gibson, "Additive manufacturing: rapid prototyping comes of age," *Rapid Prototyp. J.*, vol. 18, no. 4, pp. 255–258, 2012.

[3] S. H. Huang, P. Liu, A. Mokasdar, and L. Hou, "Additive manufacturing and its societal impact: A literature review," *International Journal of Advanced Manufacturing Technology*, vol. 67, no. 5–8. pp. 1191–1203, 2013.

[4] W. E. Frazier, "Metal additive manufacturing: A review," *Journal of Materials Engineering and Performance*, vol. 23, no. 6. pp. 1917–1928, 2014.

[5] N. Guo and M. C. Leu, "Additive manufacturing: Technology, applications and research needs," *Frontiers of Mechanical Engineering*, vol. 8, no. 3. pp. 215–243, 2013.

[6] S. Trouton, "A Deloitte series on additive manufacturing," *Deloitte Univ. Press*, 2016.

[7] V. Bhavar, P. Kattire, V. Patil, S. Khot, K. Gujar, and R. Singh, "A Review on Powder Bed Fusion Technology of Metal Additive Manufacturing," *Mater. Sci. Technol. 2014*, pp. 251–262, 2014.

[8] J.-P. Kruth, "Materials and Processing Issues in Powder Fusion Additive Manufacturing," 2013.

[9] R. M. Mahamood, E. T. Akinlabi, M. Shukla, and S. Pityana, "Material Efficiency of Laser Metal Deposited Ti6A14V: Effect of Laser Power," *Eng. Lett.*, vol. 21, no. 1, pp. 18–22, 2013.

[10] B. Liu, R. Wildman, C. Tuck, I. Ashcroft, and R. Hague, "Investigation the effect of particle size distribution on processing parameters optimisation in selective laser melting process," *Int. solid Free. Fabr. Symp. an Addit. Manuf. Conf.*, no. mm, pp. 227–238, 2011.

[11] A. Aversa *et al.*, "Effect of Process and Post-Process Conditions on the Mechanical Properties of an A357 Alloy Produced via Laser Powder Bed Fusion," *Metals (Basel).*, vol. 7, no. 3, p. 68, 2017.

[12] K. H. Leitz *et al.*, "Fundamental analysis of the influence of powder characteristics in Selective Laser Melting of molybdenum based on a multi-physical simulation model," *Int. J. Refract. Met. Hard Mater.*, vol. 72, no. December 2017, pp. 1–8, 2018.

[13] D. Manfredi, F. Calignano, M. Krishnan, R. Canali, E. P. Ambrosio, and E. Atzeni, "From powders to dense metal parts: Characterization of a commercial alsimg alloy processed through direct metal laser sintering," *Materials (Basel).*, vol. 6, no. 3, pp. 856–869, 2013.

[14] N. Kang, P. Coddet, L. Dembinski, H. Liao, and C. Coddet, "Microstructure and strength analysis of eutectic Al-Si alloy in-situ manufactured using selective laser melting from elemental powder mixture," *J. Alloys Compd.*, vol. 691, pp. 316–322, 2017.

[15] A. Aversa, "Development and Characterisation of Aluminium Alloys and Aluminium Matrix Composites Produced via Laser Powder Bed Fusion By," 2017.

[16] I. Yadroitsev, L. Thivillon, P. Bertrand, and I. Smurov, "Strategy of manufacturing components with designed internal structure by selective laser melting of metallic powder," *Appl. Surf. Sci.*, vol. 254, no. 4, pp. 980–983, 2007.

[17] K. G. Prashanth *et al.*, "Microstructure and mechanical properties of Al-12Si produced by selective laser melting: Effect of heat treatment," *Mater. Sci. Eng. A*, vol. 590, pp. 153–160, 2014.

[18] K. Kempen, L. Thijs, J. Van Humbeeck, and J.-P. Kruth, "Mechanical Properties of AlSi10Mg Produced by Selective Laser Melting," *Phys. Procedia*, vol. 39, pp. 439–446, 2012.

[19] L. Wang, J. Jue, M. Xia, L. Guo, B. Yan, and D. Gu, "Effect of the Thermodynamic Behavior of Selective Laser Melting on the Formation of In situ Oxide Dispersion-Strengthened Aluminum-Based Composites," *Metals (Basel).*, vol. 6, no. 11, p. 286, 2016.

[20] J. Kruth, P. Mercelis, J. Van Vaerenbergh, and T. Craeghs, "Feedback control of Selective Laser Melting," *Proc. 3rd Int. Conf. Adv. Res. Virtual Rapid Prototyp.*, pp. 1–7, 2007.

[21] M. Entezarian, F. Allaire, P. Tsantrizos, and R. A. L. Drew, “Plasma atomization: A new process for the production of fine, spherical powders,” *JOM*, vol. 48, no. 6, pp. 53–55, 1996.

[22] EOS GmbH - Electro Optical Systems, “Material information Compatibility DMLS Materials – EOSINT M 280,” p. 82152.

[23] S. Hegde and K. N. Prabhu, “Modification of eutectic silicon in Al-Si alloys,” *J. Mater. Sci.*, vol. 43, no. 9, pp. 3009–3027, 2008.

[24] W. Li *et al.*, “Effect of heat treatment on AlSi10Mg alloy fabricated by selective laser melting: Microstructure evolution, mechanical properties and fracture mechanism,” *Mater. Sci. Eng. A*, vol. 663, pp. 116–125, 2016.

[25] N. T. Aboulkhair, N. M. Everitt, I. Ashcroft, and C. Tuck, “Reducing porosity in AlSi10Mg parts processed by selective laser melting,” *Addit. Manuf.*, vol. 1, pp. 77–86, 2014.

[26] B. Duman and M. C. Kayacan, “Doğrudan Metal Lazer Sinterleme / Ergitme Yöntemi ile İmal Edilecek Parçanın Mekanik Özelliklerinin Tahmini Predicting The Mechanical Properties Of The Part Produced By Direct Metal Laser Sintering / Melting Method,” 2017.

[27] EOS GmbH, “EOS M290 Datasheet Status 09/2017,” 2017.

[28] A. Popovich and V. Sufiiarov, “Metal Powder Additive Manufacturing,” *New Trends 3D Print.*, 2016.

[29] Fritsch, “Operating Instructions Analysette 22.”

[30] M. Fitzpatrick, A. Fry, P. Holdway, F. Kandil, J. Shackleton, and L. Suominen, “Determination of Residual Stresses by X-ray Diffraction - Issue 2,” *Meas. Good Pract. Guid.*, no. 52, p. 74, 2005.

[31] JEOL, “Scanning Electron Microscope A To Z,” *Serv. Adv. Technol.*, p. 32, 2006.

[32] 1.Rosenthal, I., Stern, A. & Frage, N. Strain rate sensitivity and fracture mechanism of AlSi10Mg parts produced by Selective Laser Melting. *Mater. Sci. Eng. A* **682,** 509–517 (2017).

[33] 1.Mertens, A., Dedry, O., Reuter, D., Rigo, O. & Lecomte-Beckers, J. THERMAL TREATMENTS OF AlSi10Mg PROCESSED BY LASER BEAM MELTING. 1007–1016

[34]1.Aboulkhair, N. T., Everitt, N. M., Ashcroft, I. & Tuck, C. Reducing porosity in AlSi10Mg parts processed by selective laser melting. *Addit. Manuf.* **1,** 77–86 (2014).

Ringraziamenti

Molte sono le persone che mi hanno supportata in questo lavoro di tesi e che mi sento in dovere ringraziare. Ringrazio innanzitutto di cuore il Prof. Claudio Badini per avermi dato l'opportunità di poter svolgere questo lavoro , per avermi seguita costantemente , per la sua gentilezza , disponibilità. Un grazie va al Dott Fabio D'Aiuto , che mi ha dato l'opportunità di collaborare a pieno nel progetto ed a Flavia Gili che mi ha seguita durante questo percorso e che stimo molto per la sua preparazione e per la sua umanità Un sentito grazie va alla Dottoressa Elisa Padovano per la sua professionalità, per la sua pazienza ,gentilezza, per avermi seguita passo per passo dandomi l'opportunità di imparare molto e per aver creduto in me .